Elucidation of DNA methylation changes in response to ionizing radiation induced double strand breaks

Untersuchung von Änderungen der DNA Methylierung als Antwort auf Doppelstrangbrüche, induziert durch ionisierende Strahlung

Vom Fachbereich Biologie der Technischen Universität Darmstadt zur Erlangung des akademischen Grades eines Doctor rerum naturalium genehmigte Dissertation von Diplom Bioinformatikerin Maren Linda Herrlitz aus Darmstadt

TECHNISCHE UNIVERSITÄT DARMSTADT

Elucidation of DNA methylation changes in response to ionizing radiation induced double strand breaks

Untersuchung von Änderungen der DNA Methylierung als Antwort auf Doppelstrangbrüche, induziert durch ionisierende Strahlung

Vom Fachbereich Biologie der Technischen Universität Darmstadt

zur

Erlangung des akademischen Grades

eines Doctor rerum naturalium

genehmigte

Dissertation von

Diplom Bioinformatikerin Maren Linda Herrlitz

aus Darmstadt

1. Referent: Prof. Dr. Marco Durante

2. Referentin: Prof. Dr. Cristina Cardoso

Tag der Einreichung: 16.05.2014

Tag der mündlichen Prüfung: 04.07.2014

Darmstadt 2014

D 17

Table of Contents

List of Figures

List of Tables

Abbreviations

5caC	5-Carboxylcytosine
5fC	5-Formylcytosine
5hmC	5-Hydroxymethylcytosine
5hmU	5−hydroxymethyluracil
5mC	5-Methylcytosine
α	Alpha
A	Ampere
AEBSF	4-(2-Aminoethyl)-benzolsulfonylfluorid
AID	Activation-induced cytidine deaminase
AP site	Apyrimidinic/Apurinic site
APE1	AP Endonuclease-1
APOBEC	Apolipoprotein B mRNA editing enzyme, catalytic polypeptide-like
APS	Ammoniumpersulfat
ATCC	American Type Culture Collection
ATM	Ataxia telangiectasia-mutated
ATR	ATM and Rad3-related
β	Beta
BER	Base excision repair
bp	Base pair
BSA	Bovine serum albumin
c	Centi/Speed of light
C	Cytosine
CDH1	Cadherin 1
CDK	Cyclin dependent kinase
Chk1/2	Checkpoint kinase 1/2
CPD	Cumulative population doublings
CpG	Cytosine and guanine separated by one phosphate
δ	Delta
D	Dose
Da	Dalton
DAPI	4′,6-Diamidin-2-phenylindol
DDR	DNA damage response
DMEM	Dulbecco's minimal essential medium
DMSO	Dimethylsulfoxid
DNA	Deoxyribonucleic acid
DNA-PK	DNA-dependent protein kinase
DNA-PKcs	DNA-dependent protein kinase catalytic subunit
DNMT1/3	DNA methyltransferase 1/3
DSB	Double strand break
DSBH	Double-stranded β-helix
DTT	Dithiothreitol
E	Energy
e.g.	For example
ECL	Enhanced chemoluminescence
EDTA	Ethylenediaminetetraacetic acid

ELISA	Enzyme-linked immunosorbent assay
EMEM	Eagle's Minimum Essential Medium
ERRC1	Excision Repair Cross-Complementing Group-1
ESC/mESC	Embryonic stem cells/mouse ESC
eV	Electronvolt
F	Fluence
FCS	Fetal calf serum
FEN1	Flap Endonuclease-1
FOXC1	Forkhead box C1
γ	Gamma
Gadd45	Growth arrest and DNA damage-inducible protein 45
G-CSF	Granulocyte colony stimulating factor
GFP	Green fluorescent protein
GG-NER	Global genome NER
Gy	Gray
HAT	Histone acetyltransferase
HCF1	Host Cell Factor 1
HDAC	Histone deacetylase
HR	Homologous recombination
HRP	Horseradish peroxidase
HSPC	Human hematopoietic stem and progenitor cells
ICA	Intensity correlation analysis
ICQ	Intensity correlation quotient
IDAX	Inhibition of the Dvl and axin complex
IR	Ionizing radiation
IRIF	Ionizing radiation induced foci
J	Joule
JBP1/2	J-binding protein 1/2
k	Kilo
kb	Kilobasepair
kg	Kilogram
λ	Lambda
LET	Linear energy transfer
LINE1	Long Interspersed Elements
μ	micro
m	Mass; milli
M	Molar; Mega
MBD1/2/3 and MeCP2	Methyl-CpG-binding domain protein family
MDC1	Mediator of DNA-damage checkpoint 1
MEF	Mouse embryonic fibroblast
MGMT	O6-methylguanine-DNA methyltransferase
miRNA	microRNA
MLL1	Mixed-lineage leukaemia 1
mm	Millimeter
MRE11	Meiotic recombination protein
ν	Ny (Frequency)
n	Nano

NBS1	Nijmegan breakage syndrom 1
NER	Nucleotide excision repair
NFκB	Nuclear factor-kappa B
NHEJ	Nonhomologous end joining
NPC	Neuronal progenitor cells
OD_{600}	Optical density, of a sample measured at a wavelength of 600 nm
OGT	O-GlcNAc transferase
p16	Cyclin-dependent kinase inhibitor 2A
PAGE	Polyacrylamidegelelectrophoresis
PBL	Peripheral blood lymphocytes
PBS	Phosphate buffered saline
PCNA	Proliferating cell nuclear antigen
PCR	Polymerase chain reaction
PGC	Primordial germ cells
PDM	Product of the difference from the mean
pDNA-PKcs	Phosphorylated DNA-PKcs
Pol β	Polymerase β
PVDF	Polyvinylidenfluoride
Rad	Radiation Repair Protein
rDNA	Ribosomal DNA
RFC	Replication factor C
RNA	Ribonucleic acid
RPA	Replication Protein A
RPM	Rounds per minute
RPMI	Roswell Park Memorial Institute
RT	Room temperature
S	Stopping power
SAM	S-adenosylmethionine
SDS	Sodium dodecyl sulfate
SDS-PAGE	SDS-Polyacrylamide gel electrophoresis
SSB	Single strand break
ssDNA	Single stranded DNA
TBS	Tris buffered saline
TC-NER	Transcription coupled NER
TDG	Thymine DNA glycosylase
TEMED	Tetramethylethylenediamine
TET1/2/3	Ten eleven translocation 1/2/3
TET2CD-GFP	Cys-rich and catalytic domain of TET2
TFFIIH	Transcription factor IIH
TRAPPC9	Traficking protein particle complex 9
TSLC1	Tumor suppressor in lung cancer 1
UHRF	Ubiquitin-like PHD and RING finger domain-containing protein
UV	Ultraviolet
V	Volts
v	Velocity
v/v	Percent by volume
w/v	Weight/volume

XPC	Xeroderma pigmentosum, complementation group C
XRCC4	X-ray-complementing Chinese hamster gene 4
ZBTB	Zinc finger and BTB domain-containing proteins

1 Summary/Zusammenfassung

Recent studies indicate that epigenetic modifications like DNA methylation are involved in the DNA damage response to ionizing radiation (IR).

In this doctoral thesis DNA methylation changes after treatment with IR within one replication cycle time frame (≤ 24 hours) were investigated and a decrease in DNA methylation at short times after IR was observed. This fast decrease cannot be explained by a passive, replication-dependent mechanism due to reduced DNMT (DNA methyltransferase) expression. Rather it is conceivable that changing the enzymatic activity of enzymes may lead to changes in DNA methylation as a response to IR. In this context especially TET (ten eleven translocation) enzymes might play a role. These oxidize Methylcytosine (5mC) to Hydroxymethylcytosine (5hmC) and further to formylcytosine (5fC) and carboxylcytosine (5caC), being eventually replaced by cytosine via base excision repair (BER) mechanism.

For the analysis of a TET-dependent DNA demethylation an appropriate experimental cellular system was established. Therefore, global 5mC levels, TET2 expression levels and 5hmC levels in different cell lines were investigated. An anti-correlation between 5mC levels and TET2 expression was shown for all cell lines, while 5hmC and 5mC levels were correlated only in a part of the investigated cell lines and no correlation between 5hmC and TET2 expression was observed. NIH/3T3 cells, showing no TET2 expression, were chosen for experiments in which the catalytic domain of TET2 (TET2CD-GFP) was overexpressed. Using two different techniques (immunofluorescence and ELISA-based colorimetric analysis), an increase in 5hmC abundance was demonstrated as a response to TET2CD-GFP overexpression, indicating that ectopically expressed TET2 is active. Similar results were obtained when TET2CD-GFP was overexpressed in U-2 OS cells, which have a high expression level of TET2. TET2CD-GFP overexpression also led to its accumulation in nucleoli. Whether this observation would be an effect of overexpression or be indicative of a possible function in these nuclear sub-compartments is yet to be elucidated. Additionally, by using flow cytometry analysis, exposure to IR and concomitant overexpression of TET2CD-GFP strongly induced 5hmC formation, therefore suggesting a function of TET2 in response to irradiation.

Recruitment analysis showed that the TET2 catalytic domain was recruited to UV laser-induced but not X-rays- or heavy ion-induced damage sites. Endogenous TET2, which was analyzed in high TET2 expressing human fibroblasts, was recruited to damage sites after irradiation with heavy ions or X-rays. As 5hmC is the direct product of the catalytic activity of TET enzymes, local 5hmC formation and abundance at damage sites was investigated. It was observed that 5hmC accumulated at heavy ion- as well as X-ray-induced DNA double strand breaks (DSBs). In addition, investigating 5hmC foci over time after irradiation with X-rays revealed that 5hmC formation and kinetics is similar to that of γH2AX foci, whereby every 5hmC focus co-localized with γH2AX. However, this did not hold true for all γH2AX foci, whose total number was always higher than that of 5hmC. Furthermore, 5hmC (and γH2AX) foci formation was almost unaffected by the inhibition of DNA-PKcs' enzymatic activity. Conversely, 5hmC and γH2AX foci persistence was significantly delayed after DNA-PKcs inhibition.

Results obtained in this thesis show that DNA methylation changes (5hmC formation) take place within the time frame of one replication cycle after exposure to IR and that these changes can be observed at sites of DSBs. 5hmC at DSBs might be formed by the oxidative

function of TET2, which was shown to be recruited to DSBs. However, involvement of the other TET enzymes in 5hmC production cannot be excluded.

Therefore, these results suggest a role of 5hmC in the response to IR induced DSBs, whereby the here presented data suggest that the fast, radiation induced demethylation of cytosine most likely is mainly catalyzed by TET2 besides other enzymes.

Aktuelle Studien weisen darauf hin, dass epigenetische Modifikationen, wie z.B. DNA Methylierung an der DNA-Schadensantwort nach Behandlung mit ionisierender Strahlung (IR) beteiligt sind.

In dieser Doktorarbeit wurden Änderungen der DNA Methylierung nach Behandlung mit IR in einem zeitlichen Rahmen von einem Replikationszyklus (≤ 24 Stunden) untersucht und eine Abnahme der DNA Methylierung zu kurzen Zeiten nach IR beobachtet. Eine schnelle Abnahme lässt sich nicht durch einen passiven, replikationsabhängigen Mechanismus erklären, bei dem die Expression von DNA Methyltransferasen (DNMTs) inhibiert ist. Vielmehr ist es denkbar, dass die Änderung der enzymatischen Aktivität von Enzymen zu Änderungen der DNA Methylierung als Antwort auf IR beiträgt. Besonders TET (ten eleven translocation) Enzyme könnten hier eine Rolle spielen. Diese oxidieren Methylcytosin (5mC) zu Hydroxymethylcytosin (5hmC) und weiter zu Formyl- (5fC) und Carboxylcytosin (5caC), das durch Basenexzisionsreparatur (BER) durch Cytosin ersetzt werden kann.

Zur Untersuchung einer TET-abhängigen DNA Demethylierung wurde zunächst ein geeignetes zelluläres Versuchssystem etabliert. Dazu wurden die globale 5mC und 5hmC Menge sowie die Expression von TET2 in verschiedenen Zelllinien bestimmt. Hierbei konnte eine Antikorrelation zwischen der 5mC Menge und der TET2 Expression gezeigt werden. Eine Korrelation zwischen 5hmC und 5mC Menge konnte nur für einen Teil der Zelllinien beobachtet werden, wobei 5hmC und TET2 Expression nicht korreliert waren. Da NIH/3T3 Zellen kein TET2 aufwiesen, wurden sie im Folgenden für Experimente gewählt, bei denen die katalytische Domäne von TET2 (TET2CD-GFP) überexprimiert wurde. Hierbei wurde mittels Immunfluoreszenz die 5hmC Menge in TET2CD-GFP transfizierten NIH/3T3 Zellen gemessen und ein Anstieg der 5hmC Menge nach TET2CD-GFP Überexpression beobachtet. Dies zeigte, dass ektopisch exprimiertes TET2 aktiv ist und 5hmC bilden kann; dies wurde durch die Verwendung einer ELISA-basierten kolorimetrischen Methode bestätigt. Die Expression von TET2CD-GFP in U-2 OS, einer Zelllinie die eine hohe, endogene TET2 Expression aufweist, zeigte zudem vergleichbare Ergebnisse. Des Weiteren konnte beobachtet werden, dass die Überexpression von TET2CD-GFP zu seiner Akkumulation in Nukleoli führt. Ob dies nur ein Effekt der Überexpression ist, oder auf eine Funktion innerhalb dieser nukleären Subkompartimente hinweist, muss noch geklärt werden. Ferner konnte durch Durchflusszytometrie gezeigt werden, dass die Expression von TET2CD-GFP zusammen mit Bestrahlung zu einer Zunahme der 5hmC Menge führt; dies deutet auf eine Funktion von TET2 nach Bestrahlung hin.

Eine Rekrutierungsanalyse zeigte, dass die katalytische Domäne von TET2 zu UV-Laser induzierten Schäden rekrutiert wird, nicht aber zu Schäden, die durch Röntgenstrahlung oder durch Bestrahlung mit schweren Ionen induziert wurden. Endogenes TET2 in AG Zellen, mit ausgeprägter TET2 Expression, wurde allerdings zu DNA Doppelstrangbrüchen (DSBs), induziert durch Röntgenstrahlung oder nach Bestrahlung mit schweren Ionen, rekrutiert. Da 5hmC das direkte Produkt der enzymatischen Aktivität der TET Enzyme ist, wurde daraufhin untersucht ob auch 5hmC an Schäden akkumuliert. Ähnlich zu TET2 akkumulierte auch 5hmC an Schäden, die durch Bestrahlung mit schweren Ionen oder durch Röntgenstrahlung induziert wurden. Außerdem zeigte die Analyse eines zeitlichen Verlaufs von 5hmC Foci nach Röntgenbestrahlung, dass ihre Entstehung sowie ihr zeitlicher Verlauf dem von γH2AX Foci glichen. Hierbei kolokalisierte jeder 5hmC Fokus mit einem γH2AX Focus, wobei die Anzahl an γH2AX Foci immer höher war als die an 5hmC Foci. Es konnten also γH2AX Foci detektiert

werden, die nicht mit 5hmC Foci kolokalisierten. Zusätzlich wurde festgestellt, dass die Entstehung von 5hmC (und γH2AX) Foci durch die Inhibition der enzymatischen Aktivität von DNA-PKcs nahezu unbeeinflusst blieb. Im Gegensatz dazu blieben 5hmC und γH2AX Foci nach DNA-PKcs Inhibition länger am Schaden sichtbar.

Zusammenfassend konnte in dieser Arbeit gezeigt werden, dass innerhalb eines Replikationszykluses nach Bestrahlung mit IR Änderungen der DNA Methylierung (Bildung von 5hmC) erfolgen. Diese Veränderungen konnten an DSBs nachgewiesen werden. Da TET2 an DSBs rekrutiert wird, könnte 5hmC an DSBs durch die enzymatische Aktivität von TET2 entstehen. Allerdings kann eine Beteiligung anderer TET Enzyme, basierend auf diesen Beobachtungen, nicht ausgeschlossen werden.

Die Ergebnisse dieser Arbeit liefern daher erste Anhaltspunkte, die auf eine Rolle von 5hmC in der Antwort auf IR induzierte DSBs hinweisen. Die beobachtete, bestrahlungsabhängige, schnelle Cytosin Demethylierung wird dabei wohl hauptsächlich durch TET2 katalysiert; eine Beteiligung anderer Enzyme kann aber nicht ausgeschlossen werden.

2 Introduction

2.1 Physical principles of ionizing radiation

The term ionizing radiation indicates types of radiation having enough energy to eject electrons out of atoms or molecules (i.e., it ″ionizes″ the atom). These types of radiation include electromagnetic radiation (X- and γ-rays (photons)), neutron radiation, radiation of energetic charged particles like α-radiation, β-radiation, positrons, and protons as well as heavy ion radiation. Photons of low energy (< 124 eV) and ultraviolet radiation (UV-radiation) instead are not ionizing, as their energy is not sufficient to liberate electrons from target atoms. The energy of a photon can be described by the following equation:

$$E_{Photon}[J] = h\,[Js] \times \nu[s^{-1}]$$

$$with\ h = \ Planck's\ constant\ ;\nu \ = \ frequency$$

Equation 2-1

Radiation can be directly or indirectly ionizing. While charged particles are directly ionizing, meaning they disrupt atomic structures of matter they pass through and produce chemical and biological damage, electromagnetic radiations (X- and γ-rays) are indirectly ionizing. They are absorbed and produce charged particles that in turn produce the damage [Hall and Giaccia, 2012]. Depending on their energy, photons can interact with matter in different ways. The photoelectric effect (Figure 2-1 A) is predominant at low energies, while the Compton effect (Figure 2-1 B) as well as pair formation (Figure 2-1 C) mainly take place at high energies. In the photoelectric effect, the photon hitting an atom transfers all of its energy to an electron, which is emitted from the atom. In the Compton effect, only part of the energy of the incident photon is transferred to the electron and both the photon and the electron are emitted from the atom. At very high energies photons absorbed in matter can create an electron-positron pair which is emitted from the atom. The secondary electrons (δ-electrons) produced by these effects interact with matter and can cause ionization processes and damage themselves.

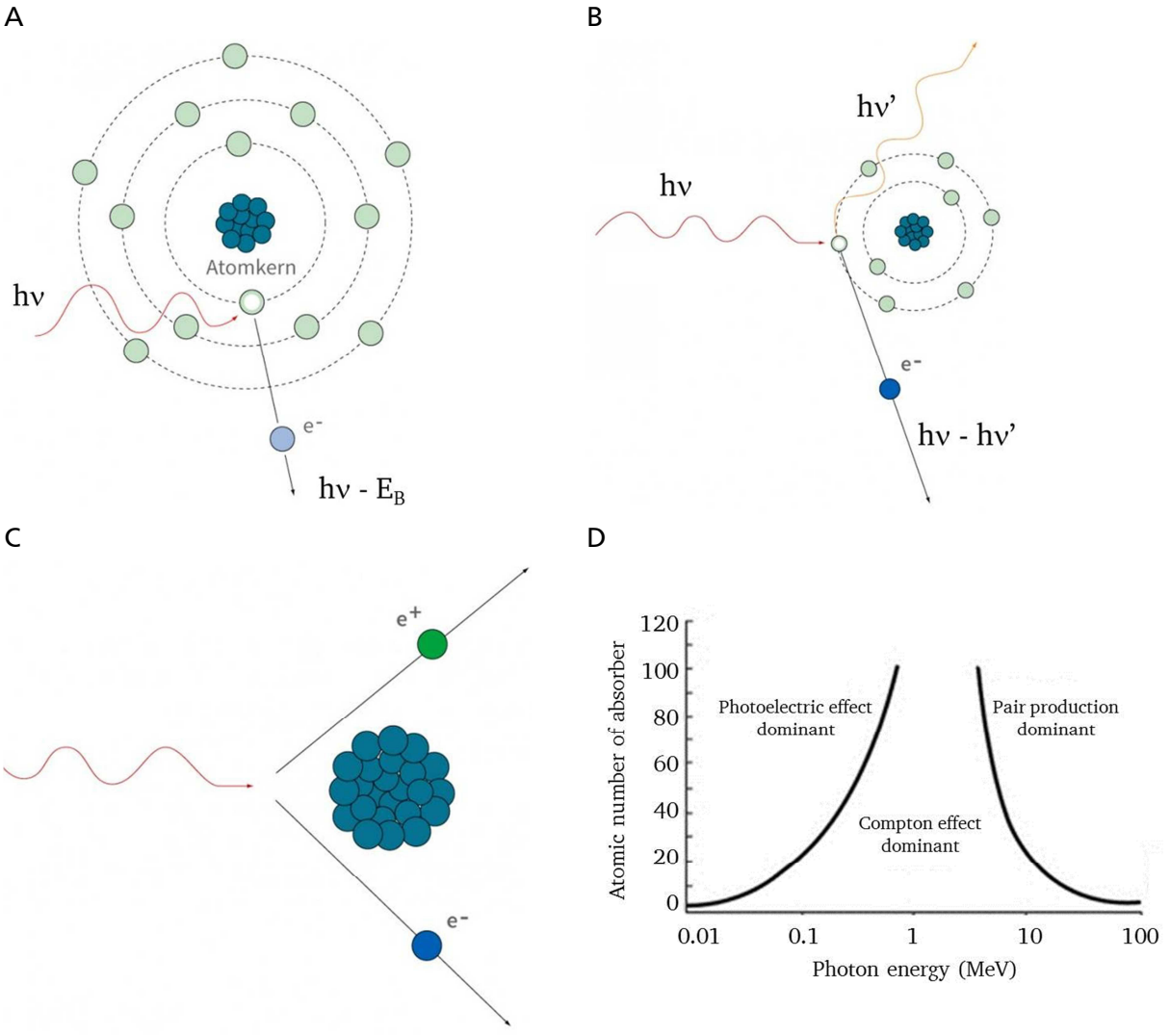

Figure 2-1: Interaction of photons with matter. The photoelectric effect (A) mainly takes place at low energies (up to 60 keV in water). Between 60 keV and 10 MeV in water the Compton effect (B) is predominant, while the pair production (C) is the dominating effect above 10 MeV in water. The relative occurrence of the three interactions is shown in (D). hν = energy of the incident photon, E_B = binding energy of the photon, e^- = electron, e^+ = positron. (Figures based on www.onmeda.de/strahlenmedizin and www.ilo.org/oshenc/part-vi/radiation-ionizing.)

2.1.1 Dose and LET

When radiation passes through matter, it deposits part (or all) of its energy. The measure of the energy (E) deposited in a medium by ionizing radiation per unit mass (m) is the absorbed dose (D), which is represented by the unit "Gray" (Gy) according to the following equation:

$$D[Gy] = \frac{E(J)}{m[kg]}$$

Equation 2-2

The dose definition in Equation 2-2 can only describe homogenous energy deposition. Since charged particles present inhomogeneous energy deposition (explained in detail in 2.1.2), a

more suitable unit is employed to describe such process. This unit, called linear energy transfer (LET), indicates how much energy an ionizing particle delivers to the penetrated matter per unit length (d) and is dependent on the energy (E) and the charge (Z_{eff}) of the particle [Bethe, 1930, Bloch, 1933], according to the following equation:

$$LET\left[\frac{keV}{\mu m}\right] = \frac{E\,[keV]}{d[\mu m]} \propto \frac{Z_{eff}^2}{\beta^2}$$

$$with\ \beta = \frac{v}{c}\ ; v = \ velocity;\ c = speed\ of\ light$$

Equation 2-3

Another unit to describe the energy loss of particle radiation passing through matter is the stopping power (S) and describes the situation from the stopping material's point of view. It is defined as the retarding force acting on the particle during the interaction with matter. Concerning unit and numerical value, LET and stopping power are identical, however S is generally indicated by a minus sign:

$$S[E] = -\frac{dE}{dx}$$

$$with\ E = energy; x = path\ length$$

Equation 2-4

In this work the LET can be assumed to be constant since only thin cell layers (up to 2 μm) were irradiated.

When energetic ions penetrate the matter, they have high velocity, give off little energy and, thus, only a few ionization events take place. On their way through matter, ions lose kinetic energy until, at the end of their paths, they deposit their remaining energy in a very limited area. This area, where enhanced ionizations take place, is called Bragg-Peak and is observed for both protons and heavy ions (Figure 2-2 A). The penetration depth for energetic ions is higher than that for ions possessing lower energy (Figure 2-2 B), while the ionization density is increasing with decreasing energy of the ion (Figure 2-2 C). In comparison to ions and depending on their energy, photons lose most of their energy in the first few centimeters upon entering matter (Figure 2-2 A). This difference in energy deposition displays advantages for ion irradiation in the treatment of tumors located deep in the tissue. Due to the inverted depth-dose profile and the possibility to adjust the penetration depth by changing the energy of the ion, most of the energy can be deposited in the tumor while healthy tissue can almost completely be spared.

Finally, the dose for charged particle irradiation is calculated taking into account (i) the LET; (ii) the density of the target material, which is water-equivalent in this study and (iii) the fluence (F), which is the number of particles traversing a given area (particles/cm^2), according to the following equation:

$$D[Gy] = 1.602 \times 10^{-9} \left[\frac{\mu m \cdot g \cdot J}{keV \cdot cm \cdot kg}\right] \cdot LET \left[\frac{keV}{\mu m}\right] \cdot F \left[\frac{1}{cm^2}\right] \cdot \frac{1}{\rho}\left[\frac{cm^3}{g}\right]$$

Equation 2-5

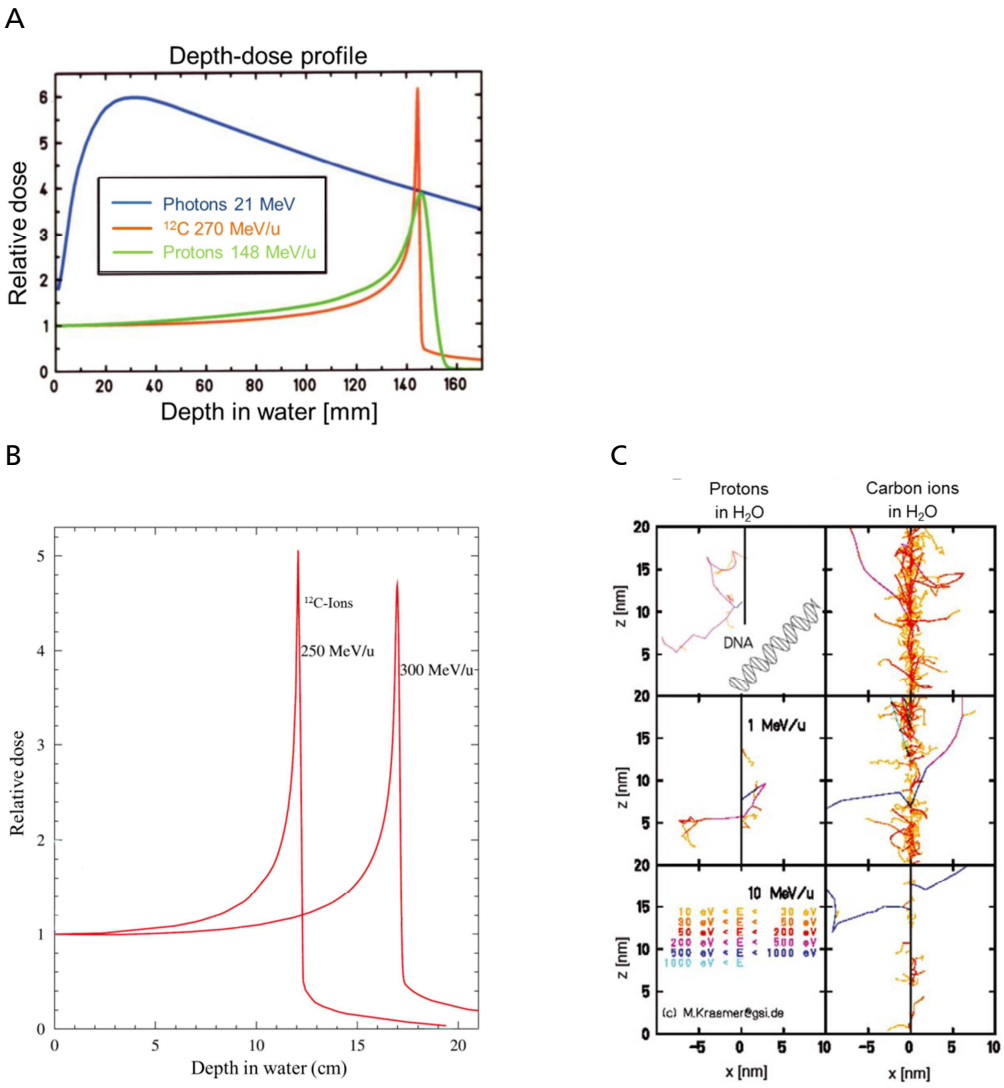

Figure 2-2: Depth-dose profile of photon- and particle radiation and comparison of particle tracks for protons and carbon ions. For photons, the dose decreases with increasing penetration depth while particles give off most of their energy in a very limited area (A). The penetration depth for ions with high energy is higher than that for ions with lower energy (B). In (C), tracks of protons and carbon ions are compared. δ-electrons are produced while the primary particle passes through matter, inducing biological damage (note the DNA cartoon). Overall, the ionization density is much higher with carbon ions compared to protons. (Figure based on [Scholz, 2003] and [Kraft, 2008])

2.1.2 Sparsely and densely ionizing radiation

Ionizing radiation can be divided into sparsely ionizing or densely ionizing radiation, according to its interactions and ionizations. X- and γ-rays belong to sparsely-ionizing radiation, in that interactions, ionizations and, ultimately, the energy are evenly deposited to

the entire irradiated area (Figure 2-3 A). Protons, α-radiation and heavy ions are densely-ionizing radiation, instead. Densely-ionizing radiation transfers its energy along its paths through matter, generating δ-electrons. The energy is deposited non-homogenously across the irradiated area and the dose is dependent on the distance from the particle trajectory. High doses are registered close to the core track while low doses (up to 10^3-fold decrease) are registered few micrometers away from the core track (Figure 2-3 B). Overall, the energy deposition along the track takes place at a confined space along the path of the single particle.

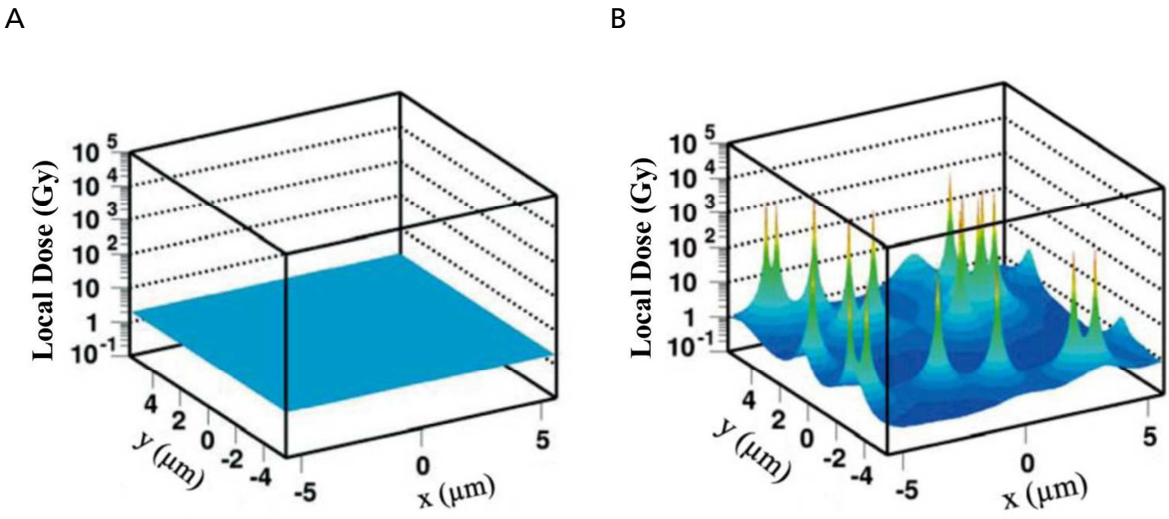

Figure 2-3: Dose distribution simulation on an area of 10 µm x 10 µm (approximate area of a cell nucleus) after photon- (A) and heavy ion- (B) irradiation. In A it is shown that the dose after X-ray irradiation is evenly distributed over the whole area. In B high doses are locally achieved by irradiation with carbon ions, while low doses are observed away from the particle track. (Figure based on [Scholz, 2003])

As just introduced, the dose is non-homogeneously distributed within the cross-section of the ion trajectory. Rather it is orders of magnitude higher in the center compared to the edge. Starting from the center of the particle track, the dose decreases according to the $1/r^2$ (r = radius) expression. The maximum range of δ-electrons is dependent on the energy of the ion and the maximum range (R_{max}) of the electron is defined by the following equation:

$$R_{max} = 0.05 \cdot E^{1.7}$$

$$with\ E = \text{Energy of the ion}$$

Equation 2-6

2.2 Principles of biology

2.2.1 The cell cycle

A cell originates from an existing cell that underwent division. For eukaryotic cells, this process comprises cell growth, DNA replication, distribution of the duplicated chromosomes to daughter cells, and cell division and is called the cell cycle (Figure 2-4). The DNA of each cell passing through the cell cycle is duplicated in S- (synthesis) phase. Then, cells pass through the G_2-phase, during which they keep growing, synthesizing and accumulating proteins, and preparing for mitosis. After G_2-phase, cells enter M-phase, where duplicated chromosomes are segregated to the newly forming daughter cells and eventually split into two cells (cytokinesis). Upon division, cells may enter G_1-phase, during which they continuously grow until they reach their former size and finally re-enter S-phase. Alternatively, depending on extracellular conditions (nutrients availability) or differentiation programs, cells may show a delayed G_1-phase, or enter a resting phase (G_0-phase), where they have left the cell cycle and have stopped dividing [Alberts et al., 2002].

2.2.2 The cell cycle control

The progression through the eukaryotic cell cycle is finely regulated via checkpoints, control mechanisms ensuring the fidelity of each cell cycle stage. The main checkpoints are found at the entry and the middle of M-phase (G_2- and metaphase-checkpoint) as well as at the end of G_1-phase (G_1-checkpoint) (Figure 2-4). They verify whether the processes at each cell cycle phase have been accurately completed before progression into the next phase. If for example DNA replication is not complete, entry in mitosis is prevented. Additionally, progression through G_1- and G_2-phase may also be halted if DNA is damaged (e.g. by radiation or chemicals). While halted at a checkpoint, the cell may attempt to repair the damage. If successful, the checkpoint releases the stall and the cell re-enters the cell cycle. Altogether, the cell cycle control system leads cells through the cell cycle, sensing signals from the environment and preventing cell division under undesirable circumstances [Alberts et al., 2002].

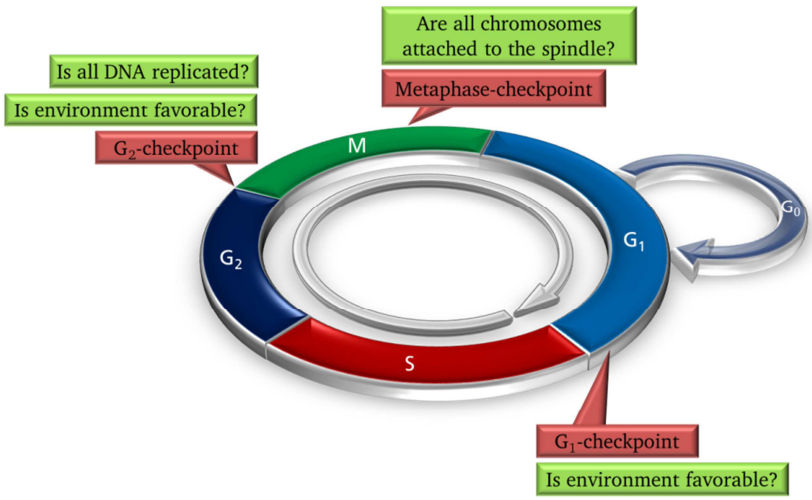

Figure 2-4: The cell cycle and the cell cycle control system The cell cycle is divided in G_1-, G_2-, S- and M-phase. Furthermore, cells can also leave the cell cycle and enter G_0-phase. The progression through cell cycle is regulated via three checkpoints (G_1-, G_2- and Metaphase-checkpoint). (Figure based on [Alberts et al., 2002])

2.2.3 DNA-damage caused by ionizing radiation

Damage to DNA, which carries the genetic information, is the main cause of biological effects of radiation [Munro, 1970]. If DNA is not properly repaired, cell death, mutations or transformation can occur. DNA can be damaged in several ways. In fact, DNA damage spontaneously occurs during replication stress and other physiological processes of cell metabolism. Exogenous genotoxic agents like mutagenic substances, UV-irradiation or ionizing radiation can account for DNA damage as well.

DNA exposed to ionizing radiation can be directly or indirectly damaged (Figure 2-5). The direct process consists of the absorption of radiation in form of X- or γ-rays, charged or uncharged particles by the biological material. Inside the cells, radiation directly interacts with all types of cellular components, leading to ionization or excitation of atoms. The direct effect is dominant when radiation possesses high LET.

The indirect process involves an intermediate moiety, which in most cases is a water molecule, since ~80 % of cellular volume is occupied by water. When radiation interacts with a water molecule, the water may lose an electron and becomes ionized. Such process can be described as follows:

$$H_2O \rightarrow H_2O^+ + e^-$$

The products of the reaction are a free electron and a H_2O^+ ion radical, being positively charged and having an unpaired electron. The former can then damage other molecules; the latter can react with another water molecule forming a highly reactive hydroxyl radical (OH·) according to the following expression:

$$H_2O^+ + H_2O \rightarrow H_3O^+ + OH\cdot$$

OH· possesses an unpaired electron and neutral charge. These features make such moiety highly reactive and diffusible. It is assumed that two thirds of damage to DNA in mammalian cells after X-ray irradiation, is caused by OH· [Hall and Giaccia, 2012].

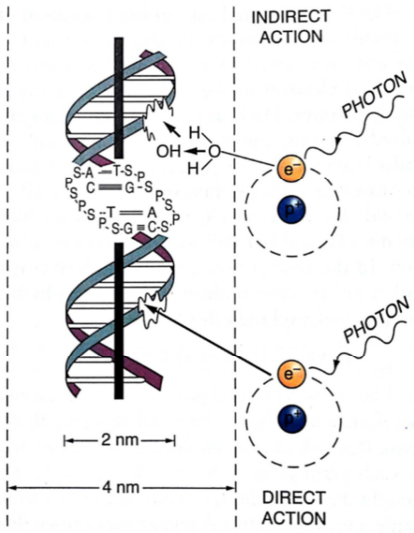

Figure 2-5: Direct and indirect damage of ionizing radiation. The direct damage is the absorption of radiation by the biological material, while in the indirect effect damage is mainly caused by a highly reactive OH·. (Figure: [Hall and Giaccia, 2012])

DNA lesions induced by ionizing radiation comprise base damage, single strand breaks (SSBs), double strand breaks (DSBs) as well as DNA protein crosslinks. According to literature [Hall and Giaccia, 2012] the numbers of DNA lesions per cell detected after a dose of 1 Gy X-rays are ~40 DSBs, ~1000 SSBs and more than 1000 base damages. Among those the most harmful DNA damage is the DSB, since both DNA strands are broken [Ward, 1975]. This may lead to mutations or chromosomal aberrations, if for example DNA ends from different genomic sites are rejoined [Agarwal et al., 2006]. As already described in chapter 2.1.2, sparsely ionizing radiation produces stochastically distributed DSBs; DSBs produced by high LET radiation are in close proximity along the ion track, instead [Ward, 1994, Goodhead, 1994]. For this reason complex "clustered DNA damage" is produced, which is extremely difficult to repair and that cannot be repaired completely [Taucher-Scholz et al., 1996].

2.2.4 Repair of DNA damage caused by ionizing radiation

2.2.4.1 The double strand break repair

DSBs can be repaired by DNA repair mechanisms. The two major DNA repair mechanisms are homologous recombination (HR) and nonhomologous end-joining (NHEJ). HR is considered to be an error-free process since the information needed for repair is copied from the undamaged homologous sister chromatid. In comparison NHEJ is considered to be error prone, since the correct information is only restored if the two DNA ends are ligated in a correct way and no intervening sequences are lost in the process. Most DSBs induced by ionizing radiation are repaired by NHEJ [Haber, 2000].

2.2.4.1.1 Immediate response of a cell to double strand breaks

Upon DSB formation, the MRN-complex, consisting of the MRE11 (meiotic recombination protein), Rad50 and NBS1 (Nijmegan breakage syndrom 1) subunits, interacts with the free DNA ends. Next, the kinases ATM (ataxia telangiectasia-mutated), ATR (ataxia telangiectasia and Rad3-related) and DNA-PKcs (DNA-dependent protein kinase catalytic subunit) are recruited to damage sites by the MRN-complex, a process leading to their activation. This, leading to activation of a cell cycle checkpoint, thus, halting the cell cycle progression. In detail, ATM phosphorylates and activates Chk2 (Checkpoint kinase 2), whereas ATR targets Chk1. Both, Chk1 as well as Chk2 are able to phosphorylate p53, leading to its stabilization. ATM and ATR can also themselves phosphorylate p53. The activation of p53 leads to the induction of p21 expression that leads to G_1 arrest by inhibition of the Cdk2-Cyclin E-PCNA complex. Chk1/2 can also phosphorylate Cdc25A that itself is degraded and is not able to activate Cdk2/Cyclin E/A complex, leading to G_1/S arrest. Furthermore, Chk1/2 may also phosphorylate Cdc25C, thus, not being able to activate Cdk1/CyclinB, which leads to G_2/M arrest (reviewed in [Christmann et al., 2003]). After activation of the checkpoint, effector kinases are activated, which in turn trigger a cascade of events involving other DSB repair, transcription or cell cycle control factors. Concomitantly, one of the earliest events of the DNA damage reponse takes place, that is the phosphorylation of H2AX (γH2AX). In principle, all three kinases, ATM, ATR and DNA-PKcs, are able to phosphorylate H2AX on serine 139 [Kinner et al., 2008]. γH2AX functions as a docking site for MDC1 (mediator of DNA-damage checkpoint 1), the latter being able to further recruit ATM and the MRN-complex, which accumulate downstream and upstream of the DSB ends. ATM accumulation ultimately leads to γH2AX spreading around the DSBs [Pardo et al., 2009]. γH2AX itself is a very important factor in recruiting repair proteins to the break and encompasses large chromatin domains

forming prominent nuclear foci that can be easily detected by immunostaining [Rogakou et al., 1999]. In the following, DSB repair is conducted either through NHEJ or HR respectively and this pathway choice is mainly dependent on the cell cycle phase. NHEJ takes place in G_0/G_1-, S- and G_2-phase. As already mentioned above, the information needed for repair by HR is copied from the undamaged homologous sister chromatid, which is only present in late S- and G_2-phase. Therefore DSB repair by HR is restricted to these cell cycle phases.

2.2.4.1.2 Nonhomologous end-joining

NHEJ is initiated by end recognition where the Ku heterodimer (composed of a 70 kDa and 80 kDa subunit) as well as DNA-PKcs bind to the ends of the DSB. Then Artemis, which possesses endonuclease activity, is recruited to the break and is phosphorylated by the Ku/DNA-PKcs complex. This in turn activates Artemis' endonuclease activity leading to end processing of 5' and 3' overhangs as well as hairpins. If blunt or compatible ends are repaired, this mechanism of end processing may not be necessarily essential. However, if the strands are processed, gaps are filled by the action of DNA polymerase μ or λ. In the following DNA-PK complexes recruit the X-ray complementing Chinese hamster gene 4 (XRCC4)-LigaseIV-Complex, which joins the ends together [Hall and Giaccia, 2012].

2.2.4.1.3 Homologous recombination

As previously stated, HR relies on the presence of the homologous sister chromatid which is used as a template. For this reason, such repair mechanism can take place in late S- as well as in G_2-phase. Reviewed by Pardo [Pardo et al., 2009], the first events of HR require ATM activated nucleases. The latter resect parts of the 5'-ends of DNA surrounding the DSB leading to a single stranded 3'-overhang (ssDNA). Next, Replication Protein A (RPA) binds to ssDNA and gets phosphorylated by PI-3-like protein kinases, thus promoting the recruitment of other involved factors. Rad51 is then recruited to the damage site and forms, together with Rad52, Rad55-Rad57 and Rad54, the Rad51-filament. This filament invades the homologous strand and the so called D-loop is formed, from which different pathways can lead to repair.

2.2.4.2 The repair of base damages

Base damages are the most common type of endogenous/physiological DNA damage. Nevertheless, base damages are also a result of exposure to IR. These damages, including alkylated and oxidative base products, abasic or AP (apyrimidinic/apurinic) sites, and misincorporated nucleotides are repaired by the base excision repair (BER) pathway. Additionally also SSBs are repaired by the same mechanism [Kim and Wilson, 2012]. The BER pathway is initiated by the recognition and subsequent removal of the incorrect or damaged site by a DNA glycosylase. By the action of the DNA glycosylase, an AP or an abasic site is generated. Subsequently this site is processed by APE1 (AP Endonuclease-1), which cleaves the phosphodiester backbone 5' to the AP site. Such cleavage results in a 3' hydroxyl group and a 5' abasic deoxyribose phosphate. The lesion is further processed by Polymerase β (Pol β) which adds one nucleotide to the 3' end of the nick and removes the 5' abasic deoxyribose phosphate. The integrity of the DNA is finally restored by DNA Ligase III, sealing the strand nick. This replacement of one damaged base is called "short-patch" BER and is the main sub-pathway of BER. If the damage is more complex, the so called "long-patch" BER pathway takes place, instead. In such case, the damage is resistant to the cleavage of Pol β,

and the 5'-sugar phosphate is not removed. Instead, replication factor C (RFC), proliferating cell nuclear antigen (PCNA) and DNA polymerase δ/ε add nucleotides to the 3'-end of the nick. Then Flap Endonuclease-1 (FEN1) takes over the removal of the flap structure and the nick is subsequently sealed by DNA Ligase I [Hegde et al., 2008, Hall and Giaccia, 2012].

2.2.4.3 The Nucleotide Excision Repair

The Nucleotide Excision Repair (NER) pathway repairs a broad spectrum of damages, although the most frequent lesions repaired by such mechanism are the photoproducts cyclobutane-pyrimidine dimers induced by UV radiation. NER can be subdivided into the global genome repair (GG-NER), where lesions are removed from coding or non-coding DNA, and transcription coupled repair (TC-NER) that only removes lesions from the transcribed strand of the DNA. GG-NER involves XPC (Xeroderma pigmentosum, complementation group C) and Rad23B scanning DNA for damaged sites and binding distortions to initiate the repair process, while in TC-NER recognition is triggered by DNA damage-mediated blockage of RNA-Pol II and the recruitment of CSB. Following recognition, which is the only part different for the two pathways of NER, TFFIIH (transcription factor IIH), XPA and RPA are recruited. Then TFFIIH helicase function unwinds the DNA next to the damage. Subsequently, the endonucleases XPG and Excision Repair Cross-Complementing Group-1 (ERRC1)/XPF cleave one strand of the DNA, and a ~30-base-long single stranded oligonucleotide is removed. The nick is filled by the polymerases δ/ε aided by RFC and PCNA and finally repaired by a DNA Ligase [Hanawalt, 2000, Hall and Giaccia, 2012, Le May et al., 2010].

So far, it is not known well enough, how the repair pathways described in this section communicate with each other to repair the different types of damage induced by irradiation with heavy ions.

2.3 Epigenetics and epigenetic changes

Epigenetic changes are heritably alterations to chromosomes without changing the DNA sequence [Berger et al., 2009]. They regulate chromatin density and therefore the accessibility of e.g. the transcriptional machinery to specific DNA regions. Furthermore epigenetic modifications serve as docking platforms promoting transcriptional activity or repression [Li et al., 2007]. In consequence, epigenetic regulation dictates specific gene expression profiles to define cellular identity and function [Orlowski et al., 2011]. The most noted and most investigated epigenetic mechanisms are DNA methylation and histone modifications, while also epigenetic events caused by small RNAs gain in importance.

2.3.1 Histone modifications

Histone modifications like acetylation, methylation, phosphorylation, or ubiquitination occur at specific histone sites. Histone modifications itself can cause changes to chromatin compaction like in the case of acetylation (see below) or can influence the binding and activity of proteins to chromatin which then could have an effect on gene regulation. Acetylation of histones, which is catalyzed by histone acetyltransferases (HATs) is mainly associated with increasing gene activity, while the removal of acetyl groups performed by histone deacetylases (HDACs) leads to a decrease in gene expression. In contrast, histone methylation shows different impacts. The methylation at lysine 4 of histone H3 (H3K4) for example, increases gene activity, while methylation at lysine 9 of the same histone (H3K9) leads to transcriptional repression (reviewed in [Tollefsbol, 2011]).

2.3.2 MicroRNAs

MicroRNAs (miRNAs) are short, 21-25-nucleotide long, non-coding single-stranded RNAs. By binding to their target-protein encoding mRNA sequence, they can regulate gene expression on a post-transcriptional level [He and Hannon, 2004]. It has been suggested that one miRNA is able to control hundreds of genes post-transcriptionally [Kim et al., 2013]. Since no investigations on microRNAs were conducted in this thesis, they will not be discussed any further.

2.3.3 DNA methylation

DNA methylation is the transfer of a methyl group from S-adenosylmethionine (SAM) to the fifth carbon position of cytosine bases. While it is known that DNA methylation can also take place in a non-CpG context [Lister et al., 2009] it mainly takes place in CpG dinucleotides. In mammals 70 – 80 % of CpG pairs are methylated [Kohli and Zhang, 2013] and can be found for example in gene bodies or transposable elements. Those CpG pairs are sparsely but globally distributed over the whole genome. Typically unmethylated CpG sites, instead, are not uniformly distributed over the genome but are concentrated in specific regions called CpG islands. CpG islands with an approximate length of 1 kilo basepair (kb) are mainly located in the upstream region from the transcriptional start site of many genes [Illingworth and Bird, 2009, Kim et al., 2013]. In vertebrates about 70 % of all gene promoters are associated with CpG islands of which the majority is unmethylated in all normal tissue types and throughout development [Deaton and Bird, 2011]. Due to the localization of CpG islands at promoter regions, especially the role in the regulation of gene expression is attributed to DNA methylation. In general, DNA hypomethylation causes increased gene expression while hypermethylation of gene promoters is associated with downregulation of gene expression and heritable silencing of gene expression can be achieved by hypermethylation of CpG islands [Antwih et al., 2013]. There are two mechanisms by which DNA methylation induces inhibition of gene expression. On the one hand methylated cytosine can directly repress transcription by blocking the binding of transcriptional activators to their DNA recognition sequence [Watt and Molloy, 1988]. On the other hand Methyl-CpG-binding-domain proteins (MBD) can elicit the repressive state of methylated DNA by recruiting co-repressors, to induce gene silencing directly [Zhang et al., 1999].

Changes in the DNA methylation pattern have been found to be related to cancer and it is commonly known, that reduced DNA methylation (global hypomethylation) as well as site-specific DNA hypermethylation take place during carcinogenesis. Global DNA hypomethylation specifically affects repetitive elements, like LINE1 (Long Interspersed Elements) or Alu [Weisenberger et al., 2005, Han et al., 2013], potentially leading to their re-activation. Repetitive elements re-activated by DNA hypomethylation might invade into functional regions of the genome, like coding regions or regulatory elements. Hypermethylation, instead, especially takes place within promoter regions and several studies have demonstrated a wide range of genes silenced by DNA hypermethylation in cancers (e.g. proteins involved in DNA repair, apoptosis or cell cycle regulation [Antwih et al., 2013]).

2.4 The regulation of DNA methylation

For quite some time DNA methylation was believed to be a rather stable epigenetic mark, newer studies however demonstrated that this modification is subjected to extensive changes. While the mechanisms behind DNA methylation are well known and studied intensively, findings about a reverse pathway are still under discussion.

2.4.1 DNA methylation

DNA methylation is catalyzed by so called DNA methyltransferases (DNMTs). DNMT1, responsible for the maintenance of DNA methylation, is targeted to hemimethylated DNA by UHRF1 (ubiquitin-like, containing PHD and RING finger domains 1) [Sharif et al., 2007] and catalyzes reestablishment of DNA methylation at the newly synthesized DNA strand [Leonhardt et al., 1992]. In comparison DNMT3A and 3B perform the *de novo* methylation, where new methyl moieties are introduced into previously unmethylated parts of DNA in a process essential for development.

2.4.2 DNA demethylation

While DNA methylation is closely related to transcriptional repression, the pivotal function of DNA demethylation is the activation of gene transcription.

While a passive DNA demethylation pathway, including loss of methylated cytosine during successive rounds of replication under the repression of the maintenance DNA methyltransferase DNMT1 (Figure 2-6 black arrow; [Wu and Zhang, 2010]) is known for quite a while, recent findings are pointing to active DNA demethylation pathway in mammals. Active demethylation was first identified in plants, where methylated cytosines are removed by a glycosylase, involving the BER pathway, leading to an abasic site. These sites then can be further processed by other enzymes finally producing unmodified cytosines [Gehring et al., 2009]. However, in mammals no such glycosylases, which could directly act on 5mC, has been identified. Moreover the methyl group cannot be removed directly due to high energetic barriers suggesting a more complex demethylation pathway [Kohli and Zhang, 2013]. In fact there are several possible pathways leading to unmodified cytosine referring to a process that includes stepwise enzymatic removal or modification of the methyl group of methylated cytosine.

2.4.2.1 Gadd45-mediated DNA demethylation

DNA demethylation may take place in a Gadd45 (Growth arrest and DNA damage-inducible protein 45) dependent manner (Figure 2-6 red arrow). Since Gadd45 has no catalytic activity itself, it is supposed that it acts as scaffold protein for DNA demethylation by NER or BER. The following mechanism is anticipated: a given gene promoter where histone H3 is trimethylated at lysine 4 (an active transcription mark) is recognized by Ing1 (Inhibitor of growth protein 1), which serves as a cofactor for the recruitment of Gadd45 to the promoter. Gadd45 itself recruits repair factors of the BER or NER mechanism that are in turn capable of replacing 5mC leading to DNA demethylation [Schaefer et al., 2013, Schomacher, 2013].

2.4.2.2 TET mediated demethylation

TET (Ten-eleven translocation) proteins are capable of oxidizing 5-Methylcytosine (5mC) to 5-Hydroxymethylcytosine (5hmC) and further to 5-Formylcytosine (5fC) and 5-Carboxylcytosine (5caC) (Figure 2-6 green arrows; [Ito et al., 2011, He et al., 2011]).

Elevated levels of 5hmC concomitant to reduced 5mC levels are found at promoter regions of phenobarbital-induced genes also showing increased levels of H3K4me2, a histone modification associated with gene activation. This indicates that DNA demethylation by 5mc oxidation is an important step in the reestablishment of transcription in previously silenced genes [Thomson et al., 2012].

Starting with 5hmC or 5fC and 5caC respectively, different pathways can further lead to demethylated cytosine, which will be discussed subsequently.

Activity of DNMT1 on 5hmC is reduced 12- to 50-fold in vitro [Hashimoto et al., 2012a, Valinluck and Sowers, 2007] suggesting that the presence of 5hmC can block methylation maintenance activity leading to a replication-dependent depletion of oxidized 5mC to unmodified cytosine (Figure 2-6 blue arrow) in a process coupling active modification of TET proteins to passive demethylation processes [Kohli and Zhang, 2013]. Other studies implicate DNMT3A and DNMT3B as well as DNMT1 to be involved in DNA demethylation processes actively converting 5hmC directly to cytosine in vitro (Figure 2-6 grey arrow) [Chen et al., 2012, Liutkeviciute et al., 2009]). It is reported that DNMT3A and DNMT3B use the same catalytic site for methylation and dehydroxymethylation and that the redox state of the enzymes determines whether they function as DNA methyltransferase or DNA dehydroxymethylase [Chen et al., 2012]. However if this reaction also takes place in cells has to be elucidated.

DNA demethylation can also be achieved by a mechanism including DNA repair enzymes of the BER pathway. Increasing evidence suggest the involvement of thymine DNA glycosylase (TDG) in this process [Dalton and Bellacosa, 2012] since it is known that TDG can directly excise 5fC and 5caC from DNA [He et al., 2011, Zhang et al., 2012]. Therefore, iterative oxidation of 5mC by TET enzymes together with TDG acting on 5fC and 5caC, as part of the BER pathway, demonstrates a plausible pathway of active DNA demethylation (Figure 2-6 dashed purple arrow).

Furthermore the AID (activation-induced cytidine deaminase) and APOBEC (apolipoprotein B mRNA editing enzyme, catalytic polypeptide-like) family enzymes have been implicated in DNA demethylation [Bhutani et al., 2010, Guo et al., 2011, Popp et al., 2010]. It is reported that they are capable of deaminating 5mC as well as 5hmC to uracils (Thymine and 5-Hydroxymethyluracil (5hmU)) (Figure 2-6 orange arrows), which can be further processed to unmodified cytosines by TDG and BER or mismatch repair. Similar is also shown for the methyl-CpG binding domain protein 4 (MBD4) which can remove thymine as well as 5hmU from DNA [Hashimoto et al., 2012b], while there is no evidence that this enzyme is able to excises 5fC or 5caC (Figure 2-6 purple arrow).

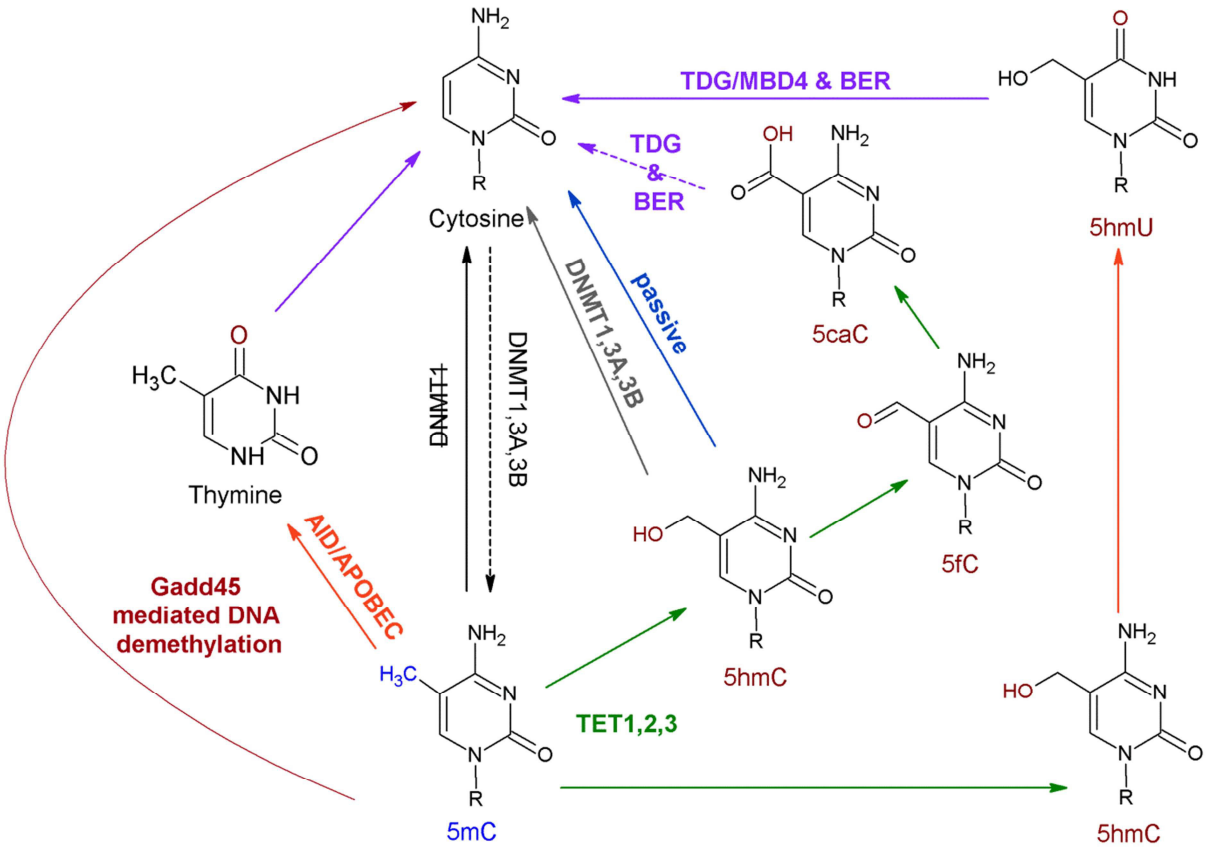

Figure 2-6: DNA demethylation pathways. The addition of a methyl group to cytosine is catalyzed by DNMT1, DNMT3A or DNMT3B (dashed black arrow) and can be iteratively oxidized to 5hmC, 5fC and 5caC by TET enzymes (green arrows). Further processing by the glycosylase activity of TDG leads to unmodified cytosine via the BER pathway (dashed purple arrows). 5mC as well as 5hmC might also be deaminated by AID/APOBEC (orange arrows) serving as a target for glycosylation by TDG or MBD4 (purple arrows), or 5hmC can be converted to unmodified cytosine by the activity of DNMT1, 3A or 3B (grey arrow). Alternatively 5mC can be converted to cytosine in a Gadd45 mediated manner including the BER or NER pathways (red arrow). Also passive mechanisms are possible, including demethylation of 5hmC (blue arrow) or 5mC in the absence of maintenance DNA methyltransferase activity (black arrow). (Figure based on [Bhutani et al., 2011])

2.5 5-Hydroxymethylation and further oxidative derivatives

The epigenetic modification 5hmC was discovered already 60 years ago by Wyatt and Cohen [Wyatt and Cohen, 1953]. But it was not until the discovery of TET enzymes converting 5mC to 5hmC and the therefore associated process of DNA demethylation that it gained in importance. 5hmC is detectable in all kind of human cells and tissues, with highest detectable levels in the brain, with 0.4 to 0.7 % of all cytosine bases converted into 5hmC [Globisch et al., 2010] and lowest levels with 0.009 % in human embryonic kidney cells (HEK-293) [Ito et al., 2011]. In comparison 5fC as well as 5caC levels are up to two orders of magnitude less abundant or even not detectable in some tissue.

In addition of being an intermediate in DNA demethylation [Wu and Zhang, 2011] conversion of 5mC to 5hmC was also found to change the binding affinities of several chromatin associated proteins to DNA and therefore could serve as an epigenetic binding platform. Substantiating a specific function of 5hmC and its derivatives, Spruijt and colleagues [Spruijt et al., 2013] identified specific readers for 5hmC in mouse embryonic stem cells (mESC), neuronal progenitor cells (NPC), and adult mouse brain tissue and compared those to readers

of 5mC, 5caC and 5fC respectively. It turned out that readers are only partially overlapping between the different modifications and that some are supremely specific. Additionally, different readers were identified for the same modification in different cell types indicating a dynamic nature of 5mC and its derivatives during development. Among others, especially DNA repair proteins, like TDG, Bloom and p53 were recruited to modified cytosines (most pronounced for 5fC), linking the DNA damage response to active DNA demethylation. Interestingly more protein readers bound 5hmC compared to 5mC in the adult brain, which was in contrast to ESCs and NPCs where more 5mC readers were found. This may indicate a particular role for 5hmC in the brain. Extended studies by the work of Iurlaro and colleagues [Iurlaro et al., 2013] showed that in mouse ESCs only few proteins specifically bound 5hmC while most of them were specific for 5fC including transcriptional regulators, DNA repair factors and chromatin regulators. Especially binding of the NuRD complex attracted the author's interest indicating that 5fC is more likely a repressive cytosine modification. In summary they conclude that 5fC may be an intermediate in DNA demethylation as well as an epigenetic signal itself. Similarly, Yildirim and co-workers [Yildirim et al., 2011] showed that the antagonistic chromatin regulators MBD3/NuRD and Brg1 (Brahma-Related Gene 1), which are important for expression or repression of certain genes in ESCs, specifically bind 5hmC but not 5mC.

Taken together, these findings suggest 5hmC and its derivatives being not only an intermediate in DNA demethylation but rather an epigenetic modification with specific functions that are mediated by the binding of proteins that themselves are able to change chromatin structure and modify genome function.

2.6 The TET Methylcytosine Dioxygenases

The family of TET proteins comprises three members, namely TET1, TET2 and TET3. They are named after the ten-eleven translocation (t(10;11)(q22;q23)) known for acute myeloid and lymphocytic leukemia, which rearranges the MLL1 (mixed-lineage leukaemia 1) gene on chromosome 10 and the TET1 gene on chromosome 11 [Lorsbach et al., 2003]. All three family members are Fe^{2+}- and 2-oxoglutarate-dependent dioxygenases able to oxidize 5mC to 5hmC, 5fC and 5caC [Tahiliani et al., 2009, Ito et al., 2011, He et al., 2011]. They were discovered in a computational search for potential mammalian enzymes that are able to convert 5mC to 5hmC. The search was based on finding homologs of J-binding protein 1 (JBP1) and JBP2 from Trypanosoma brucei, which are known to convert thymine to 5hmU. Chemical similarity of thymine conversion to 5hmU and 5mC oxidation led to the assumption that TET proteins are important factors in DNA demethylation [Tahiliani et al., 2009].

The C-terminal catalytic domain, found in all three TET enzymes (Figure 2-7), is needed for 5mC oxidation [He et al., 2011]. It comprises a double-stranded β-helix (DSBH) domain, characteristic for Fe^{2+}- and 2-oxoglutarate-dependent dioxygenases, including important metal-binding residues [Tan and Shi, 2012]. Furthermore, it contains a cys-rich insert in the n-terminal region of the DSBH domain. All metazoan TET enzymes also contain a low-complexity insert in the DSBH domain with varying length, which might be important for the interaction with other proteins [Pastor et al., 2013]. TET1 as well as TET3 contain a CXXC zincfinger domain at their N-terminus, which can mediate interaction with CpGs [Deaton and Bird, 2011]. For TET2 the exon coding for the CXXC domain probably underwent chromosomal inversion during evolution and became an independent gene coding for IDAX

(inhibition of the Dvl and axin complex; also known as CXXC4) [Ko et al., 2013]. It is reported, that IDAX plays an important role in the regulation of TET2 protein expression [Ko et al., 2013]. Furthermore, TET2 needs IDAX for DNA binding, and TET2 binding to DNA is dependent on whether IDAX binds to the particular site. Furthermore it is suggested, that TET2, like other TET proteins, may also bind DNA by the cysteine-rich region of its catalytic domain [Pastor et al., 2013].

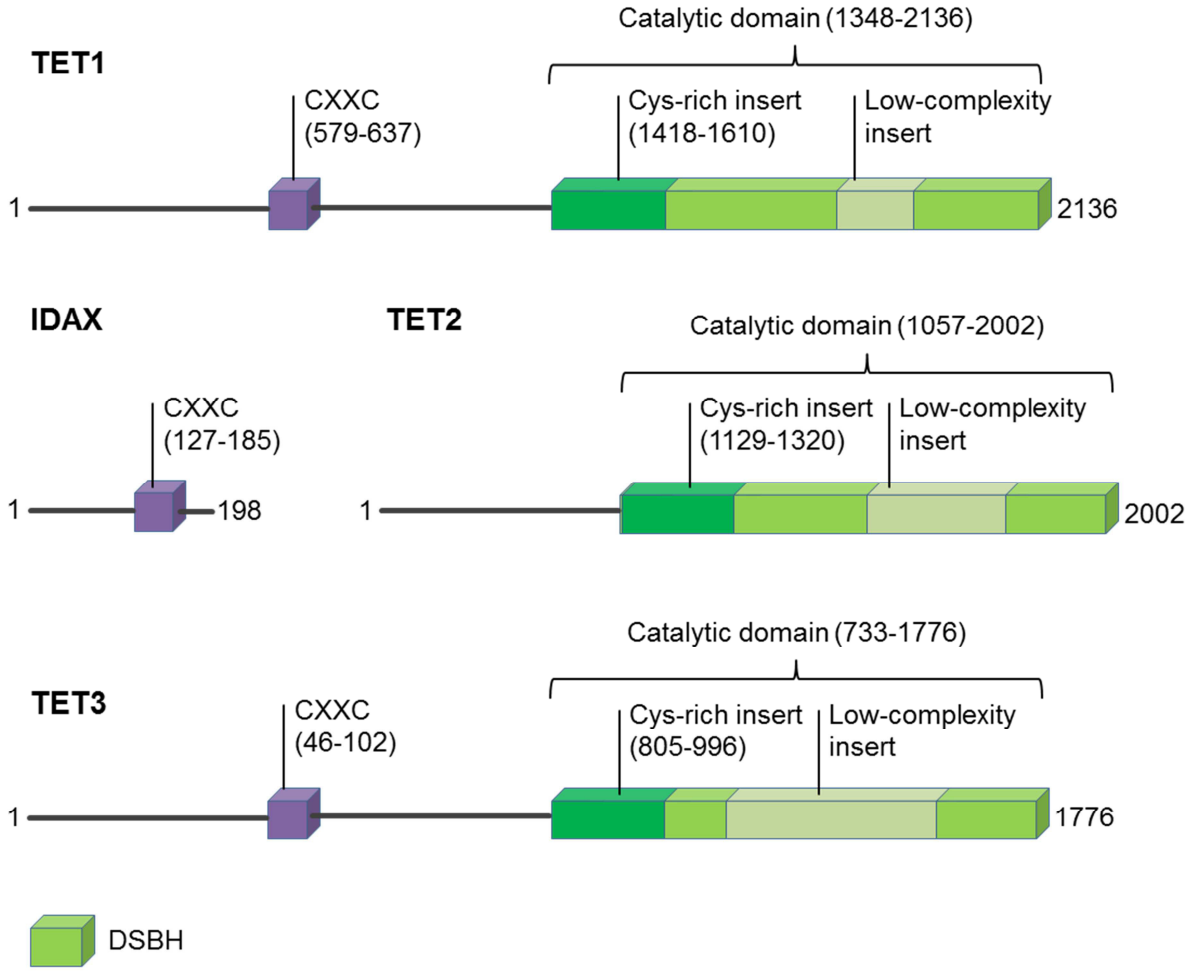

Figure 2-7: The TET enzyme family members. TET proteins comprise a double-stranded β-helix (DSBH) domain with a cys-rich insert in the n-terminal region of the DSBH domain and a low-complexity insert in the DSBH domain with varying length. TET1 and TET3 contain a CXXC zincfinger domain at their N-terminus, which can mediate interaction with CpGs, while TET2 might bind DNA via IDAX, which probably underwent chromosomal inversion during evolution and became an independent gene. The numbers of amino acids (corresponding to the human protein) are indicated. (Figure based on [Pastor et al., 2013])

For the oxidation process, which can be carried out by either full length TET protein or catalytic domain alone, the two cofactors 2-oxoglutarate and Fe^{2+} are needed [Tahiliani et al., 2009]. Recently Hu and co-workers [Hu et al., 2013] reported on TET2 structure and catalytic activity showing that DNA is located above the DSBH domain with a 5mC flipped out and inserted into the catalytic cavity. Thereby TET2 specifically recognizes 5mC in a CpG context, with weak activity on CpG-flanking regions. Furthermore DNA interaction is achieved via two

loops harbored by the Cys-rich insert and two of three zinc fingers bring the Cys-rich and DSBH domains together to stabilize areas that are important for catalysis. According to its function, the architecture of the catalytic domain allows TET proteins to accommodate also other oxidative cytosine derivatives than 5mC.

TET enzymes carry out different biological tasks. Deplus and colleagues [Deplus et al., 2013] for example report on transcriptional activation, initiated by TET2/3, interacting with OGT (O-GlcNAc transferase). OGT then promotes GlcNAcylation on HCF1 (Host Cell Factor 1), which itself is important for the formation of the SET1/COMPASS complex, an event necessary for histone H3K4me3 and subsequent transcriptional activation.

Furthermore, there is increasing evidence for TET protein function in mammalian embryonic development, where directly after fertilization the male pronucleus loses almost all its methylation. It is known that TET3 is highly abundant in the male pronucleus, while TET1 and TET2 are expressed to a lesser extent, and it is reported that TET3 is the dioxygenase catalyzing 5mC to 5hmC conversion in the paternal pronucleus [Iqbal et al., 2011]. Although the paternal pronucleus underlies this extensive demethylation, it is totally absent in the maternal pronucleus, where protein PGC7 protects maternal 5mC from demethylation mediated by TET3 [Nakamura et al., 2012]. However, why demethylation does not take place in the maternal pronucleus is currently unknown. Later in development, the group of primordial germ cells (PGCs) undergoes another demethylation process which comprises global erasure of 5mC or rather conversion to 5hmC. As in the zygote, this demethylation process takes place very quickly implicating active DNA demethylation while it is not mediated by TET3 but by TET1 and TET2 [Hackett et al., 2013]. 5mC derivatives, occurring by this demethylation process, are known to be removed by passive dilution in a replication-dependent manner [Inoue et al., 2011]. Additionally, it is known that especially TET1, and to a lesser extend TET2 are expressed in embryonic stem cells and it is suggested that TET1/2 are part of the regulatory system controlling pluripotency by regulating the expression of key ESC pluripotency factors [Ito et al., 2010, Koh et al., 2011].

Besides their function in zygotes, PGCs and ESCs, TET proteins are also involved in the active demethylation in somatic cells. For example Huang and co-workers [Huang et al., 2013] suggest a possible function of TET1 for cell proliferation that is dependent on the regulation of cyclin D1 transcription in NIH/3T3 cells.

Since aberrant DNA methylation is involved in cancer development, the question arises whether also demethylation pathways cause oncogenesis and actually a significant function in oncogenesis is ascribed to TET enzymes. The best studied member of the TET family implied in cancer progression, TET2, is known to be one of the most frequently mutated genes in myeloid malignancies and may be defined as a tumor-suppressor gene in this context [Langemeijer et al., 2009]. Furthermore, due to its fusion to MLL in patients with acute leukaemia, TET1 may also be associated to cancer, while a correlation of TET3 to cancer is not known so far. Moreover TET proteins seem to be involved in solid tumors like colorectal cancers [Kudo et al., 2012].

TET protein activity includes a broad spectrum of different functions. However the exact pathways, in which those proteins are involved, have to be elucidated.

2.7 DNA methylation changes after irradiation

Increasing evidence suggest that epigenetic mechanisms are involved in the DNA damage response after ionizing irradiation. Previous work reported that IR can induce epigenetic changes, including changes in DNA methylation. However, the results are not consistent.

For example, global CpG hypermethylation after 0.5 Gy low LET irradiation and global CpG hypomethylation after 1 Gy high LET irradiation was observed [Aypar et al., 2011]. In contrast global hypomethylation after low LET X-rays and hypermethylation after high LET iron ion irradiations were observed in another study of the same group [Goetz et al., 2011]. However both observed that neither irradiation with low LET X-rays nor treatment with high LET iron ions led to changes of promoter methylation of genes known to be differentially expressed or methylated in cancer, like of NF-κB (nuclear factor-kappa B), TSLC1 (tumor suppressor in lung cancer 1) and CDH1 (cadherin 1) [Aypar et al., 2011] or p16 (cyclin-dependent kinase inhibitor 2A) and MGMT (O6-methylguanine-DNA methyltransferase) [Goetz et al., 2011]. However, in these studies DNA methylation levels were measured several population doublings after exposure to IR. Whether or not DNA methylation changes may take place also at short times after exposure remained open.

In a study conducted by Kuhmann and co-workers [Kuhmann et al., 2011] instead, global DNA methylation was not altered in cells where IR was given in fractions (2 Gy per fraction; total dose: 10 and 20 Gy) and which were harvested 48 and 72 hours as well as 14 to 24 days after treatment. However, they found two genes, (TRAPPC9 (Traficking protein particle complex 9) and FOXC1 (Forkhead box C1)), significantly hypomethylated upon irradiation. Both demonstrated a reduction of DNA methylation when cells were harvested 48 or 72 hours after irradiation and a further decrease after a recovery period of 14 to 24 days.

Recently, Antwih and colleagues [Antwih et al., 2013] analyzed DNA methylation changes over time at more than 450 000 loci in response to X-rays. In this study, time points from 1 to 72 hours were investigated. Analyzing global DNA methylation over time, they did not find a consistent pattern of hypermethylaion or hypomethylation, while demonstrating that treatment with IR predominantly leads to changes in DNA methylation in pathways involved in cell cycle control, DNA repair, and apoptosis. These DNA methylation changes of genes directly involved in the radiation response also resulted in changes in gene expression.

Another study conducted by Chaudhry and colleagues [Chaudhry and Omaruddin, 2012] showed a decrease in DNA methylation in two different cell lines, however changes in DNA methylation were not very pronounced. In this study also DNMT expression was analyzed demonstrating no significant changes in DNMT3A/B and DNMT1 expression until the 24 hour time point. Similar results were obtained for TET1 expression analysis.

Besides the investigation of DNA methylation after IR, also investigations using UV laser irradiation were conducted. Namely, it is reported that DNMT1 is recruited to DNA damage sites after UV laser irradiation in a very short time frame [Mortusewicz et al., 2005]. The recruitment is mediated by PCNA and the presence of DNMT1 at damage sites suggests that it maintains DNA methylation patterns during the repair process, similar to its function in DNA replication. This study is extended by Ha and co-workers [Ha et al., 2011] who showed that DNMT1 also interacts with other components of the repair machinery. Furthermore, he suggests that DNMT1 may take over a function that is independent on its DNA methylation activity.

2.8 DNA methylation changes after DSB repair

Besides the studies investigating methylation changes after treatment with IR, there are also studies connecting methylation changes to DSB induction. For example, Cuozzo and colleagues [Cuozzo et al., 2007] demonstrated that single DSBs, induced in close vicinity to the respective downstream gene, which are repaired by the HR repair mechanism (only 2 – 4 % of the cells) are marked in half of the repaired molecules by *de novo* cytosine methylation flanking the cut. This process is dependent on DNMT1. In consequence they observed that the gene near the DSB was silenced due to methylation. In the other cases DNA was hypomethylated leading to the expression of the adjacent gene. This study was extended by O'Hagan and co-workers [O'Hagan et al., 2008]. They also used an experimental model in which induction of a single DSB in an exogenous promoter construct, repaired by NHEJ, leads to silencing of the downstream gene in 0.9 % of the cases. They suggest that seeding of methylation takes place by the action of DNMT3B and that methylation is expanded with passage (from ~4 methylated CpGs to 10-13 methylated CpGs in 30 passages) in a process for which DNMT1 is needed. These studies represent a possible link between DSB induction, its repair by HR/NHEJ, DNA methylation changes and the silencing of downstream genes. However, it has to be mentioned that this was observed only in a very small part of the cells. Furthermore these observations were made several population doublings after the onset of repair and therefore do not exclude a replication-dependent mechanism.

2.9 Aim of the work

Understanding cellular processes in response to IR is important to improve radiotherapy and to determine risks to human health after accidental radiation exposure. Furthermore, IR poses a risk to astronauts during long term exposure in space.

Induced by IR the DNA damage response is activated. Recently it became obvious that besides the classical response to radiation also epigenetic changes take place including changes in DNA methylation. Most of the studies investigating DNA methylation changes after IR or DSB induction however showed inconsistent results and were performed several population doublings after IR/DSB induction.

Only few recent studies report on DNA methylation changes at short times after IR. However those studies also did not show a clear trend for DNA hyper- or hypomethylation. There is no indication that DNMT activity is increased after IR and therefore rather DNA demethylation might take place at short time points after IR. In this process the involvement of DNMTs is unlikely since DNA demethylation involving DNMTs proceeds too slowly. Additionally, in the here presented work a clear decrease in DNA methylation levels was observed which led to the aim to investigate DNA demethylation processes. Instead of a contribution of DNMTs, in this work it is hypothesized that IR may induce changes in DNA methylation levels by altering (transiently or permanently) the levels of the enzymatic activities regulating such processes.

Particularly the oxidation activity of TET enzymes, a group of dioxygenases, able to convert 5mC to 5hmC and further to 5fC and 5caC might alter DNA methylation. Therefore, it was investigated, whether 5hmC as an intermediate in DNA demethylation is involved in the response to IR induced DSBs. Additionally TET involvement in DNA repair processes has not yet been addressed, which was a motive to focus on a possible TET2-driven demethylation effect during DSB repair.

3 Methods

3.1 Cell culture, inhibitor treatment, transfection and freezing cells

All cell lines used were cultivated in an incubator at 37 °C, 5 % CO_2 and a relative humidity of 95 %. Cultivation was performed in 25 cm^2 or 75 cm^2 cell culture flasks (BD Bioscience, USA). Cells were passaged every three to four days by incubating the cells with a Trypsin-EDTA-Solution (PAN Biotech) at 37 °C. Additional separation was performed by pipetting cells up and down. Trypsin was then inactivated by adding at least three trypsin volumes serum-containing medium.

To determine the number of cells, an electronic cell counter (Z2 Coulter Counter, Beckmann Coulter, Krefeld) was used. After counting, the appropriate number of cells was seeded into cell culture flasks for further cultivation or seeded in Petri dishes (Thermo Fisher Scientific Inc., Langenselbold, Germany) or on cover slips, depending on the experiment. According to the growth rate, different cell lines were seeded at different times and different densities depending on the type of experiment.

For inhibiting DNA-dependent protein kinase (DNA-PK) activity, cells were incubated as described and the specific inhibitor NU7026 was added [Peddi et al., 2010] to a final concentration of 10 μM. Cells were pre-incubated for one hour at least in presence of the inhibitor, before starting the experiments.

Transfection of mammalian cells with plasmid DNA was performed using jetPRIME (Polyplus transfection) according to manufacturer's instructions, with minor changes (half of the suggested DNA amount was used). Transfected cells were analyzed after 24 or 48 hours.

For long-term storage, cells were frozen in liquid nitrogen. Cells were harvested as described above and centrifuged at 110 × g for 10 minutes at 4 °C. After centrifugation, the supernatant was discarded and the cells were resuspended in medium containing 10 % Dimethylsulfoxid (DMSO) or 10 % of glycerin (depending on the cell line). Two million cells were transferred into cryotubes (Greiner Bio-One, Frickenhausen, Germany). Cryotubes were then placed into a container filled with isopropyl alcohol (Nalgene Cryo 1 °C Freezing Container) and cooled down to -80 °C with a mean decrease in temperature of 1 °C/minute. After 24 hours the cryotubes were transferred into a nitrogen tank with a temperature of -196 °C.

To thaw the cells, cryotubes were taken out of the nitrogen tank and thawed at 37 °C in a water bath. Afterwards, the cells were transferred into a cell culture flask (75 cm^2 or 25 cm^2) containing preheated medium. After 24 hours, medium was exchanged to remove non-attached cells and residual DMSO.

All used cells were examined for mycoplasma at regular intervals using the PCR Mycoplasma Test Kit (AppliChem, Darmstadt).

3.2 Expression of recombinant proteins in mammalian cells

3.2.1 The plasmid pCAG-GFP-TEV-CD2

The pCAG-GFP-TEV-CD2 plasmid used in this thesis was kindly provided by Prof. Dr. H. Leonhardt (LMU Munich). It comprises the cys-rich and catalytic domain of TET2 fused to the C-terminal of the pCAG-GFP-TEV vector (Figure 3-1).

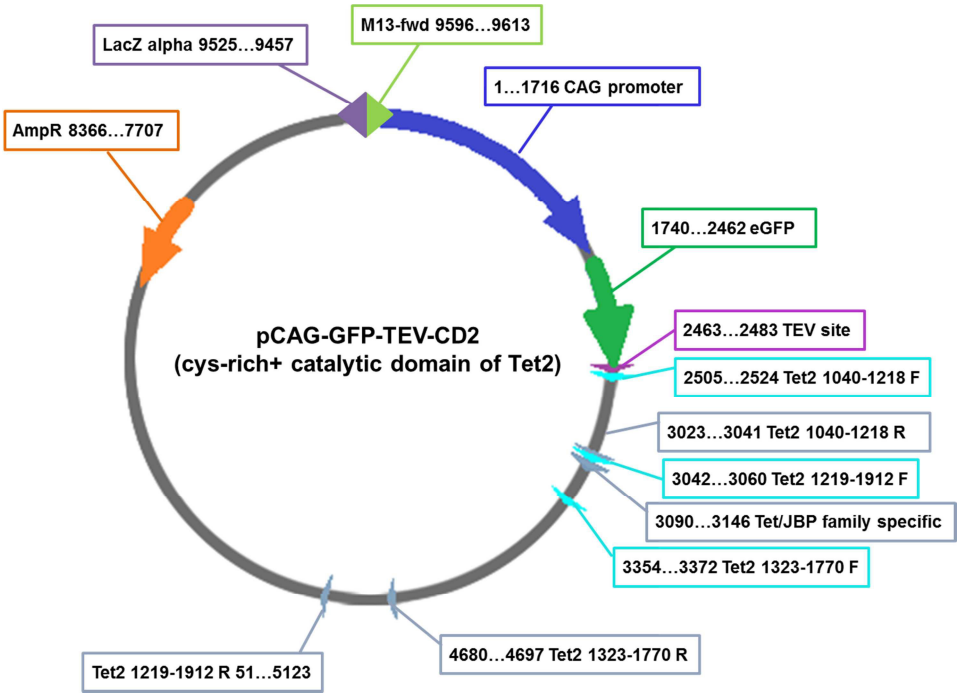

Figure 3-1: The pCAG-GFP-TEV-CD2 expression plasmid

3.2.2 Generation of competent cells

To produce competent cells from *Escherichia coli* (strain DH5α), bacterial cells were grown in LB medium at 37 °C overnight, under agitation. The next day, bacteria were transferred to preheated LB medium and agitated at 37 °C until an OD_{600} of 0.6 was reached. After centrifugation at 4000 RPM for 20 minutes at 4 °C the supernatant was discarded and the cells were resuspended in 0.1 M $CaCl_2$. Then, cells were incubated on ice for 30 minutes and again centrifuged at 4000 RPM for 20 minutes at 4 °C. The supernatant was discarded and the pellet was resuspended in 0.05 M $CaCl_2$/15 % glycerol. Afterwards, competent cells were frozen immediately in aliquots and kept at -80 °C.

3.2.3 Transformation of E. coli and plasmid purification

Amplification of the pCAG-GFP-TEV-CD2 plasmid was performed in DH5α *E. coli* cells. For transformation of the plasmid, bacteria were thawed and kept on ice while incubating together with 400 ng of plasmid DNA for 10 minutes. Then, cells were incubated for one minute at 42 °C in a water bath to make the membrane permeable for the plasmid. Immediately afterwards, cells were cooled down on ice for at least two minutes to allow plasmid uptake. Finally, the bacteria were plated on agar plates supplemented with 100 μg/ml ampicillin, and incubated at 37 °C overnight. As a negative control, non-transformed DH5α were used. The next day, cells from single colonies were used to inoculate LB medium supplemented with 100 μg/ml ampicillin and cells were grown at 37 °C overnight, under agitation. The plasmid was extracted and purified using the Plasmid Maxi KIT (25) (QIAGEN) according to manufacturer's instructions.

3.2.4 Digestion of DNA with restriction endonucleases

To validate plasmid pCAG-GFP-TEV-CD2, restriction endonuclease analysis was performed. Plasmid DNA was digested with restriction endonucleases according to manufacturer's

instructions resulting in plasmid fragments of a given length. In this case, digestion of the plasmid with *EcoRI* resulted in 2 pieces with the sizes of 3431 base pairs (bp) and 6231 bp, respectively. To determine the size of the cut plasmid DNA, agarose gel electrophoresis was used. For the analysis, a gel electrophoresis chamber (Bio-Rad) and a 1 % agarose gel with EtBr were used. The samples were diluted with 6 × loading dye (Fermentas) and applied to the gel. As a control for the size of the plasmid fragments, GeneRuler 1 kb DNA Ladder (Fermentas) was applied to the gel. The gel was run at a constant voltage of 100 V for 40 minutes.

3.3 Irradiation of cells

3.3.1 Irradiation with X-rays

Cells were irradiated with doses of 0.5, 2 and 10 Gy at a voltage of 250 kV and a current of 16 mA using the IV320-13 X-ray tube (Seifert, Germany). Dosimetry was performed using a SN4 Dosimeter (PTW Freiburg, Germany). During irradiation, the cells were kept in regular cultivation medium. Following irradiation and a given incubation time at 37 °C, cells were fixed for immunostaining or flow cytometry analysis. Additionally, whole protein lysates were prepared or genomic DNA was isolated.

3.3.2 Irradiation with heavy ions at the linear accelerator UNILAC

Irradiation at the linear accelerator UNILAC was performed using gold or uranium ions shown in Table 3-1. For irradiation, special sample holders (Figure 3-2 A) allowing perpendicular or low-angle irradiation were used. In this work only low-angle irradiation was performed. During the irradiation, up to a maximum of 3 % of the cells were not exposed to radiation, as determined by empirical assessments. After irradiation cells were fixed for immunostaining.

Ion	Accelerator	Energy [MeV/u]	LET [keV/μm]	Fluence [particles/cm^2]	Dose [Gy]
^{197}Au	UNILAC	4.6	12815	3.0 x 10^6	61.6
^{92}U	UNILAC	4.7	15000	3.0 x 10^6	72.1
^{56}Fe	SIS	1000	148	4.0 x 10^6	0.8

Table 3-1: Irradiation parameters for different ions used at the linear accelerator UNILAC and the heavy ion synchrotron SIS.

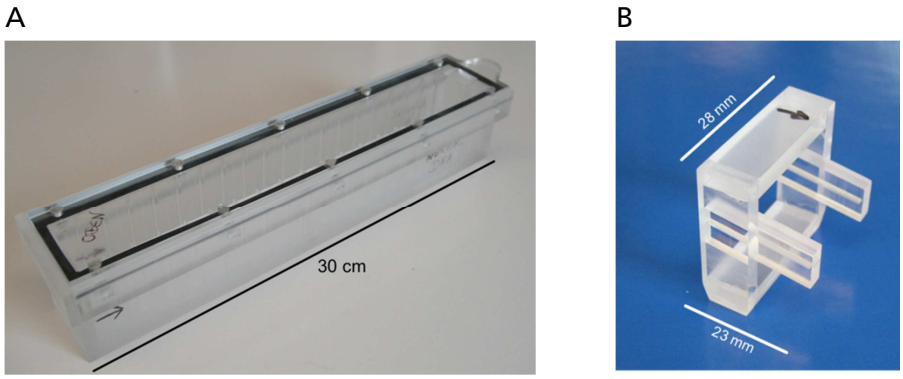

Figure 3-2: Sample holder and devices for low-angle irradiation used for the irradiation at the linear accelerator UNILAC. Up to 10 adapters for low-angle irradiation (B) can be placed into one special sample holder (A). Sample holders are placed into the irradiation unit to allow automated irradiation.

For low-angle irradiation, all cells were seeded on sterile cover slips (side length: 24 mm), set into a special adapter (Figure 3-2 B) and placed into a sample holder (Figure 3-2 A) filled with culture medium without additives. These adapters allow the irradiation of the cell monolayer at an angle of 15°. Proteins involved in DNA repair processes accumulate at the ion track and can therefore be visualized by appropriate microscopy methods [Jakob et al., 2003].

For the irradiation process, a computer-controlled robotic arm was used. It pulls each petri dish or adapter exposing them to the beam successively and putting them back to their original position in the sample holder after a certain dose was applied to the sample.

3.3.3 Irradiation at the heavy ion synchrotron SIS

Low-angle irradiation was performed at the synchrotron SIS employing iron ions (Table 3-1). Cells were seeded on sterile cover slips (side length: 24 mm) placed in a petri dish. Petri dishes were then stacked atop each other in a sample holder, which was slightly tilted (Figure 3-3). High-energy particle beam was employed, so that the target could be fully traversed.

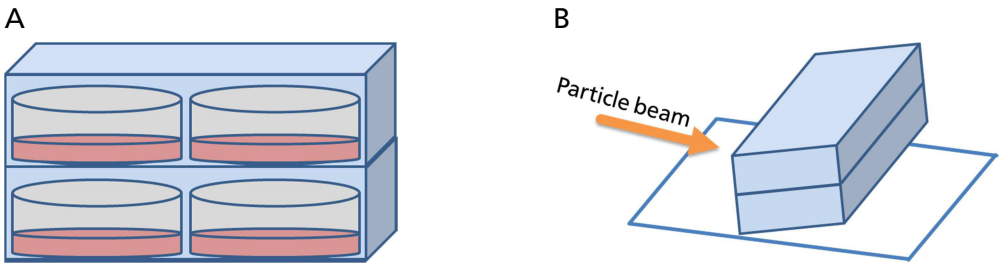

Figure 3-3: Irradiation setup used for the irradiation at the heavy ion synchrotron SIS. (A) Up to 4 petri dishes can be placed in one sample holder. (B) Samples in the sample holder are irradiated under a low angle.

3.3.4 Irradiation with UV-Laser and assessment of recruitment kinetics

For irradiation with UV-Laser, a Leica Microdissection System AS LMD equipped with a 337 nm Nitrogen Laser was used. During irradiation cells were kept at 37 °C in medium containing 10 mM Hepes to stabilize the pH. After irradiation, a time-lapse series was performed capturing 300 pictures in a time frame of two minutes using an Andor EM-CCD

camera (DU-888E-C00-#BV). For long-term observations, one picture was taken every 30 seconds for two hours in total.

For evaluation of recruitment kinetics, a time-lapse series was opened in ImageJ (National Institutes of Health) and unspecific background signal was subtracted using the plugin "BG Subtraction from ROI" (developed by Michael Cammer; Skirball Institute of Biomolecular Medicine). Movement of the cell was corrected using the plugin "StackReg". Next, the fluorescence intensity of the nucleus and the irradiated area were determined and fluorescence intensities of the irradiated areas were divided by the fluorescence intensity of the whole nucleus for each picture. For long-term observations, these values were normalized setting the first measured value to one. All the other values were converted relative to this value and were plotted as a function of time.

3.4 Cell fixation and immunostaining

Cells were fixed before immunostaining. Appropriate fixation methods were chosen depending on the employed antibodies or the experimental settings.

3.4.1 Fixation with Paraformaldehyde

All steps were performed at room temperature (RT). For fixation, medium was removed and cells were washed with PBS (calcium- and magnesium-free phosphate buffered saline (PBS) was used, unless otherwise stated). Afterwards, cells were fixed with 2 % paraformaldehyde in PBS for 15 minutes and permeabilized in 0.5 % Triton X-100 in PBS for 10 minutes. After washing the cells twice with PBS for three minutes, unspecific binding of the antibodies was blocked by incubating the cells with 0.5 % BSA (bovine serum albumin) in PBS for 20 minutes or at 4 °C overnight. Under the aforementioned conditions, cells can be stored for several weeks.

3.4.2 Cell fixation with extraction of soluble proteins (Fixation with Hepes)

In some cases, the removal of unbound proteins from the nucleus can improve the detection of target proteins (e.g. binding to damage sites). Therefore, an additional extraction step was used before fixation. Namely, medium was removed and cells were washed with PBS. Cells were then incubated on ice for 10 minutes, extracting soluble proteins using Hepes extraction buffer. Afterwards, cells were fixed in paraformaldehyde at RT (see 3.4.1).

3.4.3 Cell fixation with additional DNA denaturation

Immunofluorescent staining of DNA methylation and hydroxymethylation requires DNA denaturation. The procedure was performed as described in [Ito et al., 2010], with minor changes. All steps were performed at RT, unless otherwise stated. The medium was removed and cells were washed with PBS. Cells were then fixed with 4 % paraformaldehyde in PBS for 15 minutes and permeabilized in 0.5 % Triton X-100 in PBS for 10 minutes. Afterwards, the cells were incubated in 2 N HCl for 15 minutes to favour antibody accessibility to DNA. HCl was neutralized by incubating the cells in 100 mM Tris-HCl (pH 8) for 10 minutes. After washing three times with PBS for three minutes, unspecific binding of the antibodies was blocked by incubating the cells in 0.5 % BSA in PBS for 20 minutes or at 4 °C overnight.

3.4.4 Immunostaining of fixed cells

After cell fixation using the aforementioned fixation protocols, immunostaining was performed as follows: BSA/PBS solution was removed and primary antibody solution was added. The primary antibody was diluted in PBS supplemented with 0.5 % BSA (dilutions of primary antibodies used for immunofluorescence are listed in Table 3-2). Cells were incubated with primary antibody in a humidified chamber for one hour at RT or overnight at 4 °C. For each sample 50 μl of antibody solution was used. In order to spread the antibody solution, the sample was covered with a thin mylar foil during the incubation. Afterwards, the cells were washed three times for five minutes with PBS. In a second step, the cells were incubated with the secondary antibody in 0.5 % BSA for 45 minutes at RT (dilutions of secondary antibodies used for immunofluorescence are listed in Table 3-3). The latter and the following steps were performed in the dark to prevent bleaching of the fluorescently labeled secondary antibodies. Next, the samples were washed twice for five minutes with PBS and DNA was stained incubating the cells with 1 µg/ml DAPI (4′,6-Diamidin-2-phenylindol) solution for 20 minutes. After rinsing the cells with water, cells were mounted in Vectashield Mounting Medium (Vector Laboratories, Canada). The coverslips were sealed with nail polish to prevent the samples from drying out and were kept at 4 °C in the dark until utilization.

Antigen	Antibody	Source of supply	Species	Concentration [mg/ml]	Dilution
5-Hydroxy-methylcytosine	5-Hydroxy-methylcytosine (5-hmC) antibody (pAb)	Active Motif	Rabbit polyclonal		1:250 – 1:300
γH2AX	γH2AX (Ser139) clone JBW301	Millipore	Mouse monoclonal	1	1:500
γH2AX	Alexa Fluor 488 anti-γH2AX (Ser139)	Biozol	Mouse monoclonal	0.025	1:50
Nucleolin	C23 (H-250): sc-13057	Santa Cruz	Rabbit polyclonal	0.2	1:50 – 1:200
Rad51	Rad 51 (ab213)	Abcam	Mouse monoclonal	1	1:100
TET2	TET2 (ab94580)	Abcam	Rabbit polyclonal	1	1:100
TET3	TET3[C3], C-term	Genetex	Rabbit polyclonal	1	1:100

Table 3-2: Primary antibodies used for immunofluorescence.

Antigen	Antibody	Source of supply	Species	Concentration [mg/ml]	Dilution
Mouse-IgG	Alexa Fluor 488 anti-Mouse	Molecular Probes	Goat	2	1:400
	Alexa Fluor 568 anti-Mouse	Molecular Probes	Goat	2	1:400
	Atto 647N anti-Mouse	Sigma-Aldrich	Goat	1	1:200
Rabbit-IgG	Alexa Fluor 488 anti-Rabbit	Molecular Probes	Goat	2	1:400
	Alexa Fluor 568 anti-Rabbit	Molecular Probes	Goat	2	1:400

Table 3-3: Secondary antibodies used for immunofluorescence.

3.4.5 Verification of antibody specificity used for immunofluorescence

To determine whether binding of an antibody is specific, immunizing peptide blocking experiment was performed. Before staining, peptide corresponding to the epitope recognized by the antibody (TET2 peptide (ab106206); Abcam), was added to the antibody solution to a final concentration of 1 μg/ml and incubated for 30 minutes. Then staining was performed as described above (chapter 3.4.4). Comparing the staining from the blocked antibody with the antibody alone provides information about the antibody's specificity. Namely specific staining will be absent from the stained sample with the neutralized antibody.

3.4.6 Confocal microscopy

For the analysis of immunostained samples, a confocal Laserscanning System Leica TCS SPE equipped with an inverse DMI4000 microscope (objective: HCX PL APO 63x 1.40-0.6 OIL) and solid state lasers with excitation wavelengths of 405, 488, 532 and 635 nm was used. Alternatively, the spinning disc confocal microscope Nikon TiE (objective: CFI PLAN APO VC 60x 1.40 OIL; excitation wavelengths: 405, 488, 561 and 640 nm) was used.

To compare the signal fluorescence intensities of different samples, the settings of the laser intensity, the photomultipliers and the pinhole were kept constant.

3.4.6.1 Intensity measurements of nuclear fluorescence signal and co-localization analysis

The software ImageJ was used for the analysis and processing of pictures recorded. Unless otherwise stated, all pictures show overlays of maximum projections.

Intensity measurements of nuclear fluorescence intensity signals were performed using maximum projections. The "Threshold" function was used to highlight and select all nuclei in the picture according to their DAPI signal. Then mean gray values for all single nuclei and different channels were measured using the "Measure" function.

Co-localization analysis was performed using the Intensity Correlation Analysis plugin for ImageJ (Tony Collins; Wright Cell Imaging Facility, Toronto, Canada). For every picture, the background signal (unspecific antibody staining) in the nucleus was subtracted for each channel using the plugin "BG Subtraction from ROI". Afterwards, the nuclei were selected

according to their DAPI signal and Intensity Correlation Analysis was performed. This analysis is based on the product of the difference from the mean (PDM), which is calculated as follows:

$$PDM = (A - a)(B - b)$$

Equation 3-1

Whereby A is the fluorescence intensity of the pixel of the first channel and B is the fluorescence intensity of the pixel of the second channel, while a and b are the mean fluorescent intensities of the respective channels.

A further description of the relationship between two signals is given by the ICQ (intensity correlation quotient) value. The ICQ value is equal to the ratio of the number of positive PDM values to the total number of pixel values. ICQ values are distributed between – 0.5 and + 0.5 subtracting 0.5 from this value. Therefore the ICQ value is defined by the following equation:

$$ICQ = \left(\frac{N_{pos.PDM}}{N_{total}}\right) - 0.5$$

Equation 3-2

If the correlation is random, then ICQ = ~0, if the two signals are not correlated then 0 > ICQ ≥ - 0.5, and if the two signals are correlated, then 0 < ICQ ≤ 0.5. The detailed description of the method can be found in [Li et al., 2004].

3.5 Biochemical Methods

3.5.1 Preparation of whole protein lysates from cells (Lämmli-Lysates)

For preparation of whole protein lysates, cells were kept on ice and the medium was removed from each Petri dish. After washing cells with PBS, 70 μl double concentrated SDS Lämmli buffer was added and the cells were scraped from the bottom of the dish using a cell scraper. Lysates were transferred into a reaction tube and passed through a 25-gauge needle for 10 times. Afterwards, the sample was incubated at 100 °C for 10 minutes and centrifuged for 10 minutes at 13.000 × g. The supernatant containing the proteins was transferred to a new reaction tube and stored at -20 °C. The pellet was discarded.

3.5.2 Determination of the protein concentration

To determine the protein concentration of whole protein lysates, the protocol of Lowry [Lowry et al., 1951] was used and the DC Assay (BioRad; Canada) was performed according to manufacturer's instructions. BSA in the concentrations of 0.2, 0.4, 0.8 and 1 mg/ml was used for a standard curve.

3.5.3 SDS-Polyacrylamidegelelectrophoresis (SDS-PAGE) and Western Transfer

To separate high (DNA-PKcs and pDNA-PKcs 460 kDa, TET1 235 kDa, and Vinculin 130 kDa) and low (Actin 42 kDa and Lamin A/C 74 and 65 kDa) molecular weight proteins at the same

time, precast tris-acetate gels with an acrylamide gradient of 3-8 % (NuPAGE) were used. For comparison, equal protein amounts were loaded on each lane. Depending on the protein concentration, the samples were diluted with double concentrated SDS Lämmli buffer and double concentrated SDS sample buffer containing β-mercaptoethanol was added at a ratio of 1:2. Samples were then incubated at 95 °C for three minutes to denature the proteins before being applied to the gel. As a control for the molecular weight, a high molecular weight protein ladder (HiMark™ Pre-Stained Protein Standard, life technologies) was applied to the gel. To run the gel, the inner chamber of the PAGE apparatus was filled with running buffer complemented with antioxidant, while the outer chamber was filled with running buffer only. The gels were run at a constant voltage of 200 V and a current of about 50 mA for about one hour.

Afterwards, proteins were transferred to a Polyvinylidenfluoride- (PVDF-) membrane using the NuPAGE system. Membranes, filter paper and pads were soaked in transfer buffer complemented with antioxidant. The hydrophobic membrane was pre-equilibrated in methanol before soaking in transfer buffer. For the transfer, the gel and the membrane were positioned between two filter papers and two to three pads on each side and adjusted between the electrodes of the tank-blotting apparatus, which was filled with transfer buffer. The transfer was carried out at a constant voltage of 30 V at 270 – 330 mA for 70 minutes. To avoid overheating of the system, the outer chamber of the tank-blotting apparatus was filled with iced water.

In addition to precast gels, gels with an acrylamide percentage of 8 % were used to verify the expression of the cys-rich and catalytic domain of TET2 fused to GFP in transfected cells. Samples were prepared as indicated above. As a molecular weight marker, a protein ladder (Page Ruler^{TM} Plus Prestained Protein Ladder; Fermentas GmbH, St. Leon-Rot, Germany) was used. Gels were run in SDS running buffer at a constant current of 45 mA and proteins were transferred to a PVDF-membrane using the SemiDry apparatus of Hoefer SemiPhor (GE HealthCare, UK) afterwards. Namely, gels and membranes were framed with filter paper (soaked with transfer buffer), and placed between two electrodes. The electric field was applied perpendicular to the original running direction of the proteins, which allows transfer of proteins from the gel matrix to the membrane. The membrane was equilibrated in advance using methanol and transfer buffer. Transfer was carried out at RT for 45 minutes at a constant current of 65 mA.

3.5.4 Antibody staining and detection

After the transfer, the membranes were incubated in blocking solution for 30 minutes to block unspecific binding of antibodies. The primary antibody was diluted in blocking solution and the membrane was incubated overnight at 4 °C (dilutions of primary antibodies used for the detection of the Western transfer are listed in Table 3-4). On the next day, the membranes were washed in 1 × TBST three times for five minutes each. The secondary antibody, which is coupled to a horseradish peroxidase (HRP), was diluted in 1 × TBST, spread over the membranes and incubated for further 60 minutes at RT (dilutions of secondary antibodies used for the detection of the Western transfer are listed in Table 3-5). After the incubation, the membranes were washed four times for five minutes in 1 × TBST and were incubated with ECL Plus solution (Thermo) for five minutes in the dark. The oxidation of the Lumigen PS-3 Acridin substrate by HRP leads to a chemiluminescence signal that can be detected either on X-ray films or by an appropriate camera. The exposition times varied according to the

investigated protein. As a loading control, the housekeeping proteins actin, lamin A, lamin C, and vinculin were used. To quantify the expression of certain proteins, the signals were detected using the imaging instrument FUSION FX7^{TM} (Peqlab) and the quantification of chemiluminescence signal in the linear range was accomplished using the FUSION software. The images were pre-processed using linear background subtraction. Then, the intensity of each band of both the proteins of interest and the housekeeping proteins (loading control) were measured. To determine the expression levels of a protein, the value of its intensity was normalized over the value of the intensity of the housekeeping gene. Since Lamin A/C is not expressed in all cell lines analyzed, Vinculin was used.

Antigen	Antibody	Source of supply	Species	Concentration [mg/ml]	Dilution
Actin	β-Actin (ab34731)	Abcam	Rabbit polyclonal	1	1:3000
DNA-PKcs	DNA-PKcs Ab-4 (Cocktail)	Lab Vision	Mouse monoclonal	0.2	1:5000
pDNA-PKcs	pDNA-PKcs (phospho-S2056)	Abcam	Rabbit polyclonal	1	1:1000
GFP	GFP	Imgenex	Rabbit polyclonal	0.5	1:250
Lamin A/C	Lamin A/C, clone 14	Upstate	Mouse monoclonal	0.2	1:3000
TET1	TET1 [N3C1]	Genetex	Rabbit polyclonal	1	1:1000-1:5000
TET2	TET2 (ab94580)	Abcam	Rabbit polyclonal	1	1:100
TET3	TET3[C3], C-term	Genetex	Rabbit polyclonal	1	1:500
Vinculin	Vinculin (ab18058)	Abcam	Mouse monoclonal	0.2	1:20000

Table 3-4: Primary antibodies used for Western blot.

Antigen	Antibody	Source of supply	Species	Concentration [mg/ml]	Dilution
Mouse-IgG	Mouse-IgG HRP-conjugated	GE Healthcare UK	Sheep	1.0	1:10000
Rabbit-IgG	Rabbit-IgG HRP-conjugated	GE Healthcare UK	Sheep	1.0	1:10000

Table 3-5: Secondary antibodies used for Western blot.

3.5.5 Stripping and reprobing of membranes in Western Analysis

Re-probing of membranes is possible once primary and secondary antibodies are removed. This was achieved by washing the membrane in stripping buffer for 30 minutes at 50 °C in a water bath under agitation. Afterwards, the membrane was washed four times for five minutes in 1 × TBST and incubated in blocking solution for 30 minutes to block unspecific

binding of antibodies. To ensure successful stripping, the membrane was incubated with ECL Plus solution (Thermo) for five minutes in the dark and detection of the signal was performed afterwards. If no signal was detected, stripping was considered successful and the membrane could be re-probed. The stripped membrane was then washed four times for five minutes in 1 × TBST and incubated with primary and secondary antibody as described above (Chapter 3.5.4).

3.5.6 Verification of antibody specificity used in Western Analysis

As described for immunostaining (chapter 3.4.5), specificity of antibody-binding was also determined for Western Analysis performing immunizing peptide blocking experiment. Therefore the same amount of immunizing peptide (TET2 peptide (ab106206); Abcam) was added to the antibody solution, which was incubated for 30 minutes before performing staining and detection (chapter 3.5.4). Comparing the staining from the blocked antibody with the antibody alone provides information about the antibody's specificity. Namely specific staining will be absent from the Western blot with the neutralized antibody.

3.6 Colorimetric analysis of DNA (hydroxy) methylation

3.6.1 Isolation of DNA from cells and determination of the DNA concentration

Total DNA was isolated using the DNeasy Blood & Tissue Kit (QIAGEN) according to manufacturer's instructions. The concentration of the DNA was determined photometrically using the BioPhotometer (Eppendorf). Therefore DNA was diluted in 1 × TE buffer and for each sample concentration was measured three times. Values were averaged and concentration was calculated taking the dilution factor into account.

3.6.2 Enzyme-linked immunosorbent assay (ELISA)-based quantification of global methylation and hydroxymethylation levels

For colorimetric quantification of DNA methylation and DNA hydroxymethylation the MethylFlash™ Methylated or Hydroxymethylated DNA Quantification Kit (Epigentek) was used and analysis was performed according to manufacturer's instructions. Positive and negative controls (two technical replicates each) were used as a reference in all experiments.

3.7 Flow cytometry

3.7.1 Fixation of samples for flow cytometry

For flow cytometry analysis, the cells were incubated with a Trypsin-EDTA-solution at 37 °C, to detach the cells from the dish. Afterwards, the cells were transferred to a 15 ml tube and two volumes of PBS were added. Cells were centrifuged for five minutes at 300 × g and the supernatant was discarded. The pellet was resuspended in PBS. For fixation, one volume of 8 % paraformaldehyde was added to a final concentration of 4 %, while vortexing. Cells were then incubated at RT for 15 minutes. To permeabilize the cells, the samples were centrifuged for seven minutes at 350 × g, the supernatant was discarded and the pellet was resuspended in 0.5 % Triton-X-100 and incubated for eight minutes at RT. Samples were centrifuged at 350 × g for seven minutes and the pellet was resuspended and incubated for 10 minutes in 2 N HCl to denature DNA and allow proper binding of anti-DNA hydroxymethylation antibodies. After centrifugation at 350 × g for five minutes, HCl was removed and pH was neutralized by resuspending the cell pellet in 100 mM Tris-HCl (pH 8). Resuspended cells were then incubated at RT for five minutes and centrifuged at 350 × g for five minutes. The

pellet was washed in PBS and cells were centrifuged for eight minutes at 350 × g. To block unspecific binding of antibodies, the pellet was resuspended in 0.5 % BSA in PBS and incubated at RT for 30 minutes.

3.7.2 Staining of samples for flow cytometry

For staining, the samples were centrifuged for seven minutes at 350 × g and the supernatant was discarded. The primary antibodies were diluted in 0.5 % BSA in PBS and cells were resuspended with the antibody solution and incubated overnight at 4 °C (dilutions of primary antibodies used for flow cytometry are listed in Table 3-6). Afterwards, PBS was added and the samples were centrifuged for seven minutes at 350 × g. Secondary antibody staining was performed resuspending the cells in secondary antibody solution diluted in 0.5 % BSA in PBS and incubating them at RT for 45 minutes in the dark (dilutions of secondary antibodies used for flow cytometry are listed in Table 3-7). After the incubation, the cells were washed in PBS and centrifuged for seven minutes at 400 × g. The supernatant was discarded and the pellet was resuspended in 1 ml PBS supplied with 1 μg/ml DAPI and incubated at RT for 15 minutes. Finally, the samples were analyzed by flow cytometry.

Antigen	Antibody	Source of supply	Species	Concentration [mg/ml]	Dilution
5-Hydroxy-methylcytosine	5-Hydroxy-methylcytosine (5-hmC) antibody (pAb)	Active Motif	Rabbit polyclonal		1:300
γH2AX	γH2AX (Ser139) clone JBW301	Millipore	Mouse monoclonal	1	1:500

Table 3-6: Primary antibodies used for flow cytometry.

Antigen	Antibody	Source of supply	Species	Concentration [mg/ml]	Dilution
Mouse-IgG	Alexa Fluor 568 anti-Mouse	Molecular Probes	Goat	2	1:400
Rabbit-IgG	Alexa Fluor 680 anti-Rabbit	Life Technologies	Goat	2	1:400

Table 3-7: Secondary antibodies used for flow cytometry.

3.7.3 Flow cytometry analysis

For flow cytometry analysis, the FACS Canto II Flow Cytometer was used. Analysis was performed using cells transiently expressing the cys-rich and the catalytic domain of TET2 fused to GFP (TET2CD-GFP) and stained against 5hmC and γH2AX. DAPI was employed for DNA counter-staining and was excited using the 405 nm (violet) laser. Alexa Fluor 680 was used for the staining of 5hmC and was excited using the 633 nm (red) laser. Alexa Fluor 568, which stained γH2AX, and GFP (TET2CD-GFP) were excited by the 488 nm (blue) laser. For such reason, a compensation for GFP and Alexa Fluor 568 was made.

The samples were evaluated using the software FlowJo.

4 Materials

4.1 Cell lines, cell culture media and supplements

4.1.1 Cell lines

Cell line	Description
AG 1522 D	Human foreskin fibroblast cell line (Coriell Institute for Medical Research); adherent growth and show contact inhibition; cultivation in Eagle's Minimum Essential Medium (EMEM) with fetal calf serum (FCS) added to a final concentration of 15 %, 1 % Glutamine, 100 U/ml Penicillin and 100 µg/ml Streptomycin; the number of doublings was documented and calculated by the CPD (cumulative population doublings): $$CPD(new) = CPD(old) + \frac{ln\frac{\#\ cells\ harvested}{\#\ cells\ seeded}}{ln2}$$ Only cells with a CPD lower than 37 were used for the experiments.
HCT 116 p53 +/+	Human colorectal carcinoma cell line of an adult male with wild-type p53 genes; adherent growth and epithelial morphology; cultivation in Dulbecco's Minimal Essential Medium with 4,5 g/l Glucose (DMEM) with FCS added to a final concentration of 10 %; kindly provided by Dr. Bert Vogelstein (Johns Hopkins University School of Medicine).
HeLa	Human adenocarcinoma cell line of an 31 years adult female; adherent growth and epithelial morphology; cultivation in RPMI Medium with FCS added to a final concentration of 10 %.
MEF	Mouse embryonic fibroblast cell line; adherent growth fibroblast morphology; cultivation in DMEM with FCS added to a final concentration of 10 %.
NFFhTert	Normal foreskin fibroblasts which were transfected with human telomerase reverse transcriptase (hTert) after the protocol by [Toouli et al., 2002]; cultivation in DMEM (4,5 g/l Glucose) with FCS added to a final concentration of 15 %, 100 U/ml Penicillin and 100 µg/ml Streptomycin; kindly provided by Prof. M. Lavin (Brisbane).
NIH/3T3	Mouse embryonic fibroblast cell line; spontaneously immortalized; adherent growth and fibroblast morphology; cultivation in DMEM with FCS added to a final concentration of 10 %.
U-2 OS	Human osteosarcoma cell line of a 15 years old girl (American Type Culture Collection (ATCC), Manassas, USA); adherent growth and epithelial morphology; cultivation in DMEM with FCS added to a final concentration of 10 %.

Cell line	Description
WI-38	Human diploid cell line which was derived by Leonard Hayflick from normal embryonic (3 months gestation) lung tissue (ATCC); adherent growth and fibroblast morphology; cultivation in EMEM with FCS added to a final concentration of 10 %; the number of doublings was documented and calculated by the CPD and only cells with a CPD lower than 31 were used for the experiments.
PBL	Peripheral blood lymphocytes taken from whole blood samples of healthy donors (GSI Helmholtzzentrum für Schwerionenforschung (Darmstadt)); after isolation PBL were directly used for experiments
HSPC	Human hematopoietic stem and progenitor cells taken from mobilized peripheral blood samples (Blutspendedienst Baden-Württemberg-Hessen, Deutsches Rotes Kreuz, Frankfurt am Main) of healthy donors; enriched with G-CSF (granulocyte colony stimulating factor) and isolated using CD34 positive selection; after isolation HSPCs were directly used for experiments

4.1.2 Cell culture media and supplements

Solutions	Company
Dimethylsulfoxid (DMSO)	Roth
Dulbecco's Minimal Essential Medium with 4,5 g/l Glucose (DMEM)	Biochrom
Eagle's Minimum Essential Medium (EMEM) with EBSS	Lonza
Fetal calf serum (FCS)	Biochrom
Glycerin	Sigma
L-Alanyl-L-Glutamin	Biochrom
Penicillin/Streptomycin (10000 U/ml /10000 μg/ml)	Biochrom
Phosphate buffered saline (PBS)	Biochrom
RPMI Medium	Biochrom
Trypsin/EDTA	PAN Biotech

4.2 Bacterial strains, media and supplements

4.2.1 Strains

Strain	Description
***E.Coli* DH5α**	Subcloning Efficiency DH5α Competent Cells; Invitrogen

4.2.2 Media and supplements

Media	Chemical composition
LB Agar (liquid medium)	1 % (w/v) yeast extract, 1.6 % (w/v) Tryptone, 0.5 % (w/v) NaCl
LB Agar plates	3.5 % (w/v) LB-Agar, 0.5 % (w/v) yeast extract, 0.5 % (w/v) Tryptone

Supplements	Company
Ampicillin (50 mg/ml stock solution)	AppliChem
LB-Agar	AppliChem
Tryptone	AppliChem
Yeast-extract	AppliChem
$CaCl_2$	Merck
Glycerol	Sigma

4.3 Chemicals

Chemical	Company
1x Proteinase Cocktail Complete	Roche
4‘,6-Diamidin-2-phenylindol (DAPI)	AppliChem
6x loading dye	Fermentas
30 % Acrylamid/Bisacrylamid (29:1)	Roth
AEBSF	AppliChem
Agarose GTQ (DNAse- and RNAse-free)	Roth
Ammonium persulfate	Sigma
Antioxidant	Life Technologies
APS	Sigma
Bicine	Sigma
Bis-Tris	AppliChem
Bromphenol blue	Serva
BSA	Roth
Developer solution	AGFA
DMSO	Roth
DNA-Ladder GeneRuler 1 kb DNA Ladder	Fermentas
DNA-PK-Inhibitor NU7026	Sigma-Aldrich
DTT	AppliChem

Chemical	Company
ECL Plus	GE Healthcare
EDTA	Sigma
Ethanol	AppliChem
Ethidiumbromide	AppliChem
Fixer	AGFA
Glycine	Roth
Hepes	Biochrom
Hydrochloric acid (37 %)	Merck
Immersion oil (DIN58884)	Merck
Isopropyl alcohol	Roth
jetPRIME and jetPRIME buffer	Peqlab
Löffler's Methylene Blue solution	Roth
Magnesium chloride	Roth
Methanol 99.9 %	Roth
Mounting Medium Vectashield	Vector Laboratories
NF-Acrylamid/Bis-Solution 30 %	Roth
Paraformaldehyde	AppliChem
Potassium chloride	Merck
Protein standards: HiMark™ Pre-Stained Protein Standard Page Ruler™ Plus Prestained Protein Ladder	Life Technologies Fermentas
Ribonuclease A	AppliChem
SDS	Sigma
Skim milk powder	
Sodium acetate	AppliChem
Sodium azide	Sigma
Sodium chloride	AppliChem
TEMED	Merck
Trichostatin A	Cayman
Tricine	AppliChem
Tris HCl	Merck
Tris-Base	Roth
Triton X-100	AppliChem
Tween 20	Sigma-Aldrich

4.4 Buffers and solutions

Buffers and solutions	Chemical composition
Blocking solution	5 % skim milk powder in 1 × TBST
Hepes extraction buffer	10 mM Hepes,10 mM KCl, 1.5 mM MgCl2, 0.1 % Triton X-100, add 0.5 mM DTT directly before use
Methylen blue	30 % (v/v) Löffler's Methylenblue solution, 5 % (v/v) methanol, 0.009 % (v/v) potassium hydroxide
PBS	137 mM Sodium chloride, 7.9 mM Disodium hydrogen phosphate, 2.7 mM Potassium chloride, 1.5 mM Potassium dihydrogen phosphate
Resolving gel buffer (8 %)	According to [Sambrook et al., 1989]
Running buffer (NuPAGE)	50 mM Tricine, 50 mM Tris Base, 0.1 % (w/v) SDS
SDS Lämmli buffer (2x concentrated)	100 mM Tris-HCl (pH 6.8), 2 % SDS, 20 % Glycerin
SDS running buffer (for non-gradient gels)	25 mM Tris Base, 192 mM Glycine, 0.1 % (w/v) SDS
SDS sample buffer (2x concentrated)	100 mM Tris-HCl (pH 6.8), 50 % (v/v) Glycerin, 4 % (w/v) SDS, 0.2 % (w/v) Bromphenol blue, 10 % (v/v) β-Mercaptoethanol
Stacking gel (5 %)	According to [Sambrook et al., 1989]
Stripping buffer	2 % (w/v) SDS, 60 mM Tris HCl (pH 6.7), 0.7 % (v/v) β-Mercaptoethanol
10 × TAE	400 mM Tris Base, 50 mM Sodium acetate, 10 mM EDTA
1 × TBST	20 mM Tris Base, 137mM NaCl, 0.1 % Tween 20
10 × TE (pH 8.0)	0.1 M Tris-base, 0.01 M EDTA
Transfer buffer (NuPAGE)	25 mM Bicine, 25 mM Bis-Tris, 1 mM EDTA
Transfer buffer (Semi-dry transfer)	19.2 mM Glycine, 25 mM Tris Base, 0.037 % (w/v) SDS
DNA-PK Inhibitor stock solution (NU7026)	5 mM Nu7026 in DMSO

4.5 Kits, Software, machines and apparatuses

4.5.1 Kits

Kit	Company
DC Assay	BioRad
DNeasy Blood & Tissue Kit	QIAGEN
MethylFlash Hydroxymethylated DNA Quantification Kit	EPIGENTEK
MethylFlash Methylated DNA Quantification Kit	EPIGENTEK
Mycoplasma Kit	AppliChem
Plasmid Purification Maxi Kit	QIAGEN

4.5.2 Software

Software	Company
Andor iQ 1.10.3	Andor Bioimaging Division
FUSION software	Peqlab
FlowJo V7	Tree Star, Inc.
Gen5 1.00.14	Biotek Instruments, Inc.
ImageJ 1.47v	National Institutes of Health
ImageJ plugin Intensity Correlation Analysis	Tony Collins; Wright Cell Imaging Facility, Toronto, Canada
LAS AF Software	Leica
OriginPro 8.5.0G SR1	OriginLab Corporation

4.5.3 Machines and apparatuses

Machine/Apparatus	Company
Blotting apparatuses XCell II Blot Module CE Mark (NuPAGE) SemiDry apparatus (Hoefer SemiPhor)	 Invitrogen GE HealthCare
Confocal microscopes: DMI4000 Eclipse TiE	 Leica Nikon
Developement machine Curix 60	AGFA
Electrophoresis chamber	Bio-Rad
ELISA-Reader EL 808	BioTek
FACSCanto II Flow Cytometer	BD
FUSION FX7^{TM}	Peqlab
PAGE-Chambers: XCell Sure Lock Mini-Protean II	 Invitrogen Bio-Rad
Photometer	Eppendorf
SN4 Dosimeter	PTW
X-ray tube IV320-13	Seifert
Z2 Coulter Counter	Beckmann Coulter

5 Results

The aim of this work is to elucidate DNA methylation changes after exposure to IR. The majority of previous studies investigating DNA methylation changes after exposure to IR or DSB induction [Aypar et al., 2011, Goetz et al., 2011, Cuozzo et al., 2007, O'Hagan et al., 2008] were conducted several population doublings after irradiation and therefore cannot rule out the role of replication as a contribution to demethylation effects (dilution effect). Furthermore, only few studies on early DNA methylation changes after irradiation exist (e.g. [Antwih et al., 2013, Chaudhry and Omaruddin, 2012]) and no consistent pattern of hypermethylation or hypomethylation was shown. Therefore, the aim of this work is to elucidate early methylation effects, focusing on one replication cycle time frame (~24 hours) after irradiation.

5.1 Determination of global 5mC and 5hmC levels after irradiation with X-rays

Focusing on DNA methylation changes after irradiation, global 5mC changes were measured after irradiation with X-rays using colorimetric ELISA-based assays, which allows the calculation of methylated DNA in percentage of total DNA within the cells (chapter 3.6). Therefore, genomic DNA of normal human fibroblasts, isolated at different time points after irradiation with 10 Gy X-rays was investigated. 5mC levels decreased drastically down to 30 % of the initial starting value until three hours post irradiation and only slightly increased thereafter (Figure 5-1 A).

A fast DNA methylation decrease in a time frame of only three hours may not be explained by passive DNA demethylation, due to reduced DNMT expression, since those processes proceed slowly and loss of methylated cytosine is achieved during successive rounds of replication [Wu and Zhang, 2010]. Therefore a rather enzymatic decrease than a passive decrease due to reduced DNMT expression, is conceivable. In this scenario, TET enzymes are the major candidates as they are responsible for the conversion of methylcytosine (5mC) to hydroxymethylcytosine (5hmC), thus resulting in decreased DNA methylation levels. Therefore, in this study, the possible involvement of TET enzymes in the DNA double strand break repair was addressed as well.

Since TET enzymes convert 5mC to 5hmC, also global 5hmC changes were measured after irradiation with X-rays using colorimetric ELISA-based assays. AG cells were treated as was explained for the analysis of global 5mC changes. As shown in Figure 5-1 B, 5hmC levels show a trend of an early increase (until 30 minutes post irradiation) while it drops afterwards and may recover after 24 hours.

While 5mC changes showed reliable reproducible results, measurements of 5hmC changes presented high inter-experimental variability (visualized by the enormous error bars) and therefore no statistically significant assessment was obtained when measuring 5hmC changes (Figure 5-1 B). In this context it has to be mentioned, that quantification of global DNA hydroxymethylation may be challenging, since the overall amount of 5hmC is very limited (between 0.009 and 0.7 % of all bases; for comparison see also [Globisch et al., 2010, Ito et al., 2011]). Having such small numbers only slight variability can cause enormous variations, as observed in Figure 5-1 B.

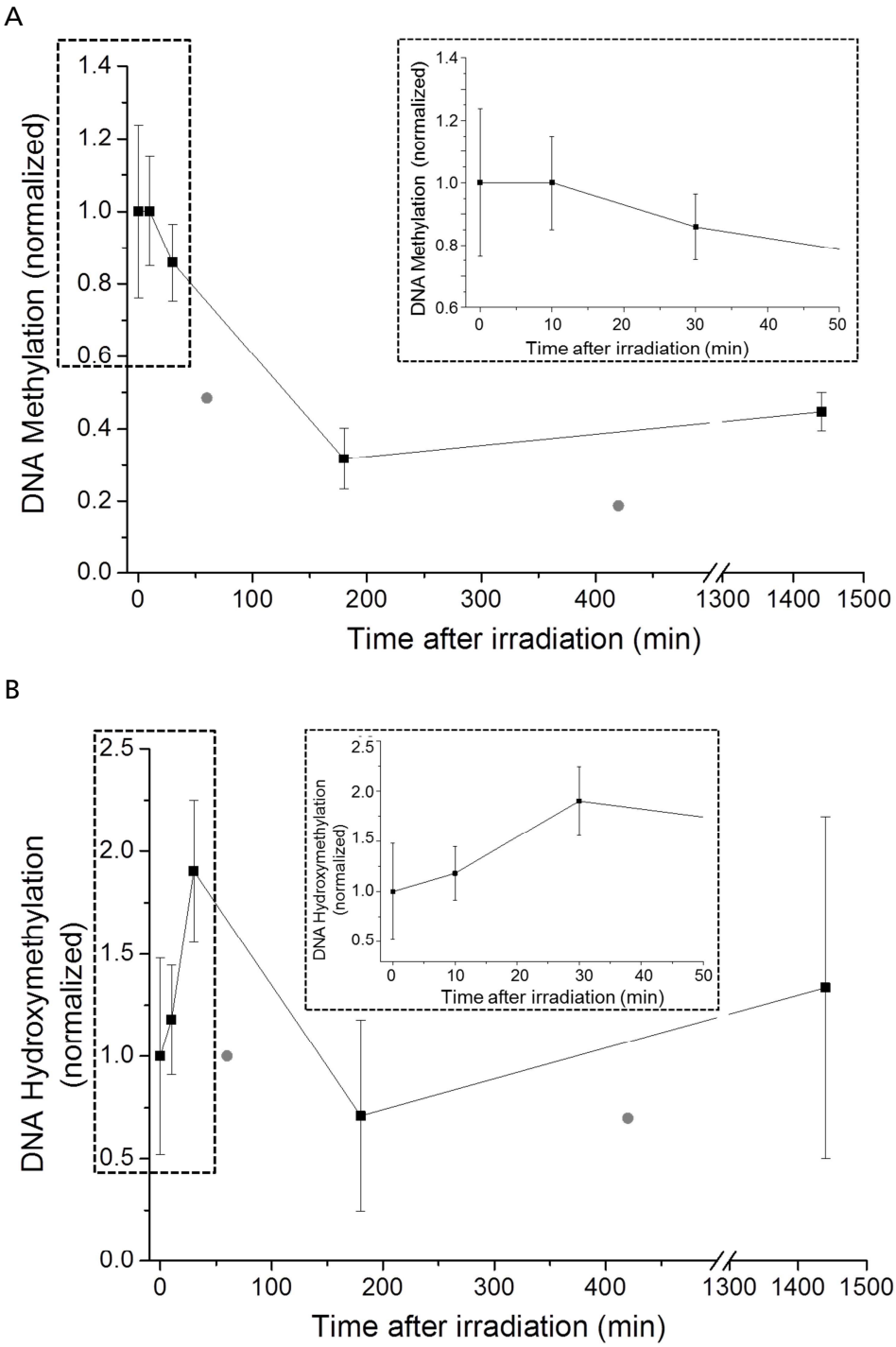

Figure 5-1: Global DNA hydroxy-/methylation changes after irradiation over time. AG human fibroblasts were irradiated with 10 Gy X-rays and incubated for 10 minutes, 30 minutes, 1 hour, 3 hours, 7 hours and 24 hours. Cells were harvested and genomic DNA was isolated at the indicated time points. An unirradiated sample was used as a control. Relative changes in global DNA methylation (A) and DNA hydroxymethylation (B) were analyzed using ELISA-based colorimetric analysis. Results for control, 10 minutes and 30 minutes are from four biological replicates; results for 3 and 24 hours are from 2 biological replicates and results for 1 hour and 7 hours are from 1 biological replicate. For each biological replicate, 2 – 4 technical replicates were analyzed. Samples with more than one biological replicate are shown as black circles, samples with only one biological replicate are shown as grey circles and are not included in the curve. Both graphs show normalized values, where the unirradiated control was set to one and all other values were converted relative to this value. The inlays show a magnified view of the time points until 30 minutes (framed by dotted lines). Error bars: Standard error.

However, with this experiment first indications of a DNA demethylation process in response to IR are given. In further studies a possible DNA demethylation process was investigated in detail. Furthermore, it was investigated whether DNA demethylation can be linked to TET enzymatic activity. Therefore the appropriate experimental system was determined first.

5.2 Establishment and validation of the experimental system

In order to investigate DNA methylation changes within one replication cycle time frame, the experimental system was established first. Many laboratory cell cultures are derived from cancer cells and it is known (reviewed in [Ting et al., 2006]) that DNA methylation and enzymes involved in DNA methylation regulation are highly variable in cancers. Additionally, there are different other factors, like age, nutrition or other environmental agents, influencing DNA methylation levels [Aguilera et al., 2010]. Therefore, hydroxy-/methylation as well as TET2 protein expression in different cell lines were investigated first.

Quantification was performed in different tumor (U-2 OS, HCT 116 p53 +/+ (HCT) and HeLa) and human and murine fibroblast cell lines (AG 1522 D (AG), NFFhTert, WI-38, NIH/3T3 and MEF). Human hematopoietic stem and progenitor cells (HSPC) as well as peripheral blood lymphocytes (PBL) from healthy donors, were used and examined for basal DNA hydroxy-/methylation and TET2 expression as a comparison to cultured cell lines. According to literature [Langemeijer et al., 2009], HSPC as well as PBL show higher TET2 mRNA levels, compared to cells of other origin.

TET1 and TET3 protein levels were also investigated, although no specific signal could be detected using commercially available antibodies (Figure 5-2 A). In contrast TET2 showed a clear signal and also immunizing peptide blocking experiment demonstrated its specificity (Figure 5-2 B).

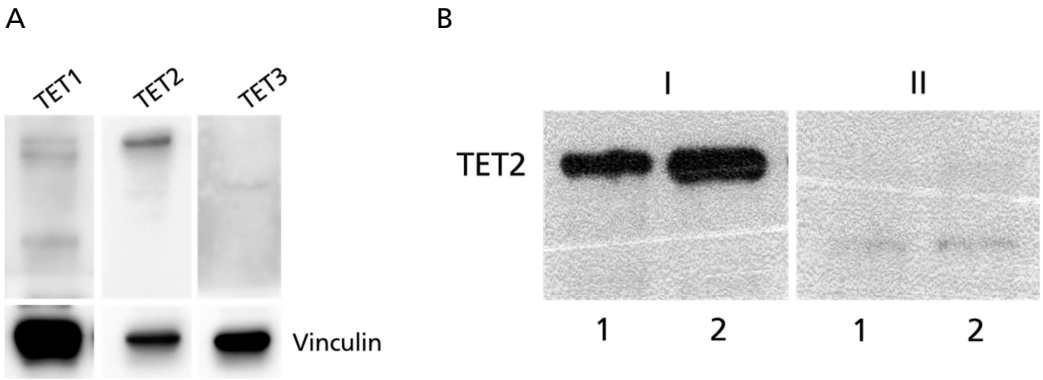

Figure 5-2: TET1/3 antibodies are not specific. A) Whole protein lysates of AG cells were analyzed for their TET1, TET2 and TET3 expression by Western analysis. While no specific signal could be detected for TET1 and TET3, TET2 showed a clear band. B) The specificity of TET2 antibody was confirmed using immunizing peptide blocking experiment on whole protein lysates of WI-38 (lane 1) and AG (lane 2) cells. Western analysis revealed TET2 expression in cells incubated with TET2 antibody (I), while no TET2 was detected when the antibody was blocked with the immunizing peptide in advance (II).

It is reported [Tahiliani et al., 2009] about the ability of TET proteins to convert 5mC to 5hmC in human embryonic kidney 293 cells and in mouse ESCs. Therefore, for the following

experiments, it was speculated that cells showing high TET2 expression would show low basal 5mC levels, while cells expressing TET2 to a low amount, would show high basal 5mC levels.

5.2.1 Basal DNA methylation levels differ among different cell lines/types and are negatively correlated to TET2 protein levels

Analysis of basal DNA methylation was performed using a colorimetric assay. The highest DNA methylation level was found in WI-38 (0.73 % ± 0.1) and the lowest 5mC level was observed for NFFhTert (0.28 % ± 0.07). The other cell lines showed 5mC levels between these two values and are depicted in Table 5-1. According to their relatively high 5mC levels, WI-38, NIH/3T3, PBL and HSPC were referred to as "high DNA methylation levels" group (Figure 5-3 A, grey columns). U-2 OS, HCT, HeLa, AG, MEF as well as NFFhTert showed comparably low levels of 5mC and were referred to as "low DNA methylation levels" group (Figure 5-3 A, green columns).

The analysis of TET2 protein expression in the same cell lines revealed highest levels in NFFhTert (0.32 ± 0.3) while TET2 protein was not detectable in NIH/3T3 and HSPC cells. The other cell lines showed TET2 expression levels between these two values (Table 5-1, Figure 5-3 B).

The color code set in Figure 5-3 A was kept in B, showing that high TET2 expression levels were mainly found in cells presenting low basal 5mC levels (compare Figure 5-3 A and Figure 5-3 B, green columns) while low TET2 expression levels were observed for cells with high 5mC amount (compare grey columns in Figure 5-3 A and Figure 5-3 B). 5mC levels were plotted as a function of TET2 protein expression (Figure 5-3 C) and calculation of Spearman's correlation coefficient indicated a strong anti-correlation of the two features ($R_{Spearman}$ = - 0.6018; p = 0.0329).

These results support the assumption that TET2 is one of the main players converting 5mC to 5hmC in the cells analyzed. Based on the anti-correlation between 5mC and TET2 protein levels, it was reasoned that a positive correlation between TET2 expression and 5hmC might be expected, as 5hmc forms the intermediate product in oxidation of 5mC catalyzed by TETs. For proving this assumption the 5hmC levels were measured in the previously analyzed cell lines.

A

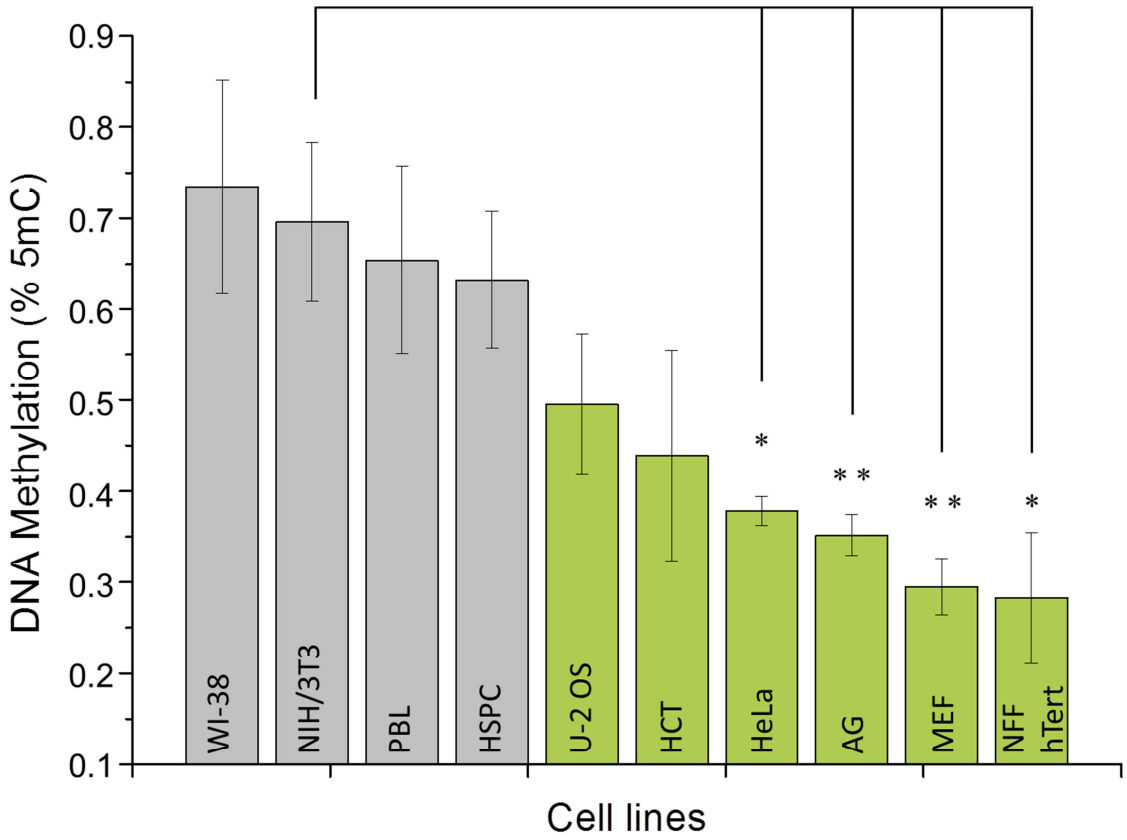

B

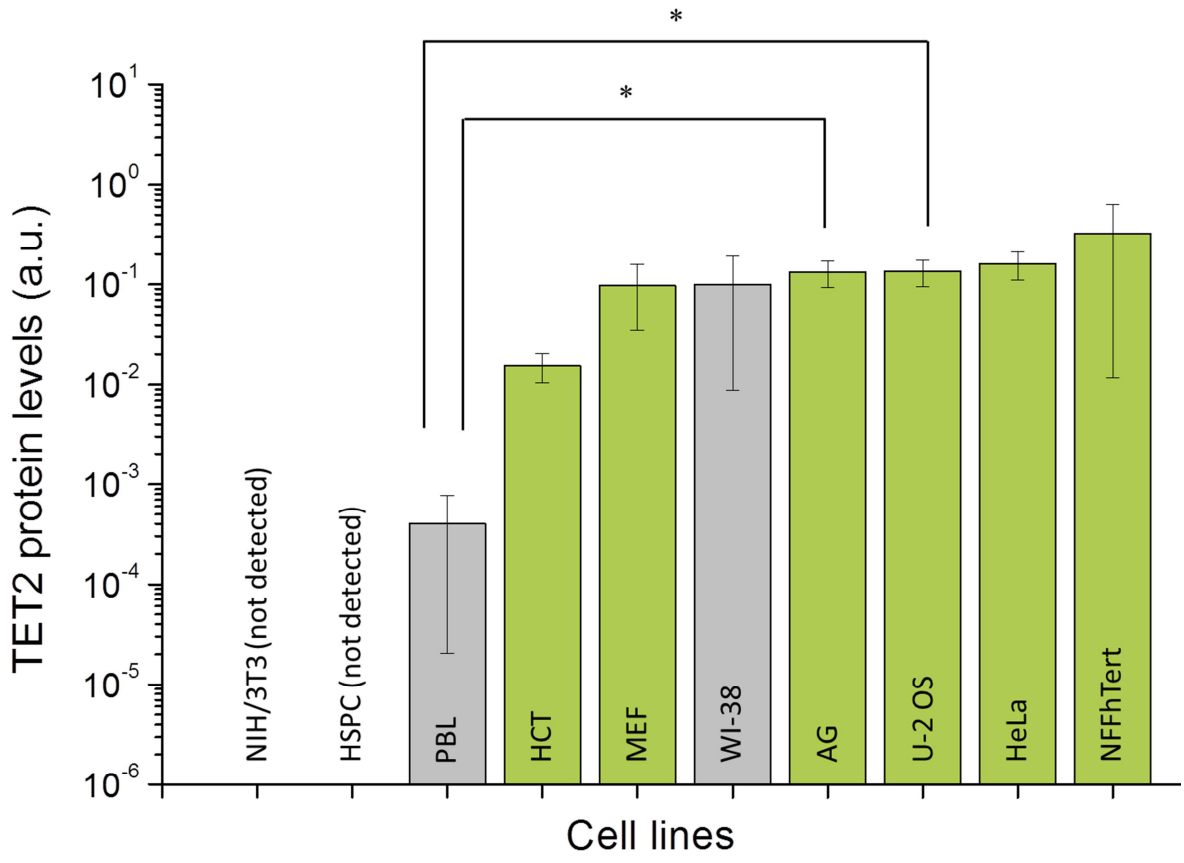

Caption see next page

Figure 5-3 continued

C

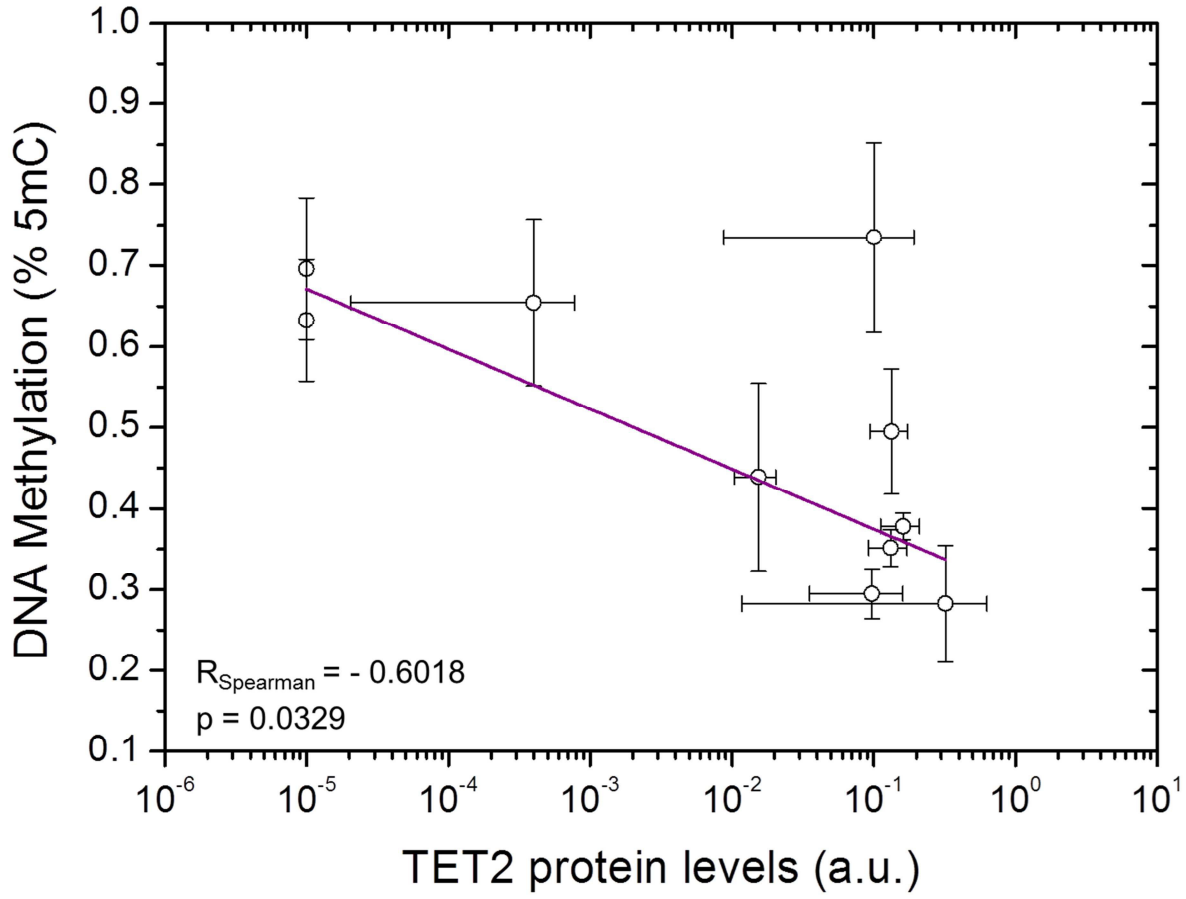

Figure 5-3: Basal global methylation and TET2 expression levels are anti-correlated in different cell lines. DNA of the indicated cell lines was isolated or whole proteins were prepared and global DNA methylation (A) and TET2 expression levels (B) were quantified using an ELISA-based colorimetric assay or SDS-PAGE and Western analysis, respectively. Numbers of biological and technical replicates for each cell line are listed in Table 5-1. A) DNA methylation is shown as percentage of 5mC in total DNA for different cell lines (the name of a certain cell line is indicated in the respective column) in descending order. Grey columns: Cells showing high DNA methylation. Green columns: cells showing low DNA methylation. B) TET2 expression was normalized to the expression of a housekeeping gene. Different cells are shown in ascending order. Color coding is adopted from A. C) Basal 5mC levels plotted as a function of TET2 protein expression of the cell lines depicted in A and B reveals strong anticorrelation of TET2 expression and basal 5mC levels ($R_{Spearman}$ = - 0.6018; p = 0.0329). Error bars: Standard error. ∗ = significantly different samples with p = 0.05. ∗∗ = significantly different samples with p = 0.01.

Cell line	5mC			TET2			5hmC		
	Levels	Number of replicates		levels	Number of replicates		levels	Number of replicates	
		Biological	Technical per biological replicate		Biological	Technical per biological replicate		Biological	Technical per biological replicate
WI-38	0.73 % ± 0.1	2	2	0.1 ± 0.09	3	2	0.024 % ± 0.002	2	2
NIH/3T3	0.7 % ± 0.09	2	2	not detectable	2	2	0.01 % ± 0.009	4	2
PBL	0.65 % ± 0.1	1	4	0.0004 ± 0.00038	1	2	0.02 % ± 0.004	1	4
HSPC	0.63 % ± 0.08	1	4	not detectable	1	2	0.03 % ± 0.003	1	4
U-2 OS	0.5 % ± 0.08	2	2	0.13 ± 0.04	2	2	0.007 % ± 0.002	4	2
HCT	0.44 % ± 0.1	4	2	0.02 ± 0.005	2	2	0.009 % ± 0.003	2	2
HeLa	0.38 % ± 0.02	2	2	0.16 ± 0.05	3	2	0.014 % ± 0.0005	2	2
AG	0.35 % ± 0.02	8	2	0.13 ± 0.04	3	2	0.015 % ± 0.004	5	2
MEF	0.29 % ± 0.03	5	2	0.1 ± 0.06	3	2	0.024 % ± 0.002	2	2
NFFhTert	0.28 % ± 0.07	2	2	0.32 ± 0.3	2	2	0.029 % ± 0.009	2	2

Table 5-1: Global 5mC, TET2 and 5hmC levels in different cell lines and biological and technical replicates used for their analysis. Global 5mC, 5hmC and TET2 expression levels were analyzed in different cell lines as explained in Figure 5-3 and Figure 5-4. Mean 5mC, TET2 and 5hmC levels and corresponding biological and technical replicates investigated for each cell line are shown. 5mC, 5hmC and TET2 expression levels were analyzed in proliferating and confluent AG cells and were pooled since results showed non-statistically significant differences. Due to the scarce availability of healthy donor samples only one biological replicate with two technical replicates was analyzed for PBL and HSPC. TET2 levels represent normalized values. Error: standard error.

5.2.2 Basal DNA hydroxymethylation levels are not correlated to endogenous TET2 protein levels

Measurements of basal 5hmC levels in the aforementioned cell lines showed highest and lowest 5hmC levels for HSPC (0.03 % ± 0.003) and U-2 OS (0.007 % ± 0.002), respectively. Basal 5hmC levels in the other cell lines were between those two values (Table 5-1; Figure 5-4 A).

Comparison of DNA methylation and hydroxymethylation in the analyzed cell lines (Figure 5-4 A) suggested an anti-correlation for cells of the "low DNA methylation levels" group (U-2 OS, HCT, HeLa, AG, MEF and NFFhTert), while no correlation between 5mC and 5hmC levels could be found for the cells of the "high DNA methylation levels" group (WI-38, NIH/3T3, PBL and HSPC). Plotting 5hmC levels as a function of TET2 expression levels (Figure 5-4 B) revealed no correlation between the two features ($R_{Spearman} = -0.0671$; $p = 0.427$).

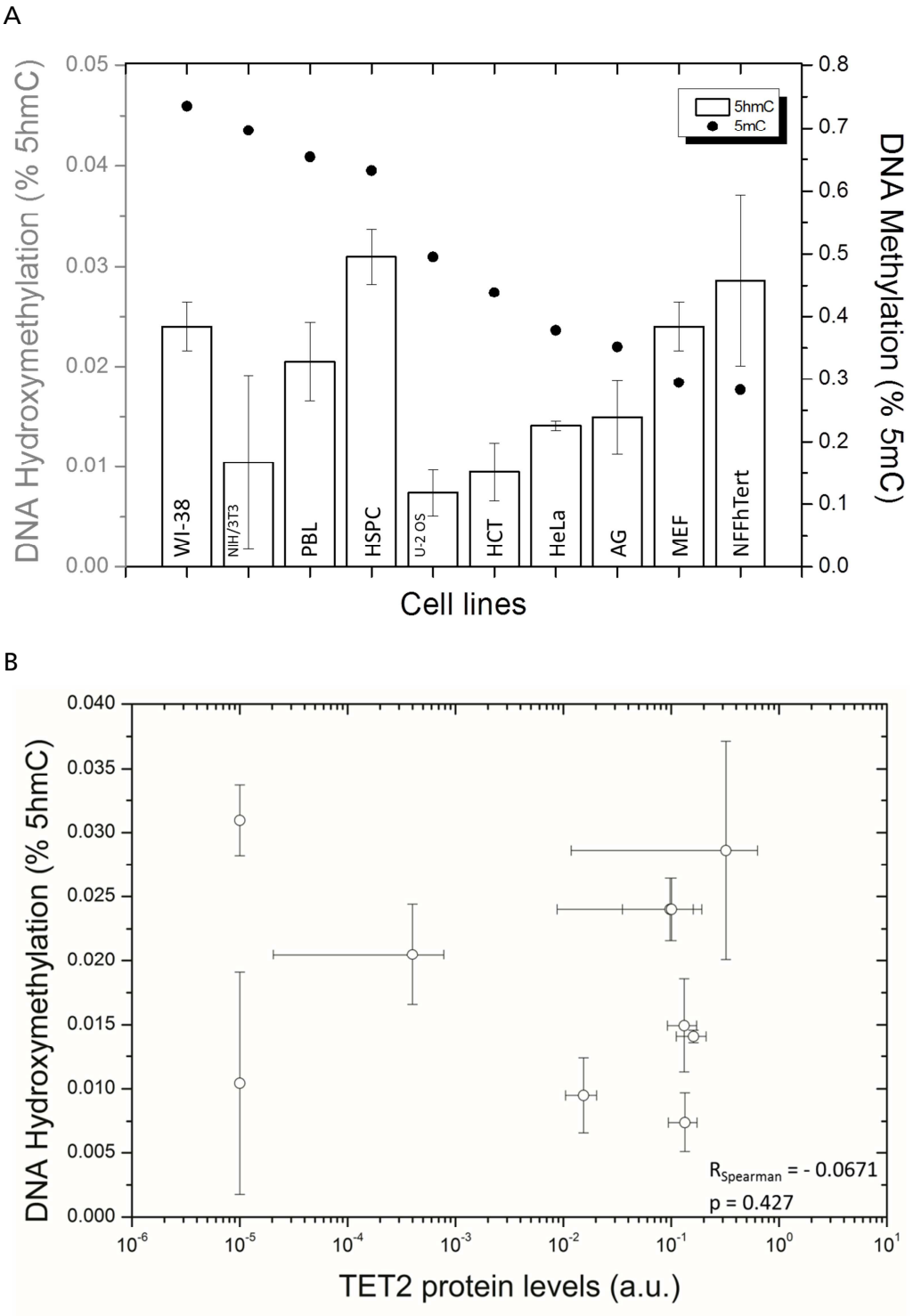

Figure 5-4: Comparison of basal global 5mC and 5hmC levels as well as TET2 expression of different cell lines. Genomic DNA was isolated from the indicated cell lines (the name of a certain cell line is indicated in the respective column), global 5hmC levels were analyzed and results were compared to basal 5mC levels (A) or TET2 expression (B). Number of biological and technical replicates for each cell line are listed in Table 5-1. A) 5hmC levels (white columns) are shown as percentage of 5hmC in total DNA in the order of descending 5mC levels (black circles). C) Basal 5hmC levels plotted as a function of TET2 protein expression of the cell lines depicted in A reveal no correlation of TET2 expression and basal 5mC levels.

These results show that global 5mC and 5hmC levels as well as TET2 expression are highly variable in different cell lines. While 5mC levels and changes after IR can be investigated

using colorimetric analysis, analysis of endogenous 5hmC levels and 5hmC changes in response to IR are challenging due to low 5hmC abundance. Therefore, in further experiments, global methylation changes were investigated in cells where TET2 catalytic domain was overexpressed and where increased 5hmC levels were anticipated. For this purpose, NIH/3T3 cells as a cell line without TET2 protein (Figure 5-3 B) were chosen as the experimental system. Expression of TET2 catalytic domain in cells without endogenous TET2 further has the advantage that DNA methylation changes can be directly linked to TET2 enzymatic function.

5.3 DNA hydroxymethylation levels are positively correlated to expression levels of ectopically expressed TET2 catalytic domain in a time-dependent manner

In a first experiment analyzing global 5hmC abundance, it was investigated whether the catalytic domain alone is capable of converting 5mC to 5hmC. Therefore, nuclear 5hmC and TET2CD-GFP signal intensities were analyzed microscopically. Clear fluorescence intensity differences of 5hmC and TET2CD-GFP signal could be detected between TET2CD-GFP transfected and non-transfected samples. Namely, cells with high TET2CD-GFP expression level also showed high 5hmC levels (Figure 5-5, lower row) whereas un-transfected cells showed low 5hmC levels (Figure 5-5, upper row).

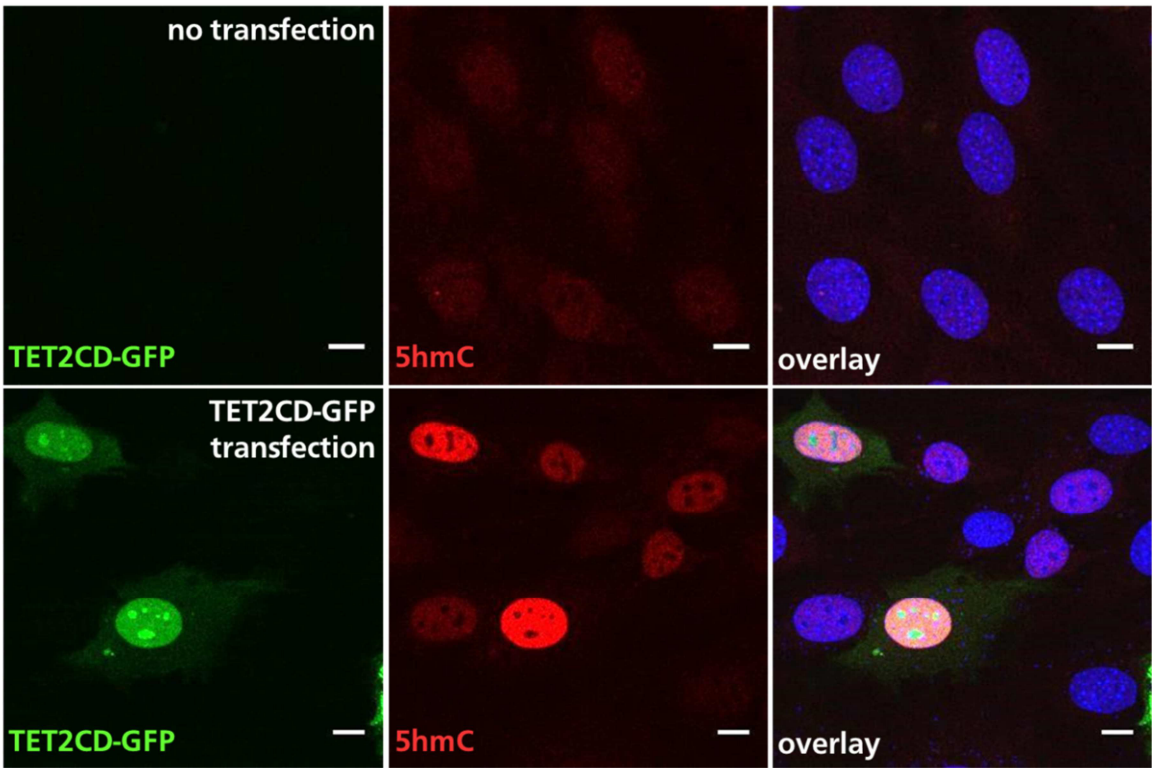

Figure 5-5: TET2 catalytic domain is expressed in NIH/3T3 and is positively correlated to DNA hydroxymethylation levels. In un-transfected or TET2CD-GFP-transfected NIH/3T3 cells, DNA denaturation with 2 N HCl and fixation with paraformaldehyde was performed 24 or 48 hours after transfection. Finally, samples were stained against 5hmC and analyzed microscopically. 24 hours after transfection, TET2CD-GFP expression (lower row; green) leads to a clear increase in 5hmC signal (red) whereas un-transfected cells (upper row) show no GFP and little if none 5hmC signal (red). Scale bar: 10 µm.

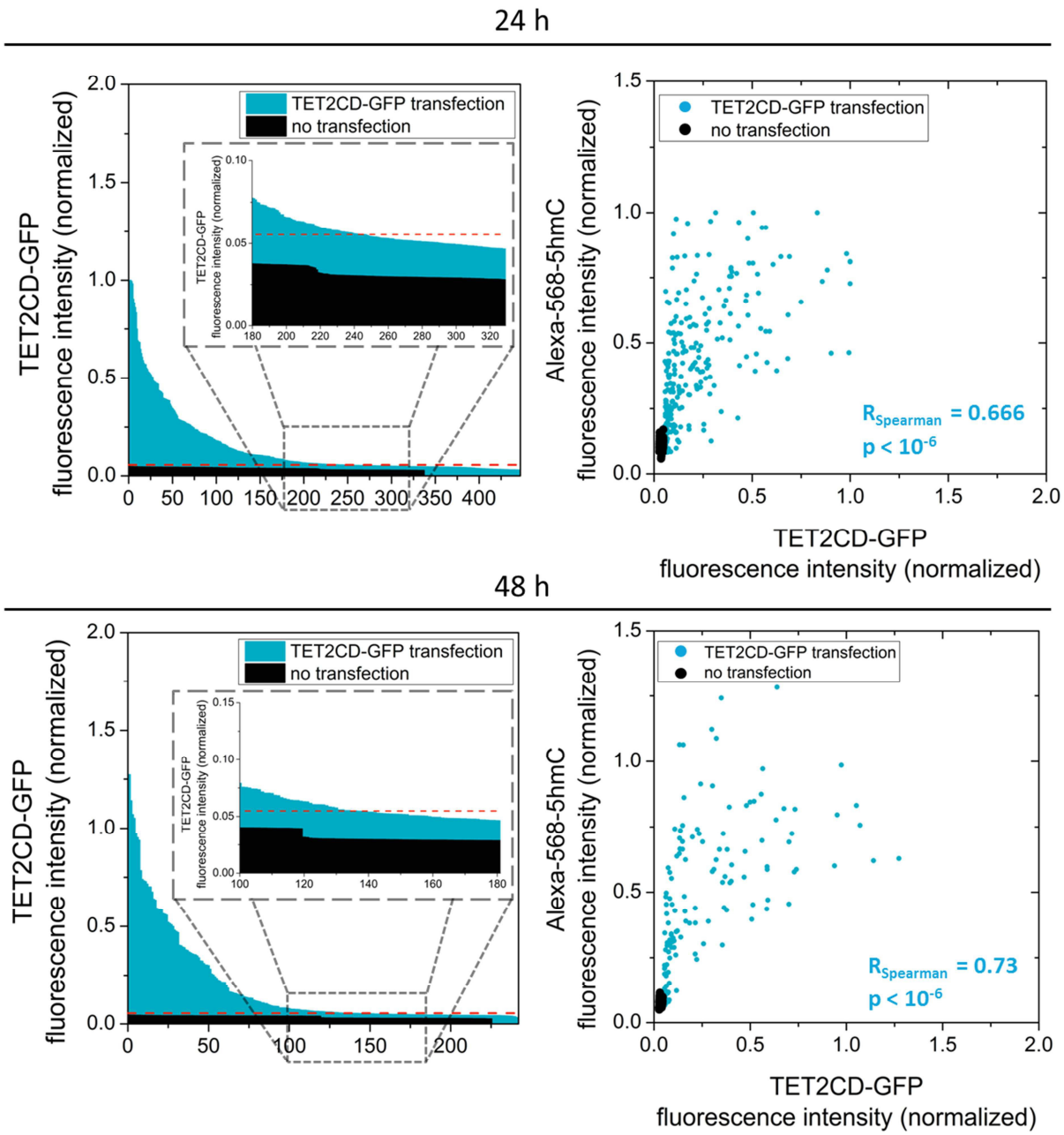

Figure 5-6: DNA hydroxymethylation levels of NIH/3T3 cells are positively correlated to the expression levels of ectopically expressed TET2 catalytic domain in a time-dependent manner. NIH/3T3 cells were treated as in Figure 5-5. Nuclear fluorescence intensities of 5hmC and GFP were determined microscopically and intensity values were normalized so that different experiments (independent transfections) could be combined. To this purpose, the highest 5hmC as well as the highest GFP fluorescence intensity values in transfected samples incubated for 24 hours in different experiments were set to one. All the other values were converted relative to these values and normalized values of all experiments were sorted according to their GFP fluorescence intensity in a descending order (top- and bottom-left; x-axis: number of cells analyzed in total). A threshold was set 3 x standard deviation above the mean GFP fluorescence intensity of un-transfected cells (dashed red line, top- and bottom-left; magnified in the inlay). Fluorescence intensity values above the threshold were considered as "GFP-positive". Top- and bottom-right: 5hmC fluorescence intensities from GFP-positive cells are plotted as a function of their corresponding GFP fluorescence intensities (blue circles). In contrast to un-transfected cells (black circles), 5hmC fluorescence intensities increase with increasing GFP fluorescence intensities. Results for TET2CD-GFP transfection and no transfection (24 hours) are from 3 independent experiments while results for TET2CD-GFP transfection and no transfection (48 hours) are from two independent experiments. Up to 160 cells were analyzed in each experiment.

In order to quantify 5hmC fluorescence signal intensities upon transfection, up to ~160 cells per experiment were imaged. Nuclear 5hmC and TET2CD-GFP fluorescence signal intensities were measured using ImageJ (chapter 3.4.6.1) and intensity values were normalized so that different experiments could be combined. GFP background fluorescence intensities were defined for both time points and a threshold was set (Figure 5-6 first figure in both rows, dashed red line). For further experiments, only those cells in transfected samples with GFP fluorescence intensities higher than the threshold were considered GFP-positive and were taken into account. Based on that, ~55 % of TET2CD-GFP transfected cells were GFP-positive after 24 hours of incubation and transfection efficiency was ~57 % after 48 hours.

Nuclear 5hmC fluorescence signal intensities were plotted as a function of GFP fluorescence signal intensities in GFP-positive cells, revealing a positive correlation between the 5hmC mark and the expression of the catalytic domain of TET2 (Figure 5-6, right, blue circles). The effect was comparable in samples transfected for 24 ($R_{Spearman} = 0.666$, $p < 10^{-6}$) or 48 hours ($R_{Spearman} = 0.734$, $p < 10^{-6}$). If TET2CD-GFP expression was high, also high 5hmC levels could be observed. However, a relatively low TET2CD-GFP expression led to large variations in 5hmC fluorescence signal intensity. Furthermore data points for transfected samples were slightly more spread after 48 hours, adopting higher values for GFP as well as 5hmC fluorescence intensities. In un-transfected cells, GFP and 5hmC intensities remained unvaried at low levels up to 48 hours (Figure 5-6, right, black circles). Overall, the overexpression of TET2 catalytic domain in NIH/3T3 cells, which lack endogenous TET2 protein, induces the conversion of 5mC in 5hmC.

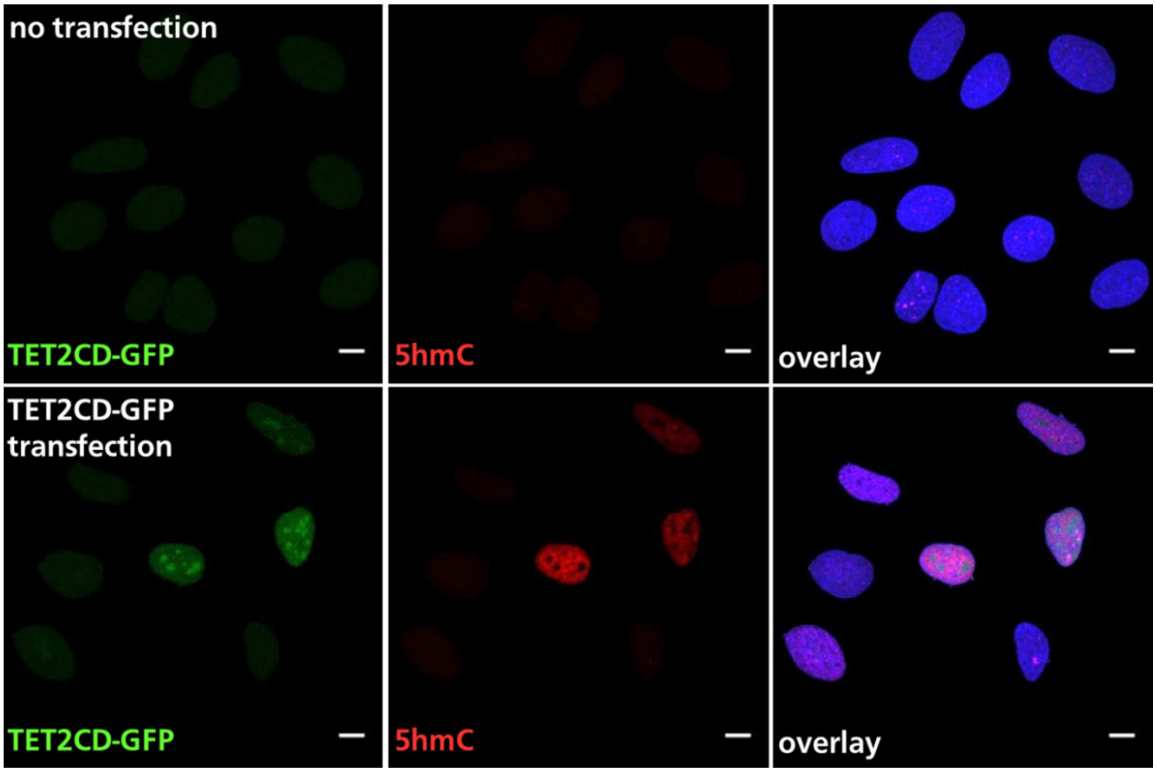

Figure 5-7: TET2 catalytic domain is expressed in U-2 OS cells and is positively correlated to DNA hydroxymethylation levels. U-2 OS un-transfected or TET2CD-GFP transfected cells were treated as in Figure 5-5 and then analyzed microscopically. 24 hours after transfection, TET2CD-GFP expression (lower row; green) leads to a clear increase in 5hmC signal (red), while un-transfected cells (upper row) show little if none GFP (green) and 5hmC signal (red). Scale bar: 10 µm.

The experiment was repeated in U-2 OS cells expressing TET2 at high levels (Figure 5-3 B). Un-transfected U-2 OS cells were compared to cells transfected for 24 or 48 hours with TET2 catalytic domain.

Also in U-2 OS cells, distinct intensity differences of 5hmC and TET2CD-GFP fluorescence signal could be observed between TET2CD-GFP transfected and un-transfected samples. Namely, cells with strong GFP fluorescence signal and therefore with high expression of ectopically expressed TET2 catalytic domain display high 5hmC fluorescence signal intensities (Figure 5-7, lower row). In contrast 5hmC and GFP fluorescence intensities were low in un-transfected cells (Figure 5-7, upper row).

TET2CD-GFP and 5hmC nuclear fluorescence intensities were quantified from pictures of up to ~120 cells per sample per experiment using ImageJ (chapter 3.4.6.1). As for NIH/3T3 cells, intensity values were normalized, GFP background fluorescence intensities were defined and a threshold was set. For further experiments, only those cells in transfected samples with GFP fluorescence intensities higher than the threshold were considered GFP-positive and were taken into account. Based on that, ~64 % of TET2CD-GFP transfected cells were GFP-positive after 24 hours of incubation while transfection efficiency was ~81 % after 48 hours.

As for NIH/3T3 cells, nuclear 5hmC fluorescence signal intensities were plotted as a function of GFP fluorescence signal intensities in GFP-positive cells, revealing a positive correlation between the 5hmC mark and the expression of the catalytic domain of TET2 (Figure 5-8, right, blue circles). The effect was strong in samples transfected for 24 hours ($R_{Spearman} = 0.6, p < 10^{-6}$) and moderate in samples transfected for 48 hours ($R_{Spearman} = 0.485, p < 10^{-6}$). In un-transfected cells, GFP and 5hmC intensities remained unvaried at low levels up to 48 hours (Figure 5-8, right, black circles). It is interesting to note that GFP fluorescence signal intensities further increase in TET2CD-GFP transfected cells after 48 hours, while 5hmC intensities do not increase simultaneously. The effect is also mirrored in an only moderate correlation after 48 hours. This might indicate a further TET2 mediated conversion of 5hmC that is fast enough to produce downstream metabolites (5fC and 5caC) within 48 hours. Independent on that, this experiment shows that the overexpression of TET2 catalytic domain in U-2 OS cells, expressing endogenous TET2 at high levels, induced the conversion of 5mC to 5hmC.

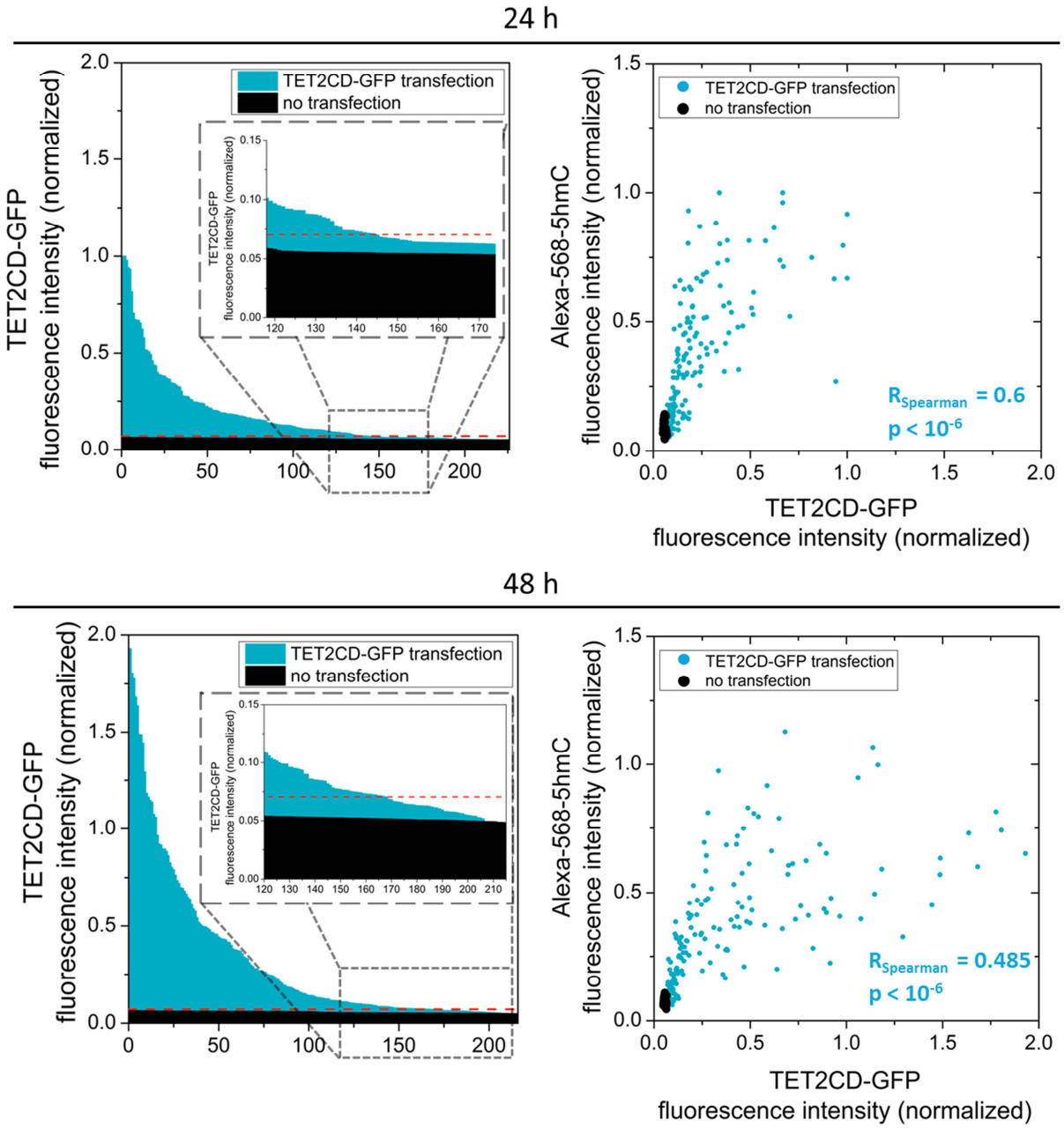

Figure 5-8: DNA hydroxymethylation levels of U-2 OS cells are positively correlated to the expression levels of ectopically expressed TET2 catalytic domain in a time-dependent manner. U-2 OS cells were treated as in Figure 5-5. Nuclear fluorescence intensities of 5hmC and GFP were determined microscopically and intensity values were normalized as described in Figure 5-6. Normalized values of all experiments were sorted according to their GFP fluorescence intensity in a descending order (top- and bottom-left; x-axis: number of cells analyzed in total). A threshold was set 3 × standard deviation above the mean GFP fluorescence intensity of un-transfected cells (dashed red line, top- and bottom-left, magnified in the inlay). Fluorescence intensity values above the threshold were considered as "GFP-positive". Top- and bottom-right: 5hmC fluorescence intensities of GFP-positive cells are plotted as a function of their corresponding GFP fluorescence intensities (blue circles). Although expressing endogenous TET2, un-transfected cells (black circles) did not show significant changes of 5hmC fluorescence intensities, compared to transfected cells where 5hmC fluorescence intensities increase with increasing GFP fluorescence intensities. Results for all samples are from 2 independent experiments and up to 120 cells were imaged per experiment.

In the previous experiment TET2CD-GFP transfected cells were compared to un-transfected (medium-exchange) cells. To exclude an effect of the transfection reagent on changes of 5hmC levels, mock-transfected (treated with transfection reagent only) and un-transfected (control) NIH/3T3 and U-2 OS cells were compared. For control cells a medium exchange was performed before incubating cells for 24 or 48 hours. Next, cells were treated as described above, stained against 5hmC and analyzed microscopically. Comparison was performed on normalized values.

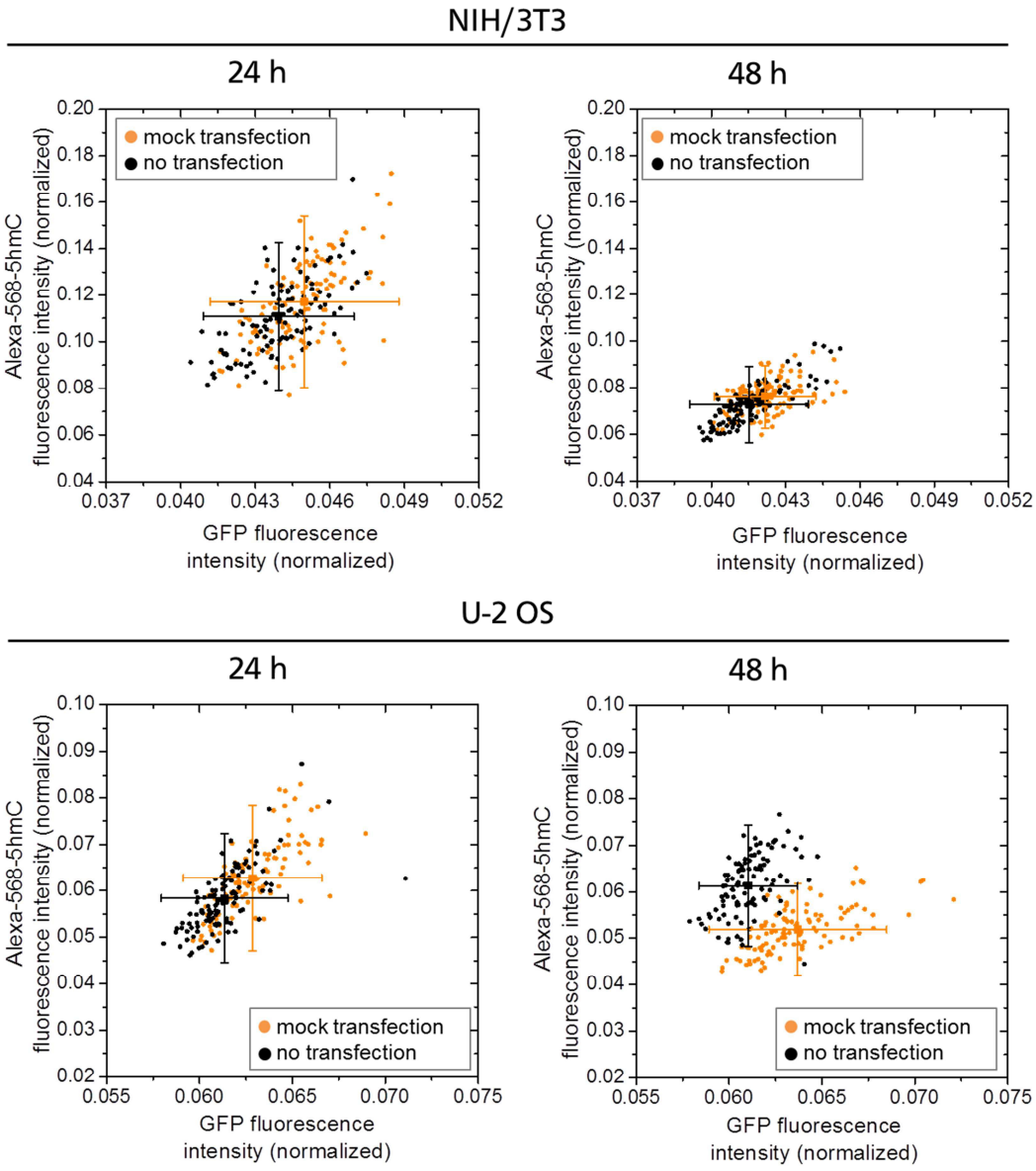

Figure 5-9: The effect of mock-transfection on 5hmC signal is negligible. Un-transfected (black circles) or mock-transfected (orange circles) NIH/3T3 and U-2 OS cells were treated as in Figure 5-5. Nuclear fluorescence intensities of 5hmC and GFP were determined and intensity values were normalized. To this purpose, all values were converted relative to the same values as for the comparison of TET2CD-GFP transfected and un-transfected cells (Figure 5-6 and Figure 5-8). Mean and standard deviation were calculated for each dataset. If the mean of one data set was within the range of two times the standard deviation (error bars) of the other data set (which approximately corresponds to a 95% confidence interval), then the two datasets were considered to be in agreement and not as statistically different. Transfection itself has no influence on 5hmC and GFP background signals after 24 (upper- and lower-left) and 48 (upper- and lower-right) hours in NIH/3T3 and U-2 OS. For each dataset around 100 cells were imaged.

Nuclear 5hmC fluorescence signal intensities were plotted as a function of GFP fluorescence signal intensities in mock-transfected (Figure 5-9; orange circles) and un-transfected (Figure 5-9; black circles) NIH/3T3 and U-2 OS cells for both time points. Mean 5hmC and GFP fluorescence intensity values and their respective standard deviations were calculated for all data sets. If the mean of one data set was within the range of two times the standard deviation of the other data set (which approximately corresponds to a 95 % confidence interval), then the two datasets were considered to be in agreement and not as statistically different.

The analysis of NIH/3T3 and U-2 OS cells revealed that transfection itself had no effect on nuclear 5hmC and GFP fluorescence intensities after 24 and 48 hours incubation. Both datasets of the two different samples show similar distributions.

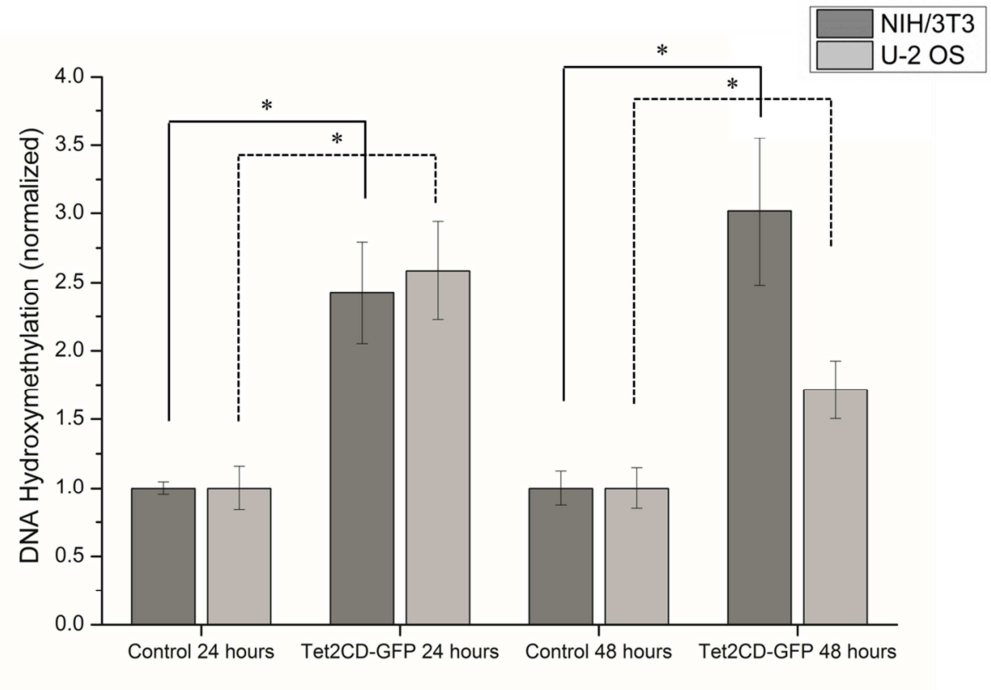

Figure 5-10: DNA hydroxymethylation levels are positively correlated to ectopically expressed TET2 catalytic domain levels. TET2CD-GFP was overexpressed in NIH/3T3 (dark grey columns) and U-2 OS cells (light grey columns), DNA was isolated and 5hmC levels were analyzed 24 and 48 hours after transfection using colorimetric ELISA-based analysis. For all samples one biological replicate with two technical replicates was used. In all cases, 5hmC levels increased in response to TET2CD-GFP overexpression. Error bar: standard error of the mean. *: significantly different samples with p = 0.05.

It was shown by immunofluorescence analysis that TET2 catalytic domain alone is capable of converting 5mC to 5hmC in two different cellular systems. This was confirmed using colorimetric ELISA-based analysis (chapter 3.6). Therefore TET2CD-GFP was overexpressed in NIH/3T3 as well as in U-2 OS cells. As in the previous experiment, samples were compared to un-transfected controls. After incubation of 24 and 48 hours, genomic DNA from transfected or un-transfected samples was isolated and global 5hmC levels were measured (chapter 3.6.1 and 3.6.2). Results were normalized to 5hmC levels in un-transfected control cells.

As shown in Figure 5-10, 5hmC amount increases in transfected specimens. Such effect is time- and cell line-dependent. Specifically, NIH/3T3 cells (dark grey columns) showed a 2.4- and 3-fold increase of 5hmC levels after 24 and 48 hours, respectively. Differently, in U-2 OS cells (light grey columns), 5hmC levels peaked after 24 hours (2.6-fold increase), and were reduced after 48 hours incubation (1.7-fold increase). These results confirm what was shown in in the experiment using immunostaining and microscopical analysis (Figure 5-6 and Figure 5-8). Namely, while 5hmC fluorescence intensities in NIH/3T3 cells increased 48 hours after transfection, they do not change in U-2 OS cells.

It has to be noted that under such experimental conditions, where a global increase of 5hmC was expected due to ectopically increased TET2 enzymatic activity, the assessment of 5hmC levels by the ELISA-based colorimetric assay produced reliable results.

5.3.1.1 TET2CD-GFP accumulates in nucleoli

Microscopical analysis of TET2CD-GFP transfected in NIH/3T3 and U-2 OS cells revealed that in those cells where expression of TET2 catalytic domain was pronounced, TET2CD-GFP accumulated in sub-nuclear regions corresponding to nucleoli. To confirm this, NIH/3T3 and U-2 OS cells transfected with TET2CD-GFP were stained against nucleolin, which localizes to dense fibrillar regions of the nucleolus. Co-staining with nucleolin (Figure 5-11) revealed co-localiation of nucleolin with TET2CD-GFP, thus confirming the TET2CD-GFP localization to nucleoli in both NIH/3T3 (Figure 5-11 A, lower row) and U-2 OS cells (Figure 5-11 B, lower row).

A

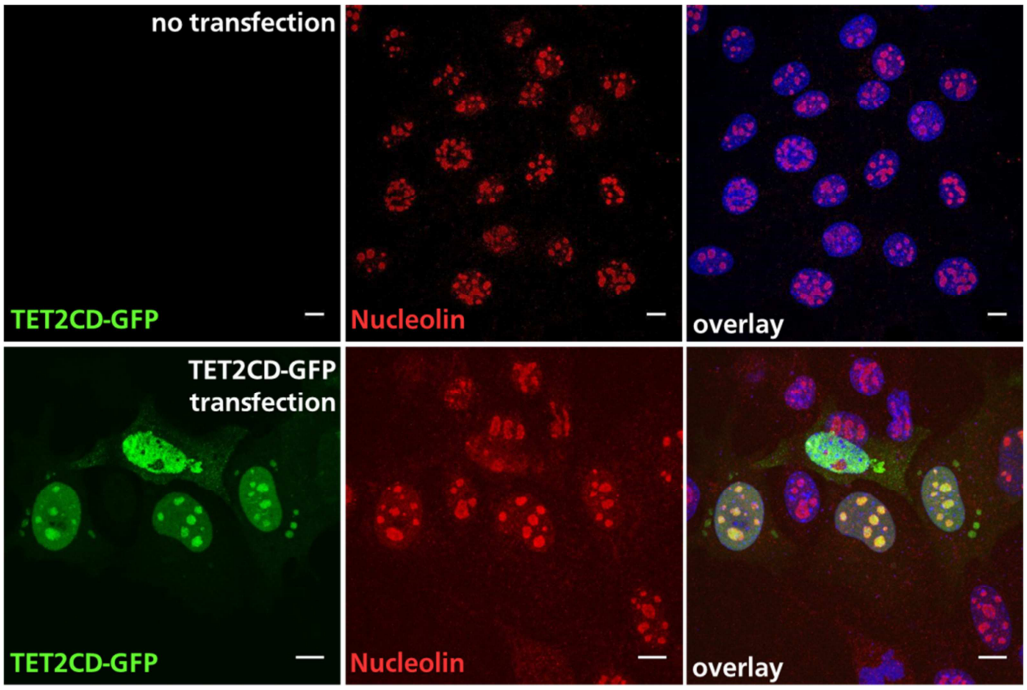

Caption see next page

Figure 5-11 continued

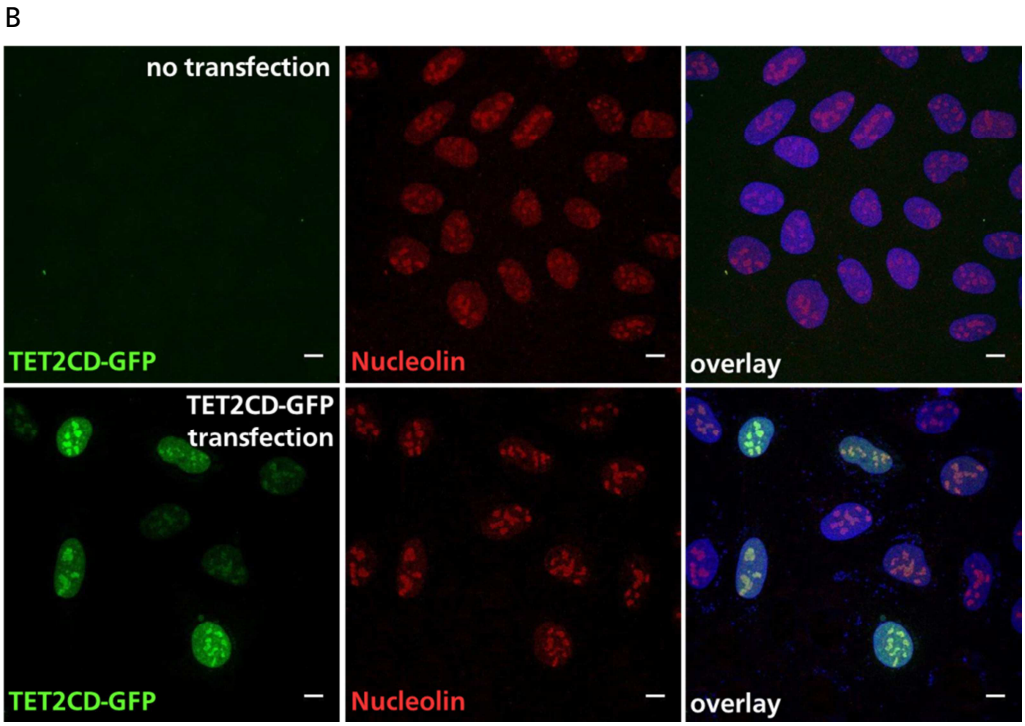

Figure 5-11: TET2 catalytic domain accumulates at nucleoli. Un-transfected (A and B upper row) or TET2CD-GFP transfected (A and B lower row) NIH/3T3 and U-2 OS cells were fixed with paraformaldehyde 24 hours after transfection and stained against nucleolin (red). DNA was stained with DAPI and is shown in blue. Samples were analyzed microscopically. TET2CD-GFP (green) co-localizes with nucleolin (red) in TET2CD-GFP transfected NIH/3T3 (A, lower row) and U-2 OS (B, lower row). Scale bar: 10 µm.

5.3.1.2 Verification of TET2CD-GFP expression

The expression of ectopic TET2CD-GFP was verified using Western analysis (Figure 5-12). Whole protein lysates from NIH/3T3 and U-2 OS cells were prepared 24 hours after transfection with TET2CD-GFP. Western analysis for GFP was performed as indicated in chapters 3.5.3 and 3.5.4. Actin was employed as loading control (lower lanes). Un-transfected NIH/3T3 and U-2 OS cells (lane 1 and 3) do not express TET2CD-GFP while NIH/3T3 and U-2 OS transfected with TET2CD-GFP display GFP signal (lane 2 and 4). The expected size of TET2CD-GFP protein is around 130 kDa and clear bands could be observed at this height for the transfected samples.

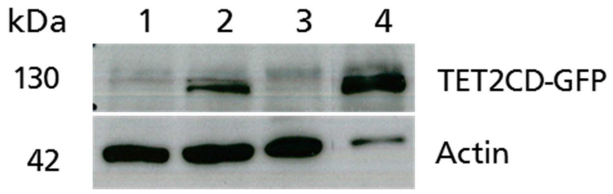

Figure 5-12: Verification of TET2CD-GFP expression in NIH/3T3 and U-2 OS cells. 24 hours after transfection of NIH/3T3 and U-2 OS cells with TET2 catalytic domain whole protein lysates were prepared and GFP was detected by Western analysis. TET2CD-GFP is expressed in transfected NIH/3T3 (lane 2) as well as in transfected U-2 OS cells (lane 4), while un-transfected cells do not show TET2CD-GFP expression (NIH/3T3: lane 1; U-2 OS: lane 3). Actin was used as a loading control.

In conclusion, results shown in chapter 5.3 reveal that TET2 catalytic domain alone is functional in different cellular systems, being able to convert 5mC to 5hmC. This was demonstrated using immunostaining and microscopical analysis and was confirmed using ELISA-based colorimetric techniques. Furthermore, it was shown that transfection reagent itself had no influence on changes of GFP and 5hmC fluorescence intensities in the cellular systems analyzed. Those results provide a good basis for the examination of methylation changes in response to IR and the involvement of TET2 in the DNA damage response (DDR).

5.4 Expression of TET2 catalytic domain concomitant to IR contribute to formation of 5hmC

Following the establishment of the experimental system, it was investigated whether IR had an influence on 5hmC formation in presence or absence of TET2 enzymatic activity. For this purpose NIH/3T3 cells, which lack endogenous TET2, were chosen. The advantage is that the effect of irradiation can be measured independent on TET2 function as well as in addition to TET2 function.

Since 5mC levels can be measured by flow cytometry (see for example [Milutinovic et al., 2003]), a protocol allowing the analysis of 5hmC levels within the cells was established, which will make the analysis faster compared to microscopical techniques and will allow analysis of a higher number of cells in parallel.

For the experiment, cells were treated as depicted in Table 5-2. For each sample >20000 cells were analyzed.

	Control	TET2CD	IR	TET2CD+IR
TET2-GFP transfection	-	+	-	+
Irradiation (10 Gy X-rays)	-	-	+	+

Table 5-2: Different treatment conditions analyzed in the experiment. Un-transfected, mock-irradiated NIH/3T3 cells (Control) were compared to TET2CD-GFP transfected, mock-irradiated (TET2CD), un-transfected, irradiated (IR) and TET2CD-GFP transfected, irradiated NIH/3T3 cells (TET2+IR).

24 hours after transfection the cells were irradiated/mock-irradiated and harvested 30 minutes afterwards. Then, GFP, 5hmC and γH2AX amount was measured by flow cytometry. For interpretation, compensation was performed and cells were gated to exclude cell debris and aggregates.

Mean GFP fluorescence intensity was upregulated in sample “TET2CD” (mean: 85.3) and “TET2CD+IR” (mean: 79.3) compared to “control” (mean: 1.8) and “IR” (mean: -4.4[1]), showing that ectopic TET2CD-GFP was expressed. The effect of TET2CD-GFP transfection and irradiation on 5hmC and γH2AX amount is illustrated in Figure 5-13 and median 5hmC and γH2AX fluorescence intensity values as well as relative changes are shown in Table 5-3. 5hmC fluorescence intensity was low in control samples (median: 5.7) and slightly increased with transfection of TET2 catalytic domain (median: 7.2). Compared to control cells, almost no

[1] Negative values are caused by compensation

change in 5hmC signal intensity was observed after irradiation alone (median: 6.3). If cells transfected with TET2 were irradiated, a clear increase in 5hmC fluorescence intensity (median: 19.6) was detected. At the same time, γH2AX fluorescence intensity increased from low levels in control samples (median: 4.2) to intermediate levels in transfected cells (median: 7.6). As expected, levels for either irradiated samples showed a further increase compared to "TET2CD", and similar median values (median: 18.3 and 18.1).

These results indicate that transfection of TET2 catalytic domain together with the exposure to IR contributes to 5hmC formation.

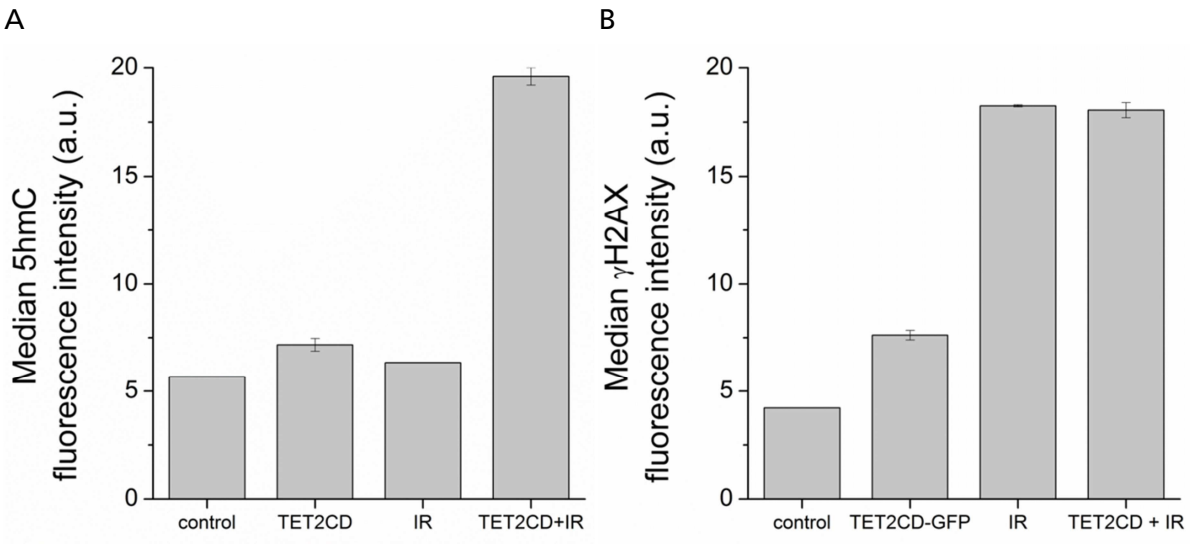

Figure 5-13: Irradiation together with transfection increases 5hmC accumulation. Un-transfected, unirradiated NIH/3T3 cells (control), were compared to NIH/3T3 cells transfected with TET2 catalytic domain (TET2CD), NIH/3T3 cells irradiated with 10 Gy X-rays (IR) and to TET2CD-GFP transfected NIH/3T3 cells irradiated with 10 Gy X-rays (TET2CD+IR) with regard to their 5hmC (A) and γH2AX fluorescence intensity (B). 24 hours after transfection medium was exchanged of "control" and "IR" sample, sample "IR" and "TET2CD+IR" were irradiated and all samples were harvested 30 minutes afterwards. Cells were stained against 5hmC and γH2AX. DNA was stained using DAPI and samples were analyzed by flow cytometry. For interpretation, compensation was performed and cells were gated to exclude cell debris and aggregates. Result for "control" is from one replicate, while results for the other samples are from two replicates. Error: standard error. Mean 5hmC and γH2AX fluorescence intensity values are depicted in Table 5-3.

	Median fluorescence intensity and relative changes	
	5hmC	γH2AX
Control	5.7	4.2
TET2CD-GFP	7.2 ± 0.3 (1.3)	7.6 ± 0.2 (1.8)
IR	6.3 ± 0.01 (1.1)	18.3 ± 0.1 (4.3)
TET2CD + IR	19.6 ± 0.4 (3.5)	18.1 ± 0.4 (4.3)

Table 5-3: Median 5hmC and γH2AX fluorescence intensity values and their relative changes. For the same experiment as in Figure 5-13 median 5hmC and γH2AX fluorescence intensity values are shown in control, TET2CD-GFP, IR and TET2CD+IR samples. Error: standard error. Fold changes compared to the control a depicted in brackets.

5.5 TET2 catalytic domain is recruited to damage sites induced by UV-Laser

For many enzymatic proteins, which are part of the repair pathways after irradiation, localization at the actual damage sites is shown (reviewed in [Polo and Jackson, 2011]). Since TET2 catalytic domain and IR, which induces local damage sites in the DNA, most likely contribute to 5hmC formation, it was investigated whether TET2CD-GFP is recruited to DNA damage sites. Since fast recruitment was expected, UV-laser irradiation and live cell microscopy was used first, which allows the observation at the time of irradiation.

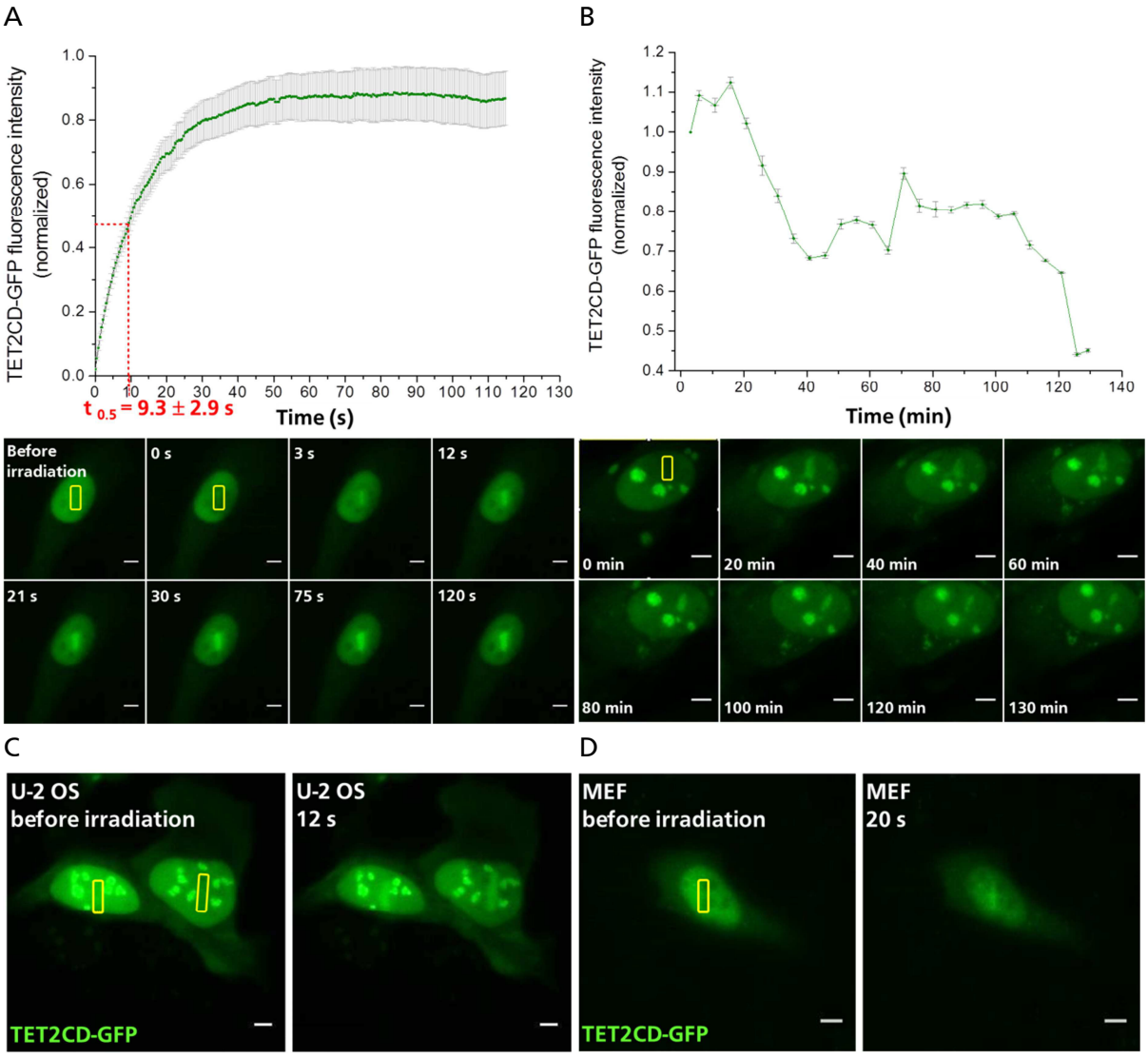

Figure 5-14: TET2CD-GFP is rapidly recruited at damages sites after UV-Laser irradiation. TET2CD-GFP transfected NIH/3T3, U-2 OS and MEF cells were UV-laser irradiated (laser wave length: 337 nm) 24 hours after transfection and short- (A, C, D) as well as long-term (B) observations were performed. A+B) Pictures in the bottom show exemplary cells and recruitment of TET2CD-GFP to damage sites (marked by a yellow box) at selected times up to ~120 seconds (A) or 130 minutes (B) after irradiation. Scale bar = 10µm. Error bars: standard error. A) N = 16 B) TET2-GFP fluorescence intensities were normalized setting the first measured value to one. All the other values were converted relative to this value. N = 1. Furthermore, recruitment of TET2CD-GFP to UV laser induced damage sites (yellow box) takes place in U-2 OS (C) and MEF (D) cells and exemplary pictures are shown for different time points. Scale bar = 5µm.

Short-term recruitment kinetics (Figure 5-14 A) revealed fast recruitment of ectopically expressed TET2CD-GFP to UV-Laser induced damage sites. Recruitment started immediately after irradiation with $t_{0.5}$ of 9.3 ± 2.9 seconds, reached a plateau region after ~50 seconds and remained stable until the end of the image acquisition (~120 seconds after irradiation).

Long-term observations were performed (chapter 3.3.4) over two hours. As depicted in Figure 5-14 B, TET2CD-GFP intensity at the irradiated site reached a maximum 15 to 20 minutes after irradiation and steadily decreased thereafter. At the end of the observation TET2CD-GFP intensity was ~45 % of the starting intensity and ~40 % of the maximum intensity.

Short-term recruitment of TET2 catalytic domain to UV laser induced damage sites was also investigated in U-2 OS and MEF cells (Figure 5-14 C and D). U-2 OS and MEF cells were treated as stated above and similar to NIH/3T3 cells fast recruitment of ectopically expressed TET2CD-GFP to UV-Laser induced damage sites was observed.

Fast recruitment of TET2CD-GFP supports the hypothesis that TET2 is involved in early DNA methylation changes after irradiation. Its persistence at damage sites indicates TET2 function at time points up to at least two hours post-IR.

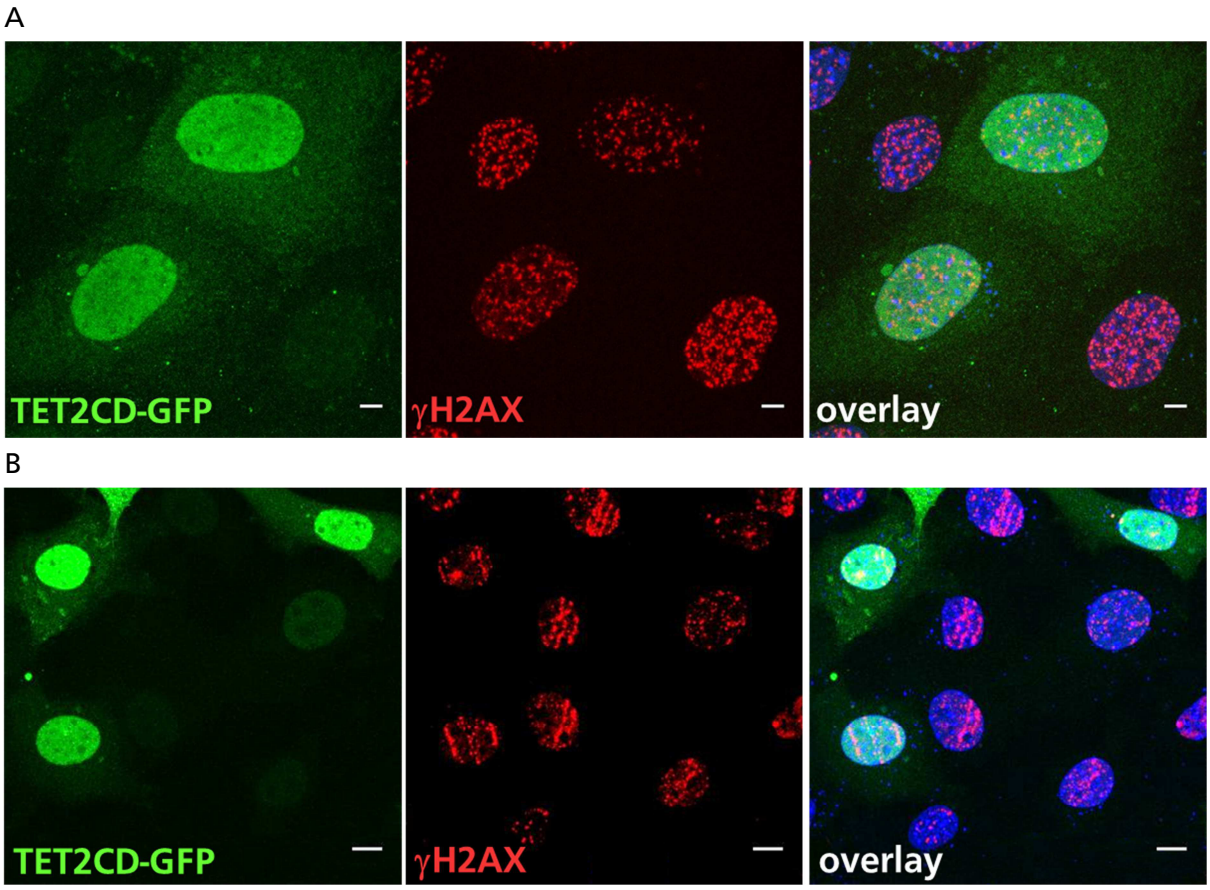

Figure 5-15: TET2 catalytic domain is not recruited to damage sites induced by X-rays and to ion induced damage sites. A) NIH/3T3 cells were irradiated with X-rays (2 Gy) or (B) ^{56}Fe ions (LET: 148 kev/µm; fluence: 4.0 x 10^6 particles/cm^2) under a low angle 24 or 30 hours after TET2CD-GFP transfection. Cells were fixed 30 minutes (X-rays) or respectively 15 minutes and 1 hour (ions) after irradiation and stained against γH2AX (red). DNA was stained with DAPI and is shown in blue. Microscopical analysis revealed no TET2CD-GFP (green) recruitment to ion induced damage sites at no time point. Scale bar = 5 µm (A), 10 µm (B).

Recruitment of TET2 catalytic domain was also analyzed in TET2CD-GFP transfected NIH/3T3 cells after irradiation with 2 Gy X-rays and iron ions (LET: 148 kev/μm; fluence: 4.0 x 10^6 particles/cm^2). In both cases γH2AX staining was used as a marker for DSBs. However TET2CD-GFP recruitment to DSBs was neither observed after irradiation with X-rays nor to ion-induced damage sites for all investigated time points (Figure 5-15).

Since TET2CD-GFP expression leads to brightly stained whole nuclei, which could mask a faint recruitment of the construct at damage sites after X-ray and ion irradiation, it was investigated whether recruitment of the endogenous protein at damage sites can be seen.

5.6 Recruitment of TET2 to damage sites

5.6.1 Endogenous TET2 is recruited to damage sites induced by heavy ions

Looking for the endogenous enzyme a cell line with high TET2 expression, namely AG cells, was chosen. Furthermore, AG cells were proliferating to analyze TET2 recruitment in all cell cycle phases, to see whether TET2 recruitment takes place in a cell cycle dependent manner.

TET2 recruitment to heavy ion induced damage sites was analyzed after irradiation with high LET gold ions at different times after irradiation (five to 10 minutes, 30 minutes, one hour and three hours). Furthermore, it was investigated whether TET2 co-localizes with γH2AX, a specific marker for DSBs, to get insights into whether TET2 is involved in the repair of DSBs. Therefore a specific antibody against γH2AX was used. Microscopical analysis revealed recruitment of endogenous TET2 to damage sites at each time point analyzed, showing co-localization of TET2 with γH2AX.

In Figure 5-16 B, an exemplary image shows co-localization of TET2 and γH2AX 30 minutes after irradiation and is compared to unirradiated cells, where TET2 co-localizes with γH2AX at replication-related foci (Figure 5-16 A).

To analyze co-localization of TET2 with γH2AX more in detail, co-localization was further analyzed using intensity profiles (Figure 5-16 C), implemented in the ImageJ macro "RGBProfilesTool". Fluorescence intensities of TET2 (green line), γH2AX (red line) and DNA (blue line) were depicted along the ion trajectory (Figure 5-16 B; white line in the overlay), indicating co-localization of TET2 and γH2AX. At most sites, where γH2AX accumulation is increased (peaks in the line profile), also TET2 could be detected to a higher degree.

To verify co-localization of TET2 with γH2AX, intensity correlation analysis (ICA) was performed using the ICA plugin for ImageJ (Tony Collins; Wright Cell Imaging Facility, Toronto, Canada). In Figure 5-16 D, exemplary ICA plots are displayed where fluorescence intensity is shown as a function of PDM values. The horizontal line represents the value of mean fluorescence signal intensities and colors represent the frequencies of the different intensities. The PDM is the product of the difference from the mean and is calculated by the equation $PDM = (A-a)\,(B-b)$, where A is the fluorescence intensity of the pixel in the first channel and B the fluorescence intensity of the pixel in the second channel, while a and b are the mean fluorescence intensities of the respective channels. If the fluorescence signals of the two channels are positively correlated, pixel intensities in the first channel and in the second channel vary in synchrony, meaning that if the pixel intensity in channel one (A) is above/below its mean (a) then the intensity of the corresponding pixel in channel two (B) is also above/below its mean (b). This will result in a positive PDM value. If the two signals are

anti-correlated instead, meaning that *A* is above mean while *B* is below mean (or vice versa), then their PDM values will be negative. Therefore in ICA plots showing an hourglass-shape, the correlation is random. The relationship between two signals can be further described by the ICQ value, which is equal to the ratio of the number of positive PDM values to the total number of pixel values ($ICQ = N_{pos.PDM} / N_{total}$). ICQ values are distributed between – 0.5 and + 0.5 subtracting 0.5 from this value. Therefore the ICQ value is defined by $ICQ = (N_{pos.PDM} / N_{total}) - 0.5$. Therefore, if the correlation is random then ICQ = ~0, if the two signals are anti-correlated then $0 > ICQ \geq -0.5$, and if the two signals are correlated then $0 < ICQ \leq 0.5$.

As demonstrated in Figure 5-16 D, TET2 PDM values increased with increasing fluorescence intensity (left figure). The effect was less pronounced for γH2AX (right figure), where many PDM values were scattered around zero. However, most PDM values were positive for both channels, and ICQ value was 0.23 ± 0.01. In conclusion, TET2 and γH2AX displayed moderate positive correlation at ion induced damage sites ($R_{Pearson} = 0.39 \pm 0.04$; $p = 0.036$).

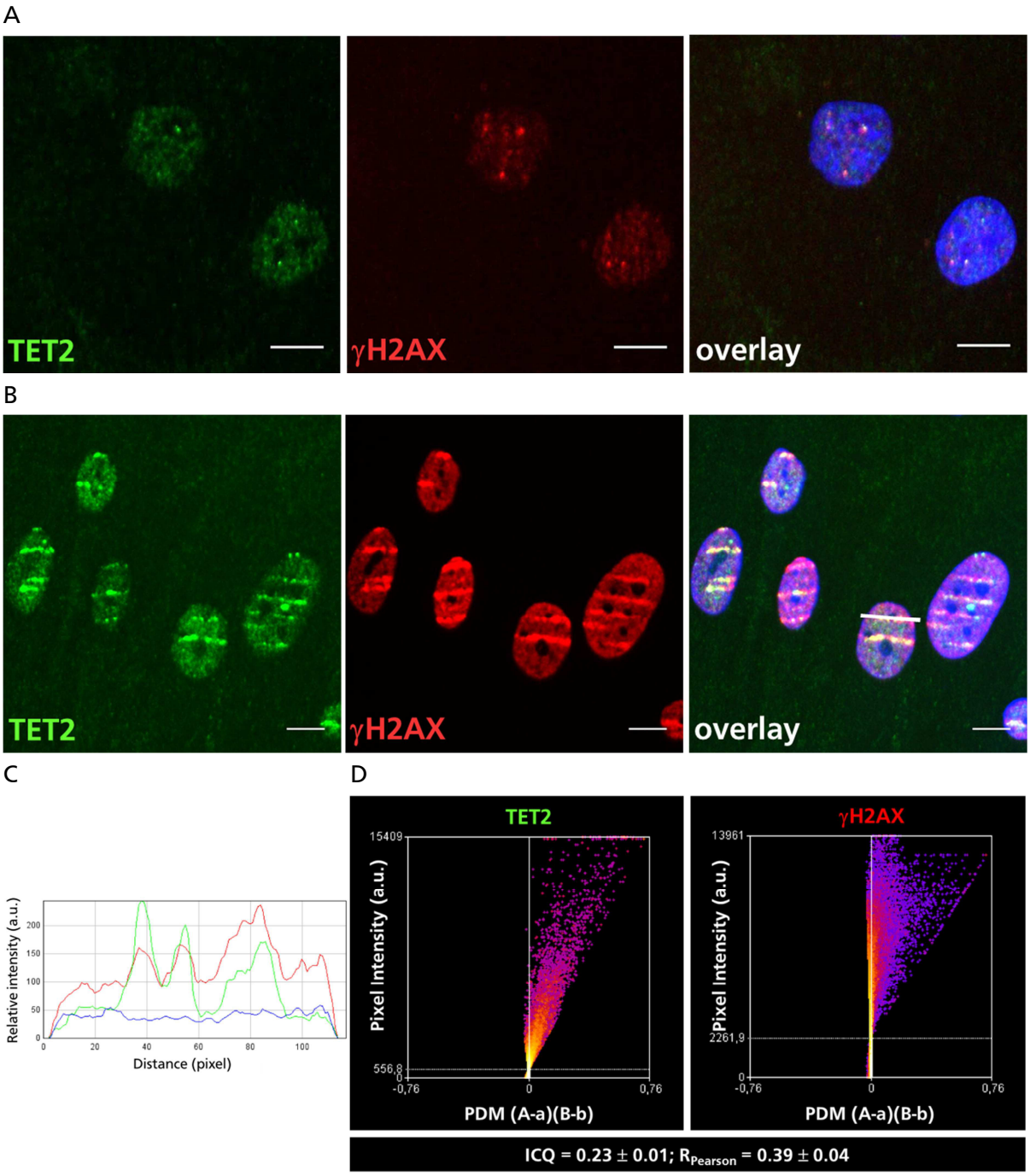

Figure 5-16: Endogenous TET2 co-localizes with γH2AX at ion induced damage sites. Proliferating AG fibroblasts were irradiated with ^{197}Au-ions (LET: 12815 kev/µm; fluence: 3.0 x 10^6 particles/cm^2) under a low angle, fixed 30min afterwards using paraformaldehyde and stained against TET2 and γH2AX. A) In unirradiated cells TET2 (green) co-localizes with γH2AX (red) at replication-related foci while after irradiation (B) TET2 and γH2AX co-localize at ion induced damage sites. DNA is shown in blue. Scale bar = 10 µm. C) Co-localization of TET2 and γH2AX is illustrated using intensity profiles along the ion trajectory, marked by the white line in the overlay in B. D) Intensity correlation analysis of the green (TET2) and red (γH2AX) channel. With increasing signal intensity, PDM values increase. The horizontal line shows the mean of the fluorescence signal intensities and colors represent the frequencies of the different intensities. ICQ = 0.23 ± 0.01. $R_{Pearson}$ = 0.39 ± 0.04; p = 0.036. Error = standard error.

In this experiment, fixation with paraformaldehyde was compared to fixation with extraction of soluble proteins (fixation with Hepes) described in chapter 3.4.1 and 3.4.2 since in some cases, the removal of unbound proteins from the nucleus can improve the detection of target proteins.

Analyzing TET2 recruitment kinetics the occurrence of TET2 positive streaks within the irradiated cells were counted and compared to γH2AX occurrence. Cells displaying at least one γH2AX streak were defined as γH2AX-positive. Since TET2 always co-localized with γH2AX, the proportion of cells showing streaks stained with both antibodies (TET2-positive cells) were defined.

	# Cells (Fixation with paraformaldehyde)				# Cells (Fixation with Hepes)			
Time after irradiation (min)	5-10	30	60	180	5-10	30	60	180
γH2AX-positive cells	101	100	100	125	100	102	100	100
TET2-positive cells	14	97	98	122	46	94	100	100
TET2-positive cells (%)	13.9	97	98	97.6	46	92.2	100	100

Table 5-4: TET2- and γH2AX-positive cells in proliferating AG cells different time points after irradiation. Proliferating AG cells were irradiated with ^{197}Au-ions (LET: 12815 kev/µm; fluence: 3.0 x 10^6 particles/cm^2) under a low angle at the linear accelerator UNILAC and fixed at different times after irradiation (five to 10 minutes, 30 minutes, one hour and three hours). In this experiment, fixation with paraformaldehyde was compared to fixation with extraction of soluble proteins (fixation with Hepes). Subsequently samples were stained against TET2 and γH2AX. γH2AX- and TET2-positive cells were counted. γH2AX-positive cells = cells showing at least one γH2AX streak; TET2-positive cells = cells showing at least one TET2 streak in cells that are γH2AX-positive; TET2-positive cells (%) = proportion of TET2-positive cells.

As summarized in Table 5-4, already five to 10 minutes after irradiation, 13.9 % of the cells fixed with paraformaldehyde and 46 % of the cells where soluble proteins were extracted, were TET2-positive. After 30 minutes almost all irradiated cells (92.2 – 97 %) were TET2-positive and still three hours after irradiation almost 100 % of the cells showed TET2 bound at DNA damage sites, excluding recruitment in a cell cycle dependent manner. Differences in TET2 signal were observed between fixation with paraformaldehyde compared to fixation with additional extraction of soluble proteins early after irradiation (5-10 minutes). This is maybe because TET2 signal is very weak at the beginning and detection may be improved by the removal of unbound proteins. However, both samples might not be fixed at exactly the same moment after irradiation. Since recruitment of TET2 is very fast those slight differences might also account for differences in TET2-positive cells.

5.6.2 Endogenous TET2 is recruited to damage sites induced by X-rays

Since sparsely and densely ionizing radiation differ in the complexity of damage they induce, it was investigated, whether TET2 is also recruited to damage sites after X-rays.

The recruitment of endogenous TET2 to X-ray-induced damage sites in AG cells was analyzed 30 minutes after irradiation with a dose of 2 Gy. Recruitment of TET2 to DSBs, demonstrated by TET2 co-localizing with γH2AX, was observed performing microscopic analysis (Figure 5-17 A). Out of 100 γH2AX positive cells 98 cells were also positive for TET2 30 minutes after

irradiation, whereby TET2 spot intensities differ dramatically between different cells generating two different populations with one showing only faint TET2 staining at damage sites and the other showing rather pronounced staining (compare the two cells on the right with cell on the left in Figure 5-17 A left picture).

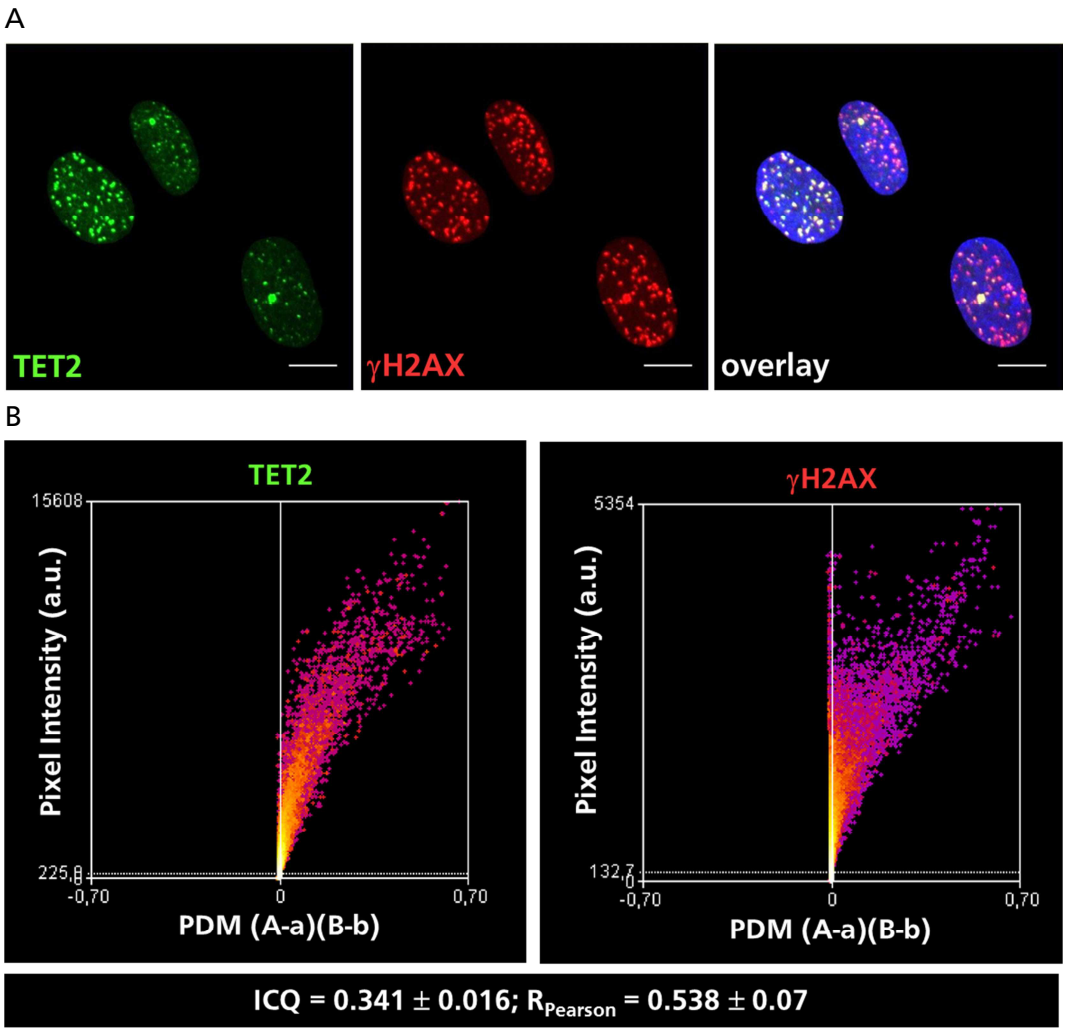

Figure 5-17: TET2 is recruited to damage sites after X-ray irradiation. Proliferating AG human fibroblasts were irradiated with 2 Gy X-rays, fixed with paraformaldehyde after 30 minutes and stained against TET2 (green) and γH2AX (red), showing co-localisation of TET2 and γH2AX at damage sites (A). DNA is shown in blue. Scale bar = 10 µm. B) Intensity correlation analysis of the green (TET2) and red (γH2AX) channel. PDM values increase with increasing signal intensity. The horizontal line shows the mean of the signal fluorescence intensities and colors represent the frequencies of the different intensities. ICQ = 0.341 ± 0.016; $R_{Pearson}$ = 0.538 ± 0.07; p = 0.044. Error = standard error.

To substantiate co-localization of TET2 and γH2AX after X-ray irradiation, ICA was performed as described above. TET2 PDM values increased with increasing fluorescence signal intensity (Figure 5-17 B, left figure). In contrast a positive tendency to high γH2AX PDM values can only be seen above ~50 % of maximal fluorescence signal intensity and γH2AX PDM values are scattered around zero for intensities below this level (Figure 5-17 B, right figure). However most PDM values are positive for both channels and calculation of ICQ resulted in a value of 0.341 ± 0.016. Together with the calculation of Pearson's correlation coefficient

($R_{Pearson} = 0.538 \pm 0.07$; $p = 0.044$) this revealed moderate positive correlation of TET2 and γH2AX at DSBs.

TET2 binding to damage sites was specific as was confirmed by immunizing peptide blocking experiment (Figure 5-18). However using a new batch of the same antibody as well as using other antibodies specific for TET2, results obtained by immunofluorescence and microscopical analysis could not be reproduced.

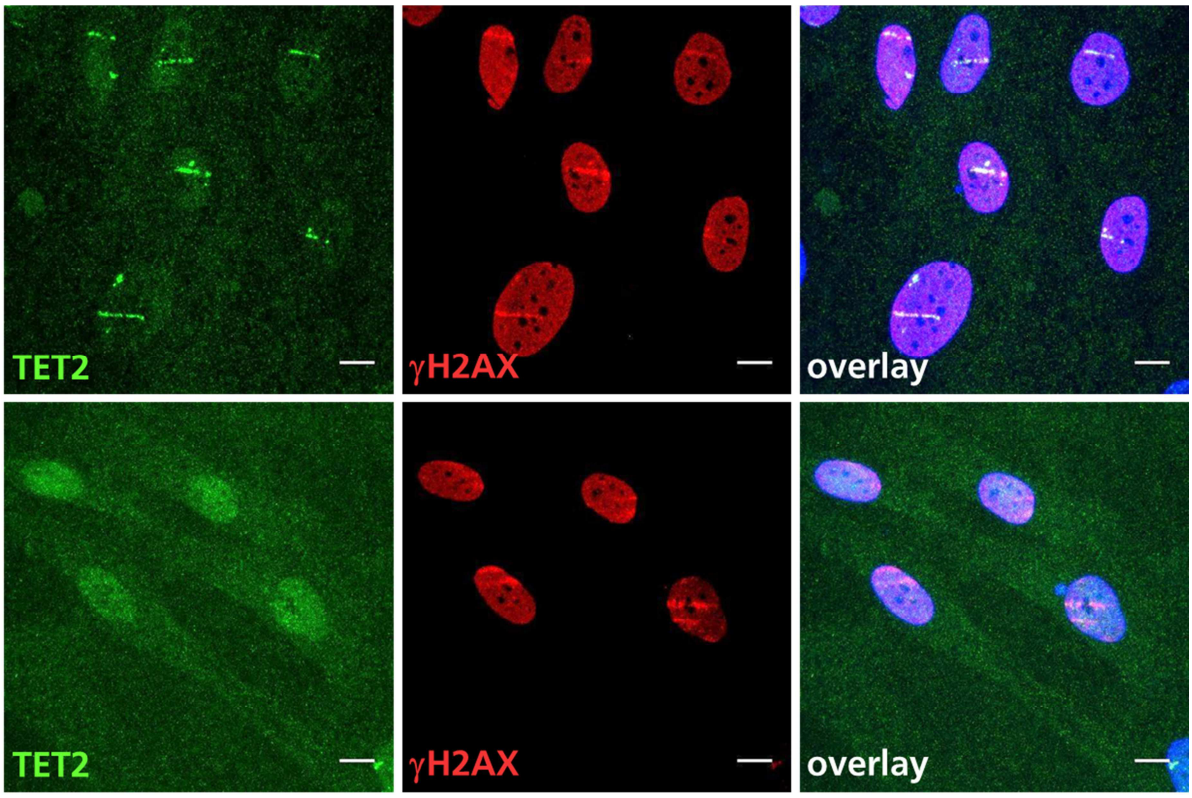

Figure 5-18: TET2 binding to damage sites is specific. AG human fibroblasts were irradiated with ^{92}U-ions (LET: 15000 kev/µm; fluence: 3.0 x 10^6 particles/cm^2) under a low angle and fixed with paraformaldehyde after one hour. Samples were either stained against TET2 (green; upper row) and γH2AX (red), showing co-localization of TET2 and γH2AX at damage sites, or with TET2 pre-incubated with immunizing peptide (green; lower row) and γH2AX (red), showing no TET2 co-localizing with γH2AX at damage sites. Scale bar = 10 µm.

These results show that endogenous TET2 is recruited to damage sites. Furthermore endogenous TET2 co-localizes with γH2AX at DSBs after irradiation with high LET ions as well as after X-ray irradiation.

In addition to TET2 recruitment analysis, it was analyzed whether also TET3 is recruited to damage sites induced by X-rays or ions. However, TET3 was neither recruited to DSBs induced by X-rays nor to ion-induced DSBs.

It was shown by flow cytometry analysis that IR concomitant to TET2CD-GFP expression induces 5hmC formation. Since TET2 was shown to be recruited to DSBs, it could locally exert its function converting 5mC to 5hmC. Therefore TET-substrate, 5hmC, was analyzed. Namely, 5hmC accumulation at damage sites, and especially at DSBs, was investigated.

5.7 Hydroxymethylation is formed at DNA damage sites following irradiation

Accumulation of 5hmC at damage sites was investigated after irradiation with iron ions and X-rays. 5hmC, which might accumulate at DSBs due to TET2-driven oxidation processes, was investigated by co-staining of γH2AX. As for recruitment analysis of endogenous TET2, AG cells were used.

5.7.1 5hmC co-localizes with γH2AX at damage sites induced by heavy ions

Despite high background signal, microscopical analysis revealed accumulation of 5hmC and co-localization with γH2AX along the ion trajectory (Figure 5-19 B) compared to unirradiated cells, where 5hmC co-localized with γH2AX at replication-related foci (Figure 5-19 A). In the experiment shown here, cells having at least one γH2AX or 5hmC streak were considered γH2AX- or 5hmC- positive. Based on such assumption, 73.6 % of the irradiated cells were γH2AX-positive, while only 26.4 % were 5hmC-positive. Nevertheless, it has to be pointed out that whenever a 5hmC streak was observed this always co-localized with a γH2AX streak. To further verify co-localization of 5hmC with γH2AX, ICA was performed as described above. Exemplary Figure 5-19 D shows that γH2AX PDM values increase with increasing fluorescence signal intensity (right figure) and there are only few data points yielding negative values. For 5hmC (left figure) instead, a positive tendency to high PDM values can only be seen above ~40 % of maximal fluorescence signal intensity. For intensities below this level, PDM values are scattered around zero. However, for both 5hmC and γH2AX most PDM values are positive and calculated ICQ was 0.236 ± 0.017, indicating positive correlation of 5hmC and γH2AX at DSBs. Moderate correlation was statistically confirmed by calculation of Pearson's correlation coefficient ($R_{Pearson} = 0.496 \pm 0.04$; $p = 1.1 \times 10^{-4}$).

Co-localization of 5hmC and γH2AX specifically at ion trajectories was further analyzed using intensity profiles (Figure 5-19 C). γH2AX fluorescence signal peaked at ionizing radiation induced foci (IRIF). The same profile was observed for 5hmC fluorescence signal. However, 5hmC and γH2AX did not co-localize at all IRIFs, rather more γH2AX IRIFs were observed compared to 5hmC IRIFs. Quantification on 51 of these intensity profiles were conducted, showing 271 γH2AX IRIF in total (5.31 ± 2.38 per streak) while only 244 5hmC IRIF were found (4.78 ± 2.23 per streak). These differences might indicate differences in 5hmC formation in different cell cycle phases, which will be addressed in chapter 5.7.3.

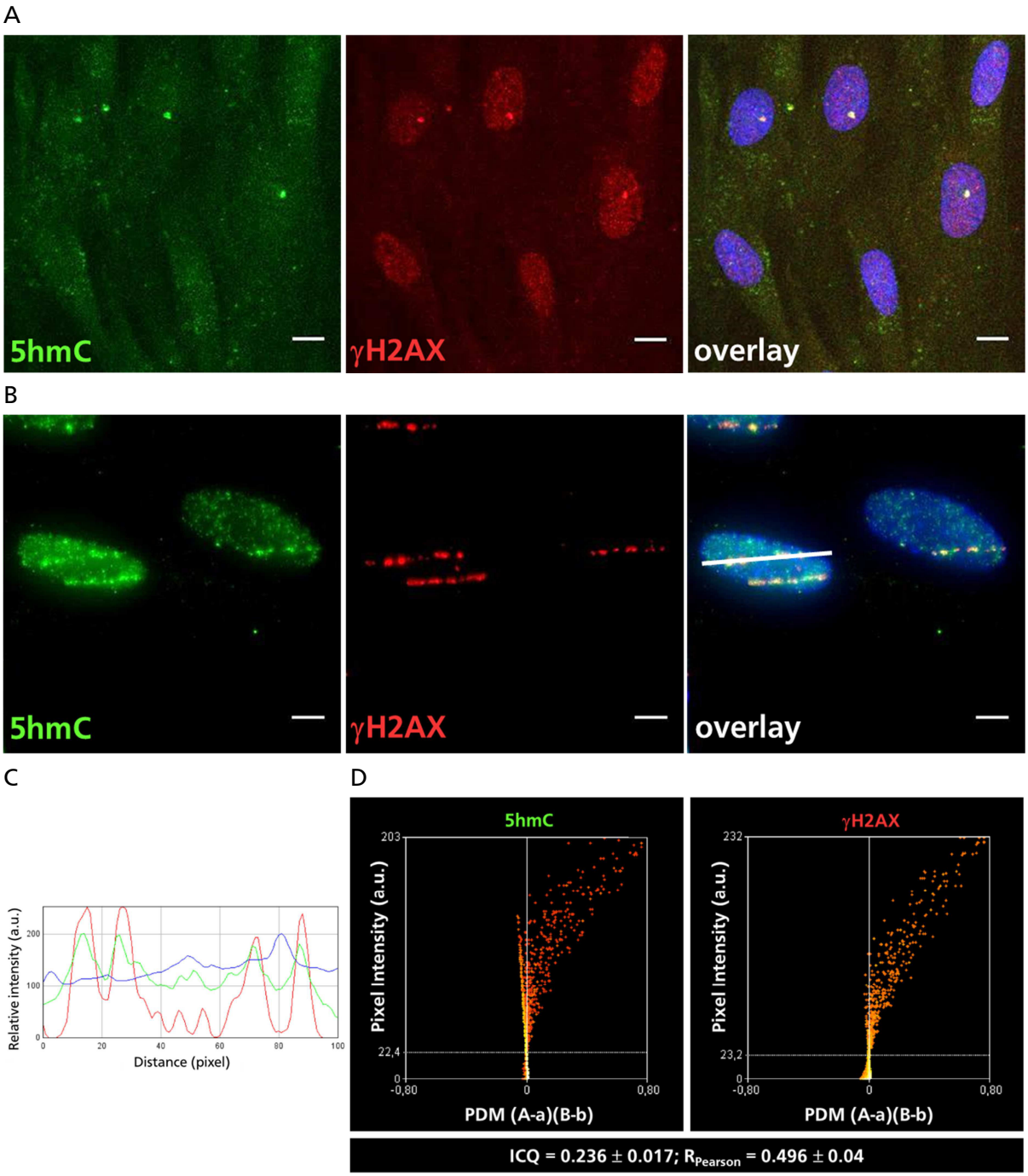

Figure 5-19: 5hmC accumulates at ion-induced damage sites. AG human fibroblasts were irradiated with ^{56}Fe-ions (LET: 148 keV/µm; fluence: 4.0 x 10^6 particles/cm^2) under low angle irradiation at the heavy ion synchrotron SIS, fixed after 30 minutes using cell fixation with additional DNA denaturation and stained against 5hmC (green) and γH2AX (red). (A) Unirradiated cells show 5hmC accumulation at replication related γH2AX foci. (B) 5hmC and γH2AX co-localize at ion induced damage sites. Scale bar = 5 µm (C) The co-localization of 5hmC (green line) and γH2AX (red line) is illustrated by the intensity profile along the ion trajectory, which is marked by the white line in the overlay picture in B. (D) Intensity correlation analysis of the green (5hmC; left) and red (γH2AX; right) channel. PDM values increase with increasing fluorescence signal intensity. The horizontal line shows the mean of the signal intensities and colors represent fluorescence intensity frequencies. ICQ = 0.236 ± 0.017; $R_{Pearson}$ = 0.496 ± 0.04; p = 1.1 x 10^{-4}. Error = standard error.

5.7.2 5hmC co-localizes with γH2AX at damage sites induced by X-rays

As for TET2 recruitment, it was investigated, whether also 5hmC accumulates at damage sites induced by sparsely ionizing X-rays.

In Figure 5-20 A, detection of nuclear 5hmC and γH2AX signals is shown. 5hmC accumulates at damage sites induced by X-rays and co-localizes with γH2AX at DSBs. While γH2AX shows larger foci, 5hmC foci are concentrated within a smaller area ("micro-foci").

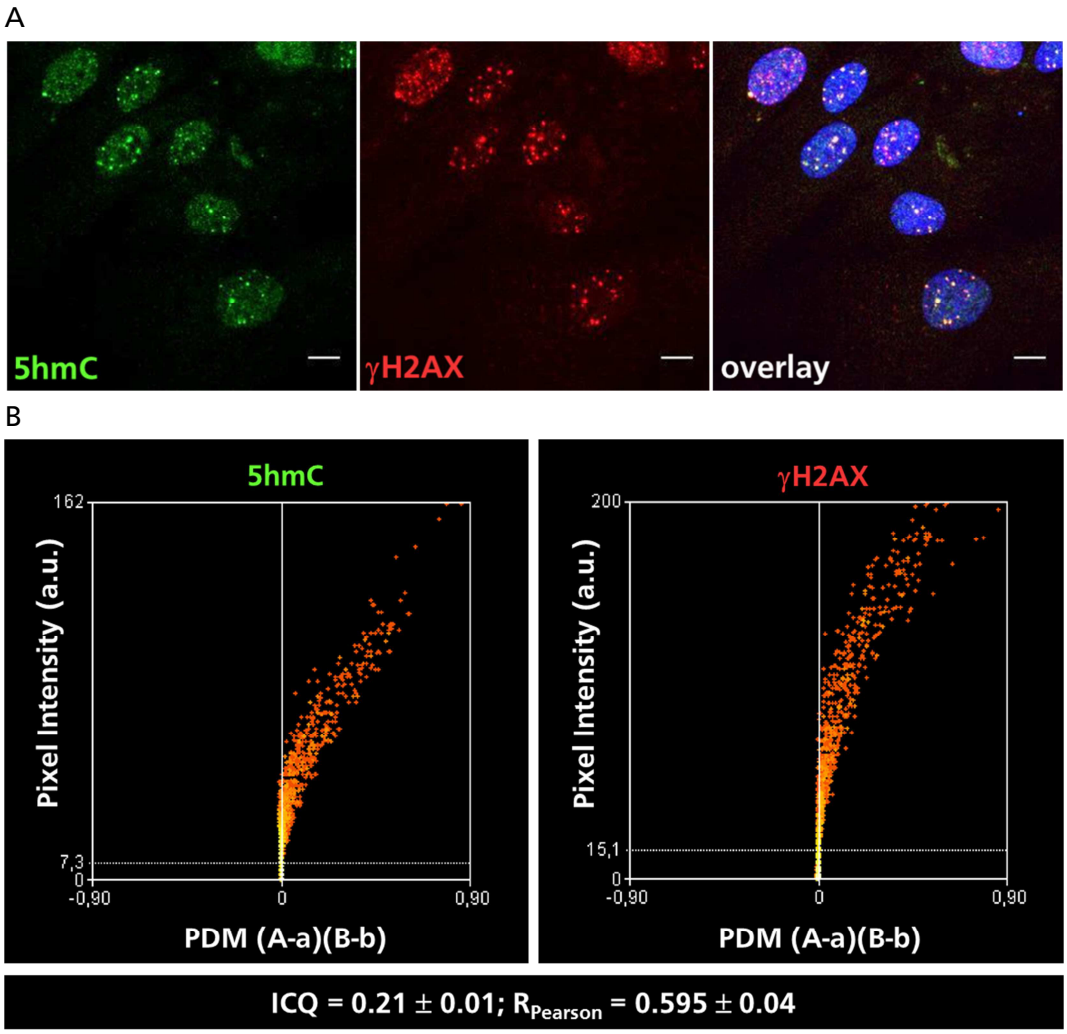

Figure 5-20: 5hmC accumulates at DSBs induced by X-rays. Proliferating AG human fibroblasts were irradiated with 0.5 Gy X-rays, fixed after 30 minutes using cell fixation with additional DNA denaturation and stained against 5hmC (green) and γH2AX (red). A) 5hmC and γH2AX co-localize at damage sites. DNA was stained using DAPI and is shown in blue. Scale bar = 10 µm. B) Intensity correlation analysis of the green (5hmC) and red (γH2AX) channel. PDM values increase with increasing signal intensity. The horizontal line shows the mean of the signal fluorescence intensities and colors represent fluorescence intensity frequencies. ICQ = 0.21 ± 0.01; $R_{Pearson}$ = 0.595 ± 0.04; p = 10^{-8}. Error = standard error.

To further verify the co-localization of 5hmC with γH2AX after X-ray irradiation, ICA was performed as described above. Exemplary Figure 5-20 B shows, that most 5hmC and γH2AX PDM values are positive. For γH2AX (Figure 5-20 B, right figure) a positive tendency to high PDM values can be seen above 30 % of maximal fluorescence intensity while for 5hmC (Figure 5-20 B, left figure) a trend to high PDM values is already obvious above 20 % of maximal fluorescence intensity. For fluorescence intensities below this level, PDM values are scattered around zero. However for both, 5hmC and γH2AX, most PDM values are positive and the ICQ adopts a value of 0.21 ± 0.01, displaying positive correlation of 5hmC and γH2AX at DSBs. Moderate correlation was statistically confirmed by calculation of Pearson's correlation coefficient ($R_{Pearson} = 0.595 \pm 0.04$; $p = 10^{-8}$).

5mC, as a repressive mark, is located in heterochromatic regions [Shen et al., 2013] of gene promoters. In contrast, 5hmC is mainly associated with euchromatin [Kubiura et al., 2012]. To analyze 5hmC spatial location, NIH/3T3 cells were used where heterochromatin is organized in clearly separated chromocenters. Cells, irradiated with iron ions, were analyzed one hour after irradiation and stained using antibodies specific for 5hmC and γH2AX. 5hmC accumulation in NIH/3T3 cells was observed only in a small fraction of irradiated cells. Nevertheless, 5hmC foci formation after irradiation with iron ions was analyzed using intensity profiles. As shown in two exemplary intensity profiles in Figure 5-21, 5hmC signal overlaps with γH2AX but not with DAPI signal, meaning that 5hmC was never observed inside of chromocenters, but rather in euchromatic regions. It is reported [Jakob et al., 2011], that lesions (marked by γH2AX) move from the interior to the periphery of irradiated heterochromatic regions. Therefore, it is tempting to speculate that 5mC located in heterochromatin is oxidized to 5hmC, the latter reaching the border of heterochromatin via the same process as γH2AX.

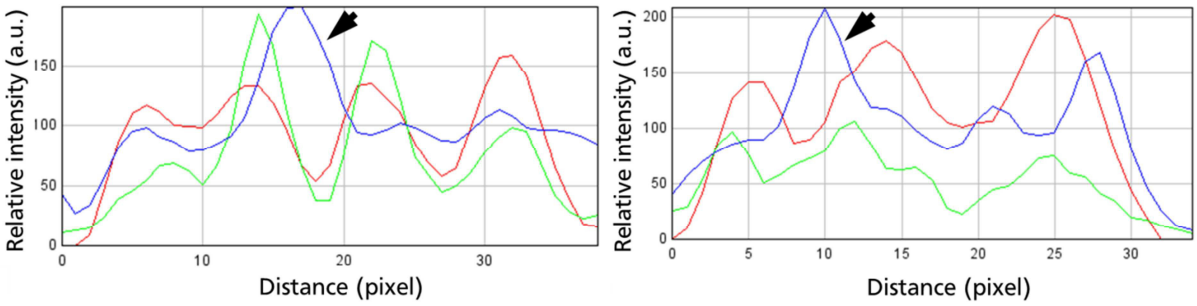

Figure 5-21: Exemplary intensity profiles of 5hmC and γH2AX along the ion trajectory. NIH/3T3 cells were treated as in Figure 5-19. One hour after irradiation cells were fixed and stained against 5hmC and γH2AX. DNA was stained using DAPI. Intensity profiles were used to analyze 5hmC spatial location. 5hmC (green line) co-localizes with γH2AX (red line) outside of heterochromatic regions (DNA peak marked by a blue line and indicated by an arrow head).

The results of this chapter, together with TET2 recruitment to damage sites, strongly suggest a radiation-dependent DNA demethylation process. Such process occurred within one replication cycle time frame and could involve TET proteins.

To investigate TET2 role in such a process, a knockdown approach was attempted, as downregulation of TET2 expression could affect 5hmC formation at damage sites. Therefore

several commercially available siRNAs as well as shRNAs were used in different cell lines. However, TET2 protein expression was only insufficiently or even not downregulated with all the approaches used (exemplary Figure 5-22).

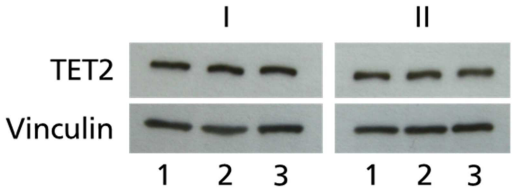

Figure 5-22: TET2 protein expression cannot be downregulated. Whole protein lysates of untreated HeLa (I) and MEF (II) cells (1) or lysates of HeLa and MEF cells incubated with different siRNAs (2, 3) were compared by Western analysis. Despite using easy transfectable cells, no downregulation of TET2 expression is seen. Vinculin was used to confirm equal protein loading. The following siRNAs and shRNAs were used: one siRNA designed using an online design tool (clontech.com), four commercially available siRNAs (each for the targeting of mouse or human genes; Gene Solution siRNA, QIAGEN) as well as 4 commercially available shRNAs (also for targeting human and mouse genes; SureSilencing shRNA, QIAGEN).

In seeking to give a deeper insight into DNA demethylation processes after IR exposure, further work was focused on 5hmC appearance and disappearance at damage sites after activation of the DDR. 5hmC foci kinetics after irradiation with X-rays were analyzed and compared to γH2AX kinetics. γH2AX can be observed after the activation of the DDR and is closely linked to the repair of DSBs.

5.7.3 The accumulation of 5hmC at damage sites follows the γH2AX accumulation and is independent on the cell cycle

Since 5hmC and γH2AX did not co-localize at all IRIFs after irradiation with ions (chapter 5.7.1), which might indicate differences in 5hmC formation in different cell cycle phases, the analysis of 5hmC foci kinetics was performed in proliferating AG cells, to investigate different cell cycle phases. AG cells, irradiated with 0.5 Gy X-rays and fixed after different times after irradiation (10 min, 30 min, 1 h, 3 h, 7 h, 16 h and 24 h) as well as an unirradiated sample were investigated. All samples were stained against 5hmC and γH2AX. To distinguish S/G_2- from G_1-cells, cells were stained against Rad51, which is only expressed in S/G_2-phase. Due to antibody specificity, a cell cycle marker could not be used.

The so handled cells were analyzed microscopically and pictures of 50 to 100 cells per sample and experiment were taken. Two independent experiments were performed and total numbers of cells analyzed per sample are shown in Table 5-5. For all samples and all pictures, 5hmC as well as γH2AX foci per cell were counted on maximum projections in ImageJ. Cells were defined as S/G_2, or G_1 cells depending on the presence or absence of Rad51 at DSBs, respectively.

Time after irradiation (min)	0 Gy	0.5 Gy						
		10	30	60	180	420	960	1440
# all cells	149	137	133	142	151	162	178	168
# cells in G_1	120	96	98	97	112	126	167	160
# cells in S/G_2	29	41	35	45	39	36	11	8

Table 5-5: Cells analyzed for 5hmC and γH2AX foci kinetics. X-ray irradiated (0.5 Gy) proliferating AG cells were fixed after indicated incubation times (10 min, 30 min, 1 h, 3 h, 7 h, 16 h and 24 h). Cells were stained against 5hmC, γH2AX and Rad51. DNA was stained with DAPI. Samples were analyzed microscopically and 5hmC as well as γH2AX foci per cell were counted in 50 to 100 cells per sample. Cells were defined as S/G_2, or G_1 cells depending on the presence or absence of Rad51 at DSBs, respectively. Two independent experiments were performed and total number of cells (# all cells), number of cells in G_1 phase (# cells in G_1) and number of cells in S/G_2 (# cells in S/G_2) are shown.

In Figure 5-23 A, percentage of cells in all cell cycle phases, showing a certain number of 5hmC foci (green columns) and γH2AX foci (red columns) are shown for each time point. In control samples (0 Gy; upper-left) 5hmC and γH2AX foci number were comparable whereby about 90 % of the cells showed one to three 5hmC and γH2AX foci. Differently, the number of γH2AX foci increased rapidly and reached a maximum 30 minutes after irradiation (0.5 Gy 30 min; upper-right, red columns). At that time point, samples showed seven to 20 foci per cell and were normally distributed. Even though 5hmC foci reached their maximum at the same time (0.5 Gy 30 min; upper-right, green columns), samples showed zero to 15 foci per cell only. Foci per cell were normally distributed; however, their total number never equaled that of γH2AX. Starting by 3 h (0.5 Gy 3 h (180 min); middle row, figure in the middle) however, when γH2AX foci number already decreased, both 5hmC and γH2AX foci numbers showed comparable levels. 16 hours after exposure to IR (0.5 Gy 16 h (960 min); lower-left), γH2AX and 5hmC foci distributions were comparable to basal levels, where about 80 % of the cells showed one to three 5hmC and γH2AX foci. Overall, each 5hmC focus co-localized with a γH2AX focus, while this observation did not hold true for γH2AX, whereby several γH2AX foci did not show 5hmC signal.

Time after irradiation (min)	0 Gy	0.5 Gy						
		10	30	60	180	420	960	1440
# γH2AX foci	1.4 ± 1.1	12.8 ± 3.6	13.8 ± 3.4	12.8 ± 4.0	6.9 ± 3.2	3.3 ± 2.2	1.3 ± 1.3	1.2 ± 1.2
# 5hmC foci	1.0 ± 1.1	4.0 ± 3.2	8.4 ± 3.9	7.5 ± 4.0	4.2 ± 2.4	2.1 ± 1.9	1.2 ± 1.1	1.2 ± 1.2
# γH2AX foci (S/G2)	2.2 ± 1.9	13.3 ± 3.5	14.6 ± 4.1	14.7 ± 3.8	9.3 ± 3.7	4.3 ± 2.3	2. 5 ± 1.9	2.3 ± 1.7
# 5hmC foci (S/G_2)	0.8 ± 0.7	3.0 ± 3.0	7.6 ± 3.9	5.5 ± 4.5	3.1 ± 2.7	1.6 ± 2.0	1.9 ± 1.6	1.6 ± 1.9
# γH2AX foci (G_1)	1.2 ± 1.2	12.5 ± 3.6	13.6 ± 3.2	11.6 ± 3.6	6.1 ± 2.5	3.1 ± 2.1	0.7 ± 1.2	1.1 ± 1.2
# 5hmC foci (G_1)	1.1 ± 1.1	4.4 ± 3.2	8.7 ± 3.8	8.1 ± 3.3	4.6 ± 2.2	2.3 ± 1.8	0.6 ± 1.1	1.2 ± 1.2

Table 5-6: Mean number of 5hmC and γH2AX foci over time. Proliferating AG cells were treated as in Table 5-5. Samples were analyzed microscopically and 5hmC as well as γH2AX foci per cell were counted. Mean γH2AX and 5hmC foci number are shown for all cells (# γH2AX foci; # 5hmC foci), for S/G_2 cells (# γH2AX foci (S/G_2); # 5hmC foci (S/G_2)) and for G_1 cells (# γH2AX foci (G_1); # 5hmC foci (G_1)) at the respective time points after irradiation (10 to 1440 minutes) and in the unirradiated control (0 Gy). Error = standard deviation of foci counts.

In Figure 5-23 B, 5hmC and γH2AX foci kinetics are shown for all cell cycle phases (green and red solid line) as well as subdivided into S/G_2 (green and red dashed line) and G_1 (green and red dotted line) cells and mean foci numbers are depicted in Table 5-6.

Total γH2AX foci per cell (red solid line) increased promptly after irradiation reached a maximum (∅ ~14 foci per cell) 30 minutes after irradiation and decreased thereafter. γH2AX foci per cell in S/G_2 cells (red dashed line) peaked (∅ ~15 foci per cell) one hour after irradiation, instead. Over time, S/G_2 cells always showed more γH2AX foci compared to the count averaged over all cell cycle phases. In contrast G_1 cells showed a lower number of γH2AX foci per cell (red dotted line) over time with a maximum (∅ ~14 foci per cell) at 30 minutes post irradiation.

Cells exposed to radiation also showed increased total 5hmC foci number per cell (green solid line), which also reached a maximum (∅ 8.4 foci per cell) 30 minutes after irradiation and decreased thereafter. 5hmC foci per cell in S/G_2 cells (green dashed line) peaked (∅ 7.6 foci per cell) 30 minutes after irradiation. In contrast to γH2AX, 5hmC foci number in S/G_2 cells was lower compared to the count averaged over all cell cycle phases except after 16 and 24 hours (960 and 1440 min), where S/G_2 cells showed more foci. G_1 cells showed a higher number of 5hmC foci per cell (green dotted line) over time (maximal value (∅ 8.7 foci per cell) at 30 minutes after irradiation) compared to the count averaged over all cell cycle phases, except for the 16 and 24 hour (960 and 1440 min) time points, where G_1 cells showed less foci. However, it has to be mentioned that for the analysis only few S/G_2 cells were taken into account (Table 5-5). Those might not be sufficient to ensure reliable results and further investigations have to be made to substantiate this effect.

These results indicate that 5hmC foci are formed together with γH2AX foci and such effect is independent of the cell cycle. 5hmC foci increase rapidly after irradiation following γH2AX and peaking within 0.5-1 hour, although their total number never equals that of γH2AX. Only at later time points both marks show comparable abundance.

In response to IR exposure, the DDR is activated leading to the accumulation of proteins of the DSB repair machinery to DSBs [Bekker-Jensen and Mailand, 2010]. 5hmC signal is also observed at DSB sites (co-localization with γH2AX) as a response to IR treatment. Therefore 5hmC might hold a function in the DDR that might be associated to the repair of DSBs.

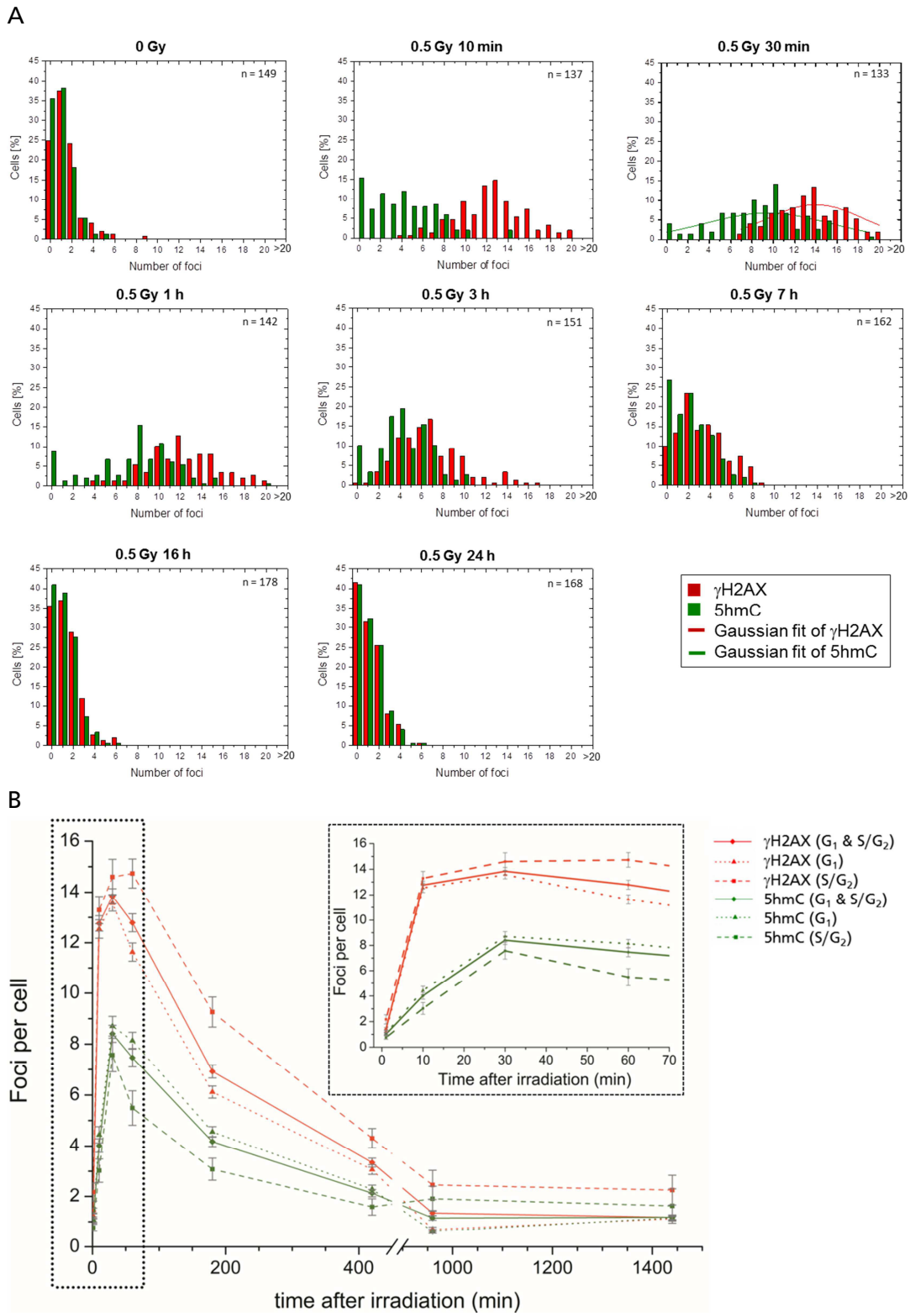

Figure 5-23: 5hmC and γH2AX foci kinetics after X-ray irradiation. X-ray irradiated (0.5 Gy) proliferating AG cells were fixed after indicated incubation times (10 min, 30 min, 1 h, 3 h, 7 h, 16 h and 24 h). Cells were stained against 5hmC, γH2AX and Rad51. DNA was stained with DAPI. Samples were analyzed microscopically and 5hmC as well as γH2AX foci per cell were counted in 50 to 100 cells per sample. A) Percentage of cells in all cell cycle phases showing a certain number of 5hmC foci (green columns) and γH2AX foci (red columns) are shown for each time point. Results are a summary of two independent experiments. n = number of cells investigated. B) 5hmC and γH2AX foci kinetics for all cell cycle phases (green and red solid line) as well as subdivided into S/G_2 (green and red dashed line) and G_1 (green and red dotted line) cells. The inlay shows a magnified view of the time points until 60 minutes (framed by dotted lines). Error bars: standard error.

5.7.4 5hmC foci kinetics is dependent on DNA-PK activity

Based on the findings that 5hmC follows γH2AX kinetics after DDR activation, it was investigated whether the inhibition of one of the main DNA repair pathways would affect 5hmC formation and kinetics. Therefore analysis of 5hmC foci kinetics after inhibition of DNA-PK, a key factor of NHEJ, was performed.

DNA-PK plays a crucial role in NHEJ, one of the main pathways of the DSB repair (chapter 2.2.4.1.2). NHEJ takes place throughout the cell cycle and predominates in G_1/G_0. Therefore confluent non-replicating AG cells were used. These cells show halted cell cycle and, therefore, little if none replication-related γH2AX foci.

AG cells treated with DNA-PK inhibitor were compared to control samples, where cells were incubated with the same volume of DMSO. After treatment, cells were irradiated with 0.5 Gy X-rays (chapter 3.3.1). Additionally, an unirradiated sample treated with DNA-PK inhibitor or DMSO was included in the experiment. After irradiation and incubation at 37 °C for convenient times (30 min, 1 h, 2h, 3 h, 7 h, 10 h and 24 h), cells were treated as described previously (chapter 5.7.3). Afterwards cells were analyzed microscopically and pictures of up to 100 cells per sample per experiment were taken. For all samples and all pictures, 5hmC as well as γH2AX foci per cell were counted using maximum projections in ImageJ.

	0 Gy	**0.5 Gy**						
Time points (min)		30	60	120	180	420	600	1440
#γH2AX foci (control)	2.1 ± 1.7	13.6 ± 3.2	13.2 ± 3.0	11.4 ± 3.0	7.7 ± 2.7	4.1 ± 2.1	3.8 ± 2.0	2.6 ± 1.4
#γH2AX foci (DNA-PKi)	2.0 ± 1.6	11.8 ± 3.5	14.2 ± 3.0	15.2 ± 3.0	12.5 ± 3.5	9.8 ± 2.3	8.3 ± 2.8	4.5 ± 2.2
# 5hmC foci (control)	1.2 ± 1.1	6.1 ± 4.7	5.3 ± 3.1	5.1 ± 3.0	4.4 ± 2.1	2.4 ± 1.6	2.9 ± 1.6	2.1 ± 1.3
# 5hmC foci (DNA-PKi)	1.1 ± 1.1	4.7 ± 4.0	5.5 ± 2.7	7.8 ± 4.2	6.6 ± 2.6	6.6 ± 2.7	6.5 ± 2.9	3.5 ± 1.8

Table 5-7: Mean number of 5hmC and γH2AX foci over time with and without inhibition of DNA-PK. # γH2AX foci (control): mean γH2AX foci number in cells treated with DMSO; # γH2AX foci (DNA-PKi): mean γH2AX foci number in cells treated with DNA-PK inhibitor; # 5hmC foci (control): mean 5hmC foci number in cells treated with DMSO; # 5hmC foci (DNA-PKi): mean 5hmC foci number in cells treated with DNA-PK inhibitor; Error = standard deviation of foci counts.

As shown in Figure 5-24 and Table 5-7, formation of γH2AX and 5hmC foci is not affected by DNA-PK inhibition. After 30 to 60 minutes, comparable γH2AX and 5hmC foci numbers are reached in inhibitor-treated (red and green dashed line) compared to control cells (red and green solid line). Conversely, repair of DSBs is strongly affected by DNA-PK inhibition, indicated by increased γH2AX foci and their persistence over time (red dashed line). One to two hours post irradiation, unrepaired DSBs accumulate and are repaired slowly over time in DNA-PK-inhibited cells, showing an up to 2-fold increase in γH2AX foci number compared to control cells. Such persistence was observed up to 24 hours post irradiation.

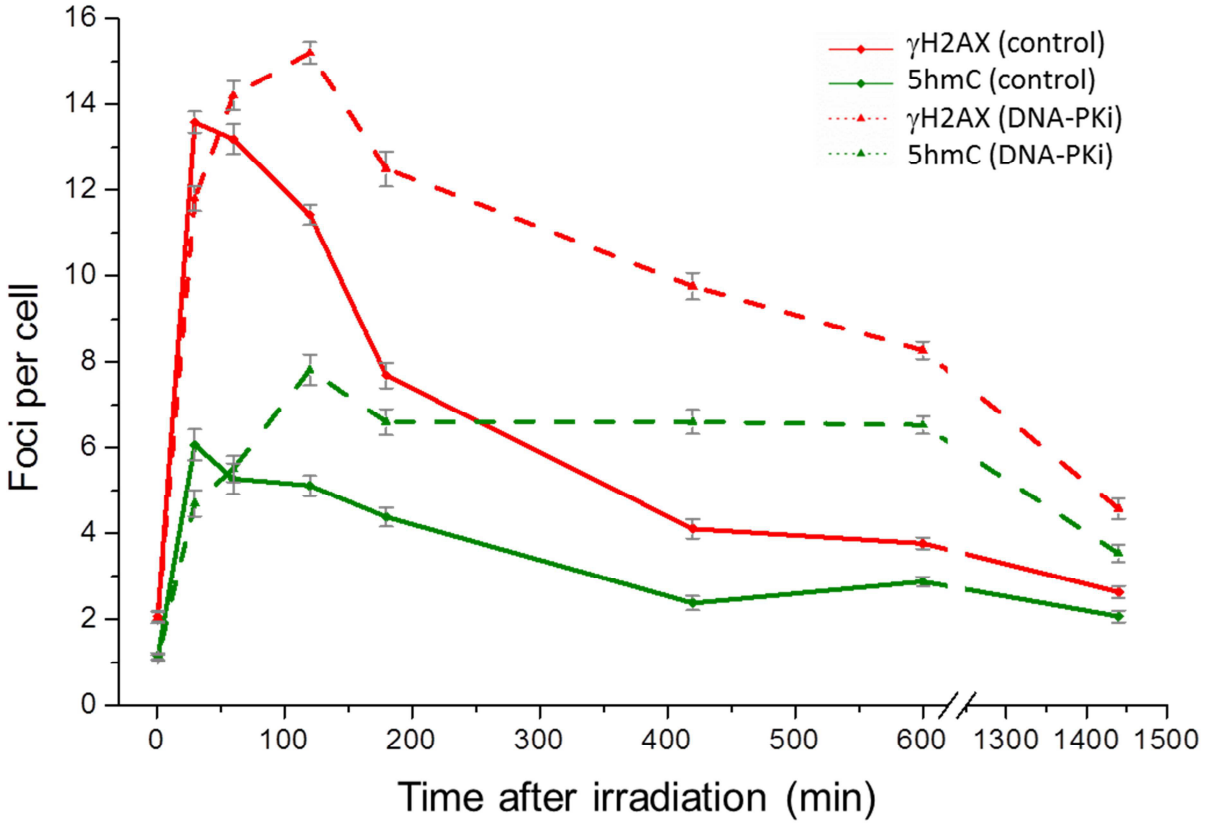

Figure 5-24: 5hmC and γH2AX foci persistence is increased after DNA-PK inhibition. Confluent AG cells treated with DNA-PK inhibitor (DNA-PKi) or DMSO (control) were irradiated with 0.5 Gy X-rays and fixed at different time points (30 min, 1 h, 2 h, 3 h, 7 h, 10 h and 24 h) after irradiation. Cells were stained against 5hmC and γH2AX. DNA was stained with DAPI and cells were analyzed microscopically, where pictures of up to 100 cells per sample and experiment were taken. For all samples and all pictures 5hmC as well as γH2AX foci per cell were counted using maximum projections in ImageJ. Result for control, 30 minutes, 2 hours and 10 hours are from two independent experiments, results for all the other samples are from one experiment. Error bars: standard error.

Similar kinetics was observed for 5hmC where foci number peaked two hours after irradiation in DNA-PK-inhibited cells (green dashed line; mean number of foci = 7.8 ± 4.2). As for γH2AX, 5hmC foci also persisted over time, showing an up to 2-fold increase compared to control cells, up to 24 hours post irradiation (compare green dashed and solid lines in Figure 5-24).

Inhibition of DNA-PK was demonstrated by Western analysis. Therefore confluent AG human fibroblasts, treated with DNA-PK inhibitor or DMSO were compared according to their abundance of activated (phosphorylated) DNA-PKcs (pS2056). As shown in Figure 5-25, activation of DNA-PK by autophosphorylation is reduced by the inhibitor (DNA-PKi compared to DMSO). However, residual signal of the phosphorylated form of DNA-PKcs is still detectable. Then, the membrane was stripped and re-probed for unmodified DNA-PKcs, to demonstrate that reduced amount of phosphorylated DNA PKcs is not due to lower abundance of DNA-PK. Since both samples have comparable amount of DNA-PKcs (Figure 5-25), inhibition is not due to lower abundance of DNA-PK.

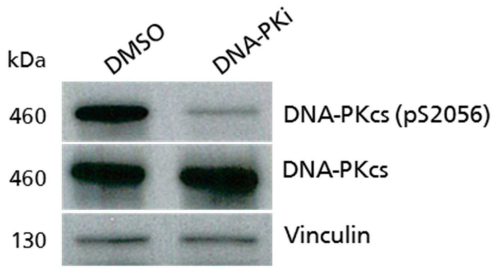

Figure 5-25: Impact of DNA-PK inhibition on DNA-PK autophosphorylation. Confluent AG cells were treated with DNA-PK inhibitor (DNA-PKi) or DMSO one hour before 10 Gy X-ray irradiation. One hour after irradiation, whole protein lysates were made and the phosphorylated form of DNA-PKcs (pS2056) was analyzed by Western blot. Vinculin was used as loading control. DNA-PKcs was detected to demonstrate that reduced amount of phosphorylated DNA-PKcs is not due to lower abundance of DNA-PK.

6 Discussion

Recent studies within the last years showed, that DNA methylation might have an impact on the response to IR. Genome-wide as well as gene-specific methylation changes were investigated [Aypar et al., 2011, Goetz et al., 2011]. However results from those studies were controversial. Another recent work [Cuozzo et al., 2007, O'Hagan et al., 2008] showed DNA methylation changes at DNA sites where a single DSB was induced, either in the upstream promoter or in the direct vicinity of downstream genes, by a sequence-specific endonuclease (*SceI* site) and repaired by NHEJ or HR. In those studies, DNA methylation of the repaired DNA segment lead to silencing of the respective downstream gene. These data demonstrated a relation between DSB repair (either through HR or NHEJ), DNA methylation and gene silencing. However, DNA methylation changes of the repaired DNA segments and the subsequent silencing of downstream genes was observed only in a very small fraction of cells. All of these studies as well as most of the work on DNA methylation changes after exposure to IR were conducted several population doublings after DSB induction. For this reason, replication dependent demethylation effects (passive "dilution" of 5mC; chapter 2.4.2) could not be ruled out.

Only two recent studies investigated DNA methylation at early timepoints after irradiation. While in one of those studies [Antwih et al., 2013] no consistent pattern of hypermethylaion or hypomethylation could be found, in the other study [Chaudhry and Omaruddin, 2012] DNA hypomethylation was observed. However also in this study, changes in DNA methylation were not very pronounced. Results obtained in the here presented thesis suggest an early decrease in DNA methylation after exposure to IR (Figure 5-1 A). Therefore it is conceivable that rather than DNA methylation, DNA demethylation processes may take place within one replication cycle time frame, conceding a rather enzymatic decrease of DNA methylation than a passive reduction of DNA methylation over decreased expression of DNMTs.

Passive DNA demethylation is the loss of methylated cytosine during successive rounds of replication under the condition that maintenance DNA methyltransferase activity of DNMT1 is repressed [Chen and Riggs, 2011]. Therefore this mechanism is too slow to account for such fast DNA demethylation observed here (Figure 5-1 A) and a rather enzymatic decrease might be involved. In this scenario TET enzymes might be the candidates.

The members of the TET family are methylcytosine dioxygenases recently discovered in the group of Anjana Rao [Tahiliani et al., 2009] and play a role in DNA demethylation processes. Namely, it is reported that TET1, TET2 as well as TET3 are able to oxidize 5mC to 5hmC and further to 5fC and 5caC, the latter being converted to cytosine via the base excision repair mechanism ([Ito et al., 2011, He et al., 2011]; chapter 2.4.2.2). Therefore, together with DNA methyltransferases, TET proteins regulate DNA methylation dynamically.

Based on the discussed observations, the aim of this study was to investigate radiation dependent DNA demethylation processes within one replication cycle time frame and a possible involvement of TET proteins in the DNA damage response.

In order to investigate DNA methylation changes within one replication cycle time frame, the experimental system was established first and hydroxy-/methylation as well as TET expression were investigated. While in this doctoral thesis, it was attempted to investigate all three TET family members, the proteins TET1 and TET3 could not be investigated in this study, since no

specific signal in Western analysis could be detected using commercially available antibodies (Figure 5-2 A). Whether this result depends on technical constrains is yet to be clarified and investigation of TET1/3 mRNA using a qPCR approach might give insights into their abundance. Therefore the relationship between 5mC, 5hmC and TET2 expression was investigated.

6.1 Low 5hmC levels cannot be determined using colorimetric techniques

In this study efforts were made to analyze global 5mC as well as 5hmC changes after irradiation over time using colorimetric ELISA-based techniques. While reasonable results were obtained for 5mC abundance after irradiation with X-rays (Figure 5-1 A), measurements of 5hmC abundance did not show reliable results and varied considerably (Figure 5-1 B). On the one hand, this may be caused by low 5hmC abundance in the cell lines investigated. As already mentioned, the total amount of 5hmC can be very limited (between 0.009 and 0.7 % of all bases [Globisch et al., 2010, Ito et al., 2011]) and therefore analysis may be difficult. On the other hand, in the experiments conducted in this work, ELISA-based colorimetric analysis might not provide sufficient sensitivity to detect small 5hmC amounts and only minor differences in 5hmC abundance induced by IR. Therefore those analyses can only give an estimate of global DNA hydroxymethylation levels. However this might not be generally valid since the colorimetric assay was successfully employed to assess global 5hmC changes in cells overexpressing TET2 catalytic domain, where a pronounced change of 5hmC abundance was expected. For the analysis of endogenous 5hmC levels, that is, in absence of TET2CD-GFP, immunofluorescence was preferred.

6.2 Dependence of DNA (hydroxy) methylation levels on TET2 expression

DNA methylation levels vary in different cell lines [Thurman et al., 2012] and there is a plethora of factors influencing methylation abundance (e.g. age, nutrition, drug exposure or exposure to other environmental agents [Aguilera et al., 2010]). Additionally, changes in DNA methylation can be linked to various cancers, diabetes, autoimmune diseases and mental illnesses. In this work DNA methylation levels and TET2 expression levels were measured in different cell lines in order to analyze interdependence between those two features (Figure 5-3). As expected a clear negative correlation with Spearman's correlation coefficient of -0.6018 ($p = 0.0329$) was observed.

Overall, global DNA methylation status is defined by the interplay between a plethora of factors promoting the addition or the (indirect) removal of 5mC.

Firstly, DNMT1, preserving 5mC patterns as well as DNMT3A and DNMT3B (*de novo* methyltransferases), which are able to add a methyl group to non-methylated substrate have a significant impact on 5mC levels (chapter 2.4.1). Furthermore, all TET enzymes are able to convert 5mC to 5hmC (chapter 2.4.2.2) and it is possible that TET1 and TET3 also contribute to 5(h)mC abundance in the cell lines analyzed in this work. TET1 is mainly expressed in ESCs. Moreover, TET2, which is also expressed in ESCs, is more ubiquitously distributed [Ito et al., 2010] and its expression in adult somatic cells has been reported [Langemeijer et al., 2009]. TET3, which carries out a special task in oocytes and one-cell zygotes (chapter 2.6), may also be found in adult tissues [Wu and Zhang, 2011, Wu and Zhang, 2014]. Additionally, methyl-CpG binding proteins including MBDs, ZBTBs and UHRFs families may also have an impact on DNA methylation abundance (chapter 2.4.1). A role in DNA demethylation (deamination of 5mC/5hmC) was also described for the AID and APOBEC enzymes (chapter

2.4.2; [Bhutani et al., 2010, Guo et al., 2011, Popp et al., 2010]) and thus changes of AID/APOBEC enzyme abundance might contribute in defining DNA methylation levels (see also below). Since DNA methylation is not only dependent on TET2 expression, the expression levels of the most critical factors influencing DNA methylation should be assessed in order to validate an appropriate experimental system. For this reason, the results presented in this work can only give preliminary information on the correlation between TET2 and DNA methylation.

5hmC levels were determined in the same cell lines in order to investigate interdependence between 5hmC and 5mC levels or TET2 expression levels. However a correlation was not seen for all the cell lines investigated. Rather 5hmC levels of cells of the group with "high DNA methylation levels" (Figure 5-3 A; grey columns) were not correlated to 5mC levels, while cells of the "low DNA methylation levels" group (Figure 5-3 A; green columns) showed anticorrelation of 5hmC and 5mC (Figure 5-4 A). If this is indicative of a possible function, discriminating high 5mC from low 5mC cells, has to be elucidated.

Like 5mC, 5hmC abundance also depends on several factors. 5hmC levels might not only depend on TET2 but also on TET1/3 enzymatic function. Additionally, also the AID and APOBEC enzymes might be involved in DNA demethylation (chapter 2.4.2; [Bhutani et al., 2010, Guo et al., 2011, Popp et al., 2010]).

On the whole, also global DNA hydroxymethylation levels are dependent on the presence and function of different factors. Even if a partial anticorrelation was found for cells of the "low DNA methylation levels" group, the results presented in this work could only give a rough estimate on global DNA hydroxymethylation levels and its correlation to other factors.

At this point it should be noted that in this experiment only global 5hmC levels were measured. However, at the local level correlation between 5hmC and 5mC or TET2 might exist and 5hmC accumulation and TET2 abundance at damage sites observed in this work (chapter 5.6 and 5.7) might give a first indication on a correlation at specific sites.

6.3 Overexpression of TET2 catalytic domain is sufficient to induce 5hmC accumulation

It was shown by Ito and co-workers [Ito et al., 2010], that overexpression of wild type TET2 catalytic domain, but not their catalytic mutant results in the generation of 5hmC. In experiments conducted during this doctoral thesis (chapter 5.3), these findings were expanded by analyzing different cell lines over time. This analysis revealed that kinetics of 5hmC formation differs between the two investigated cell lines.

After transfection of NIH/3T3 cells with TET2 catalytic domain, 5hmC levels increased (determined by immunofluorescence). This effect was observed 24 and 48 hours after transfection (Figure 5-6), while GFP and 5hmC fluorescence intensity values were higher after 48 hours than after 24 hours and also correlation of those two features was higher after 48 hours. The same was seen using ELISA-based colorimetric analysis (Figure 5-10). Namely, 5hmC levels increased as a response to TET2CD-GFP transfection, while the effect was slightly more pronounced 48 hours after transfection.

A similar effect was observed for U-2 OS cells (Figure 5-8), whereby 5hmC fluorescence intensity increased after transfection of TET2 catalytic domain. However, in contrast to NIH/3T3 cells, GFP fluorescence intensities increased after 48 hours compared to after

24 hours, while 5hmC fluorescence intensities did not increase simultaneously. Similarly, ELISA-based colorimetric analysis revealed higher increase of 5hmC amount in response to TET2CD-GFP overexpression 24 hours after transfection compared to after 48 hours.

With these experiments, it is shown that overexpression of TET2 catalytic domain is sufficient to induce 5hmC accumulation in two different cell lines. In both cell lines, TET2CD-GFP can exert its function, oxidizing 5mC to 5hmC.

There are various reasons for the different behavior: i) In U-2 OS cells TET2CD-GFP might oxidize 5hmC further to 5fC or 5caC according to its oxidative function [Ito et al., 2011, He et al., 2011]. ii) It is also possible that DNMT expression is higher in NIH/3T3 cells leading to faster 5mC formation. Since 5hmC is dependent on 5mC, 5mC production and conversion to 5hmC might reach an equilibrium state much faster than in U-2 OS. iii) IDAX, which might be needed for TET2 binding to DNA may be limited in NIH/3T3 cells. Therefore less TET2CD-GFP might bind to DNA leading to slower oxidation to 5hmC and further to 5fC and 5caC. iv) Since TET enzymatic activity is dependent on Fe^{2+} and 2-oxoglutarate abundance, it is also possible that those factors are limiting in NIH/3T3 cells leading to slower 5mC conversion.

Furthermore, it is conceivable that the expression of endogenous TET2 influences the different behaviors observed for NIH/3T3 and U-2 OS cells. U-2 OS cells express endogenous TET2, which might oxidize 5mC to 5hmC. This process may be accelerated by overexpression of TET2 catalytic domain. However after 48 hours a saturation effect may occur where much more TET2 is present as would be needed to process 5mC to 5hmC.

Therefore, for U-2 OS it would be of interest to investigate 5hmC amount at later time points after transfection. An additional decrease of 5hmC levels would further consolidate the TET2CD-GFP involving DNA demethylation pathway. In this context investigating also 5fC and 5caC abundance might be of further interest.

For NIH/3T3 cells instead, it might be interesting to investigate whether longer incubation times (e.g. 72 hours) lead to a further increase in TET2CD-GFP abundance, and if 5hmC amount varies in synchrony, or if a similar effect as for U-2 OS can be observed.

For both cell lines, it is of further interest, whether increased 5hmC staining in cells overexpressing TET2 catalytic domain is concomitant with the loss of 5mC.

In conclusion, overexpression of TET2 catalytic domain leads to 5hmC production in two different cell lines, one expressing endogenous TET2 (U-2 OS) compared to a cell line without TET2 expression (NIH/3T3). Kinetics of 5hmC formation differs between the two investigated cell lines and suggests that TET2 mediated oxidation of 5mC is not carried out the same way in both cell lines.

While in immunofluorescence analysis overexpression of TET2 catalytic domain clearly leads to 5hmC production, only a slight increase in 5hmC abundance was observed after transfection analyzed by flow cytometry (Compare Figure 5-6 and Figure 5-13).

Those differences might be explained by technical differences between microscopy and flow cytometry. For flow cytometry analysis GFP (TET2CD-GFP) was excited by the 488 nm laser. To avoid emission spectra overlap, 5hmC was stained with Alexa Fluor 680, which could be excited by the 633 nm laser. The emission maximum of Alexa Fluor 680 was not entirely covered

by the available emission filter, leading to a lower signal intensity. Therefore, it is conceivable that only cells showing high 5hmC signal could be detected. In microscopic studies, only few cells showed high 5hmC fluorescence signal intensity (Figure 5-6, top-right). If only those cells could be detected by flow cytometry, this might be the reason why only a very weak increase in 5hmC was detected.

6.3.1 TET2CD-GFP accumulates at nucleoli

Nucleoli are the places of ribosome biogenesis and are surrounded by nucleolus organizer regions on which the genes coding for ribosomal subunits (rDNA) are located. In this work it was observed that overexpressed TET2 catalytic domain accumulated to nucleoli of NIH/3T3 and U-2 OS cells. While on the one hand, the accumulation of TET2CD-GFP might be an effect of overexpression, on the other hand a function of TET2 in nucleolar compartments cannot be ruled out. A first step could be the investigation of whether TET2 as well as TET2 catalytic domain carry nucleolar localization sequences. This can be performed using tools to predict nucleolar localization sequences like the “nucleolar localization sequence detector” (“The Barton Group”; Division of computational biology, College of Life Sciences, University of Dundee).

Furthermore, it is reported [Bártová et al., 2010, Santoro and Grummt, 2005] that not only transcription of non-nucleolar genes is regulated by epigenetic changes including DNA methylation, but that epigenetic regulatory changes also take place during transcription of rDNA. Interestingly, those epigenetic regulatory changes include rDNA methylation and demethylation processes [Schmitz et al., 2009]. rDNA demethylation is reported [Schmitz et al., 2009] to be triggered by the non-enzymatic factor Gadd45a by recruiting the NER repair machinery which removes methylated cytosine, keeping the promoter of active genes in an hypomethylated state. In the study conducted by Schmitz and co-workers, a demethylation by the BER pathway was precluded, since depletion of the main BER enzyme (TDG) did not affect the methylation state of rDNA. However, the protein MBD4 (mismatch-specific thymine glycosylase) may have a vicarious function in the BER pathway. DNA demethylation promoted by Gadd45, involving MBD4 and AID/APOBEC has been reported [Rai et al., 2008, Hashimoto et al., 2012b], whereby Gadd45 may promote functional or physical interactions between AID/APOBEC and MBD4 at the site of demethylation. This process involves deamination of 5mC by AID/APOBEC resulting in thymine or 5hmU (5-hydroxymethyluracil), which are removed by MBD4 and converted to cytosine by BER. Furthermore, AID/APOBEC can also deaminate 5hmC [Hashimoto et al., 2012b] and a mechanism of DNA demethylation involving TET-mediated oxidation of 5mC to 5hmC and its deamination to 5hmU via AID/APOBEC can be hypothesized. 5hmU itself would then be removed by MBD4 as part of the BER pathway, yielding unmodified cytosine in the end. Even if this function is described for non-nucleolar DNA, a similar process on rDNA cannot be ruled out. In this thesis, localization of TET2 catalytic domain to nucleoli was shown, therefore suggesting a possible TET2 enzymatic function in rDNA demethylation processes.

In the presented work, nucleolar 5hmC fluorescence signal was absent in most of the cells (Figure 5-5 and Figure 5-7). Additionally, although TET2 catalytic domain did not always show nucleolar localization, a possible function of TET2 in nucleoli cannot be ruled out. On the one hand, it might be possible that 5hmC located in nucleoli is oxidized to 5caC or 5fC by the catalytic activity of TET2CD-GFP in nucleoli expressing TET2 catalytic domain. On the other hand, in nucleoli without TET2CD-GFP this function might be carried out by

endogenous TETs. Since TET2 is not expressed in NIH/3T3 (Figure 5-3 B), in that case the oxidative function might be carried out by TET1 or TET3. To further analyze this issue, it would be of interest to investigate the nucleolar abundance of the oxidative products 5fC or 5caC in the cell lines used in this work.

While it was observed that overexpressed TET2 catalytic domain accumulated to nucleoli of NIH/3T3 and U-2 OS cells, no accumulation of endogenous TET2 to nucleoli was observed (Figure 5-16 and Figure 5-17). This is an indication that the accumulation of TET2CD-GFP might be an effect of overexpression. Additionally, accumulation of TET2 to nucleoli does not necessarily mean that it is also active at these sites.

While TET2 might bind DNA by the cysteine-rich region of its catalytic domain [Pastor et al., 2013] also the need for IDAX is described for DNA binding. Therefore, it might be interesting to investigate, whether IDAX localizes to nucleoli.

6.4 Irradiation may enhance TET2CD-GFP-mediated 5hmC formation

Exposure to IR of TET2CD-GFP transfected cells led to a ~3.5-fold increase of 5hmC levels compared to control, transfected and irradiated cells (Figure 5-13), indicating that 5hmC production is enhanced if both conditions are combined. This shows that TET2 might have an impact on the response to IR. In this context, it is possible that irradiation triggers 5hmC accumulation by changing the levels of the enzymatic activities of TET enzymes. Such a response to radiation is already described for other proteins involved in the DNA repair pathway. ATM, for instance, exists in unirradiated cells as a dimer, is not phosphorylated and is dispersed in the nucleus. Upon irradiation instead, activated ATM monomerizes, is phosphorylated and recruited to DSBs induced by IR [Bakkenist and Kastan, 2003]. It is tempting to speculate that a similar mechanism could also regulate TET enzymes activation. This assumption may be investigated using an in vitro study, where TET1, TET2 or TET3 together with a methylated DNA oligo is irradiated and compared to an unirradiated sample with regard to 5hmC production. Maybe also just the recruitment and attachment of TET2 to damaged DNA is sufficient for its oxidizing activity. This process might also involve IDAX that may mediate TET2 binding to DNA.

In summary, these results demonstrate that treatment with IR in addition to TET2CD-GFP transfection leads to a sharp increase in 5hmC formation. In this context it is possible that irradiation activates TET enzymatic activity, however this needs to be confirmed.

6.5 DNA methylation decreases after irradiation with X-rays

Global 5mC level changes over time after irradiation with X-rays using ELISA-based techniques were measured, whereby a decrease in 5mC abundance up to three hours and a slight increase thereafter were observed (Figure 5-1 A). This might be due to conversion of 5mC to 5hmC as a response to radiation. An accumulation of 5hmC at damage sites was shown after irradiation with X-rays and ions using microscopical analysis (Figure 5-19 and Figure 5-20). Additionally, 5hmC amount increased in TET2CD-GFP transfected irradiated NIH/3T3 cells (Figure 5-13).

For direct comparison, it might be advantageous to investigate also 5mC accumulation/abundance in response to IR using microscopy or flow cytometry analysis. Additionally, investigating 5mC and 5hmC abundance after IR in TET knockdown cells would show, which TET protein is accountable for 5mC conversion.

There are also other methods that might be employed to simultaneously quantify 5mC and 5hmC changes. For example (2D-)TLC can be used to quantify 5mC and 5hmC with much higher sensitivity and can be employed to quantify not only 5(h)mC but also 5fC as well as 5caC abundance [Ito et al., 2011, He et al., 2011].

6.6 TET2 may exert its oxidative function at UV-induced damage and DSBs induced by ionizing radiation

TET2 catalytic domain was shown to be recruited to DNA damage sites induced by UV laser in NIH/3T3 cells (Figure 5-14 A and B). Recruitment was very fast ($t_{0.5}$ = 9.3 ± 2.9 seconds) and TET2CD-GFP persistence to the damaged area could be observed for at least two hours after irradiation. However, TET2 catalytic domain recruitment to DNA damage sites was not observed for X-rays- or ion-induced damage (Figure 5-15).

The recruitment of endogenous TET2 to DSBs was examined after irradiation with high LET gold ions as well as after X-ray irradiation in AG human fibroblasts (chapter 5.6). Recruitment was observed to ion induced damage sites as well as after irradiation with X-rays (Figure 5-16 and Figure 5-17). After ion irradiation TET2 co-localized with γH2AX as early as five to 10 minutes after irradiation and persisted at the damage site until at least three hours after irradiation. After irradiation with X-rays, endogenous TET2 and γH2AX coexisted in almost all of the irradiated cells.

Endogenous TET2 and TET2 catalytic domain showed pronounced differences in their recruitment, since endogenous TET2 was recruited to damage sites induced by ion and X-ray irradiation, while TET2CD-GFP was not recruited to damage induced by IR but to UV laser induced damage. One might argue that the recruitment of TET2 is dependent on 5mC amount, meaning that cells having high 5mC levels might show TET2 recruitment, while cells having low 5mC might not. Recruitment of endogenous TET2 was performed in AG cells, while recruitment of TET2 catalytic domain was analyzed in NIH/3T3 cells. As demonstrated in Figure 5-3 A, basal 5mC levels of NIH/3T3 cells are higher than for AG. Therefore, it is unlikely that TET2CD-GFP is not recruited after irradiation with X-rays or ions because of its substrate specificity to 5mC. Furthermore, recruitment of TET2CD-GFP after UV-laser irradiation was also observed in U-2 OS and in MEF cells (Figure 5-14 C and D) showing intermediate and low basal 5mC levels, respectively (Figure 5-3 A), thus substantiating the assumption that the absence of TET2CD-GFP at X-rays- or ion-induced damage sites is not dependent on 5mC amount. In addition, if TET2 recruitment was just dependent on 5mC amount, one might also observe TET2CD-GFP recruitment to X-rays- or ion-induced damage sites, which were not observed in this study.

Also, damage quality induced by UV laser compared to X-rays and ions greatly differs. While it is known that UV laser induces DSBs, SSBs as well as base damage repaired by BER mechanisms [Kong et al., 2009], the exact amount and distribution of DNA damage is not well defined. The spectrum of damage induced by ionizing radiation instead, is much more distinct. Therefore, some UV laser-induced lesions that are not induced by X-rays or heavy ion irradiation may favor TET2CD-GFP binding to UV laser-induced but not X-rays- or heavy ions-induced damage sites. Indeed, similar observations were made concerning TRF1 and TRF2 (telomere repeat-binding factors) recruitment [Williams et al., 2007, Splinter et al., 2010]. While both TRF1 and TRF2 were recruited to UV laser induced damage sites, no significant recruitment to damage sites after IR exposure was observed.

Since TET2CD-GFP comprises only the cis-rich and catalytic domain of TET2, it might lack domains that would favor the binding to X-rays- or heavy ion-induced damage sites. Maybe also the lack of a certain domain and the different damage quality play together in defining whether TET2 catalytic domain is recruited to damage sites or not. In this regard it is of interest to investigate whether also endogenous TET2 is recruited to UV laser induced damage sites.

Additionally, due to the fact that TET2 is missing a CXXC domain, which is important for CpG binding, it is possible that TET2 binds to DNA via interaction with IDAX. Therefore, it might be possible, that TET2CD-GFP binding to UV laser induced damage sites does not require interaction with IDAX, while binding to damage sites induced by X-rays or heavy ions needs the interaction with IDAX. This hypothesis would implicitly assume that IDAX is expressed in AG but not in NIH/3T3 cells. It is therefore of interest to investigate IDAX expression levels in the cell lines used for the experiments shown here.

Furthermore, IDAX binds unmethylated DNA. Therefore differences in recruitment might not be due to substrate specificity of IDAX. However, it is reported, that TET2 has a strong substrate preference on methylated DNA in a CpG-context [Hu et al., 2013]. Therefore substrate specificity as a reason for different recruitment behavior cannot be ruled out.

A more simple explanation might be that recruitment of TET2CD-GFP is not visible after irradiation with X-rays or energetic heavy ions. Generally, for recruitment analysis, heavy ions possess the advantage that their energy deposition along the track takes place at a confined space along the path of the single particle, thus producing high density of damage which is easier to detect, compared to X-rays (chapter 2.1.2). For TET2CD-GFP recruitment analysis, high-energy (1 GeV) iron ions were used. In that experiment the LET was 148 keV/μm, likely too low to produce detectable DNA lesions, especially if compared to low energy ions accelerated by the linear accelerator UNILAC (explained in chapter 2.1.1). For recruitment analysis of endogenous TET2 instead, high LET gold ions (LET = 12815 keV/μm) were used (chapter 5.6). Therefore, the difference in detection may be dependent on the LET. However, endogenous TET2 but not TET2CD-GFP was recruited after irradiation with X-rays thus ruling out an LET-dependent effect.

Additionally, TET2CD-GFP expression leads to brightly stained whole nuclei. As already mentioned, this staining might cover a faint recruitment of the construct at damage sites after X-ray and ion irradiation, and may account for the observed differences.

Overall, UV laser irradiation, but not IR, favors TET2CD-GFP recruitment to damage sites. This may be explained by structural differences between TET2CD-GFP and TET2 or between their interactors, thus influencing the recruitment to damage sites induced by IR. Nonetheless the results shown in this work suggest a possible involvement of TET2 in the DNA damage response, in particular the response to DSBs, supported by the co-localization of TET2 with γH2AX.

6.7 5hmC accumulates at damage sites induced by ionizing radiation and may be involved in the response to ionizing radiation induced double strand breaks

It was demonstrated that 5hmC accumulates at damage sites, either induced by irradiation with X-rays (Figure 5-20) or heavy ions (Figure 5-19). In both cases, co-localization of 5hmC and the DSB marker γH2AX was verified using intensity correlation analysis.

In this context, validating whether 5hmC formation is dependent on TET2 enzymatic activity is an important issue. While TET2 knockdown was not efficient (Figure 5-22), another approach is to perform this study employing catalytic mutants of TET2. It is also important to include TET1 and TET3 in this study, since these enzymes might also contribute to 5hmC formation.

5mC oxidation might also be produced independently of TETs by reactive oxygen species. So it is reported that free radicals are able to attack 5mC in vitro to produce altered bases (e.g. 5hmC) [Castro et al., 1994]. Additionally, 5fC was found to be formed in 5mC-containing DNA fragments upon γ-irradiation [Murata-Kamiya et al., 1999]. However the abundance of 5fC only reached yields of 1.5 % of all nucleosides at an irradiation dose of 400 Gy. Additionally, investigating 5mC oxidation by reactive oxygen species might be challenging due to low 5hmC abundance.

To achieve deeper knowledge into DNA demethylation processes after IR exposure, further work was focused on 5hmC appearance and disappearance at damage sites after activation of the DDR. 5hmC foci increased rapidly after irradiation following γH2AX, although their total number never equaled that of γH2AX. Only at later time points both marks show comparable abundance (Figure 5-23 and Table 5-6). The possibility that 5hmC and γH2AX foci clustering may account for a decrease in foci number can be excluded with reasonable certainty. Namely, it is demonstrated that DNA breaks produced by IR have limited diffusion in the nucleus and therefore do not form clusters [Jakob et al., 2009].

Most of DSBs (~85 %) are repaired with fast kinetics, while the repair of ~15 % of DSBs is much slower [Beucher et al., 2009]. HR represents this slow component of DSB repair and DSBs which are repaired by slow kinetics predominantly localize to heterochromatic regions [Goodarzi et al., 2010]. Since 5hmC is dependent on 5mC, which also localizes to heterochromatic regions in promoters [Shen et al., 2013], 5hmC might only be involved in HR-mediated DSB repair and therefore might be restricted to G_2-phase cells. Therefore, it was investigated whether the reduced 5hmC foci count compared to γH2AX foci was caused by reduced or missing 5hmC foci formation in G_1-phase of the cell cycle. As expected, there were more γH2AX foci in S/G_2 cells. This can simply be explained by the fact that there is an increased amount of DNA in S/G_2 cells and part of the damage sites in these cell cycle stages are repaired by HR, the slower component of DSB repair [Beucher et al., 2009]. Surprisingly, there were more 5hmC foci counted in G_1 cells compared to S/G_2 cells. Otani and colleagues [Otani et al., 2013] reported that the overall amount of 5hmC in mouse ESCs was high in G_1 and S phase, while it was low in G_2 phase, suggesting that 5hmC in mouse ESCs is regulated in a cell cycle-dependent manner. This would also explain the findings of more 5hmC labeled damage sites in this cell cycle stages. However, it has to be mentioned that for the analysis in the presented doctoral thesis only few S/G_2 cells were taken into account (Table 5-5). Those might not be sufficient to ensure reliable results and further investigations have to be performed to substantiate these effects.

Differences in foci number might also be explained by technical limitations. While γH2AX forms large “macro-foci” after irradiation with X-rays, 5hmC forms “micro-foci” that are concentrated within a smaller area, instead. Due to the size of γH2AX foci, they are easily detected by immunostaining and confocal microscopy, while detection of small 5hmC foci is more challenging. Therefore, less 5hmC foci might be counted since some of them were just not detectable. To verify this assumption, irradiation with heavy ions was used. As already

mentioned (chapter 2.2.3), irradiation with heavy ions induces a high local density of damage (clustered damage) at which accumulation of repair related factors is usually easier to detect. Therefore, γH2AX as well as 5hmC foci were counted in cells which were irradiated with iron ions. It has to be mentioned that the conditions for this kind of analysis were not optimal, since high energy ions (1GeV) were used, resulting in a relatively low LET which produces a lower local density of damage compared to high LET ions, the latter being the optimal choice for this kind of experiment. For this analysis incubation of 30 minutes after irradiation was chosen since this was the time point where 5hmC as well as γH2AX foci number reached maxima after irradiation with X-rays (Figure 5-23 and Table 5-6). The results clearly display more cells showing γH2AX (73.6 %) accumulation at the ion streak compared to 5hmC accumulation (26.4 %). Furthermore all 5hmC streaks displayed a total number of 244 IRIF, while there where 271 γH2AX IRIF at the same streaks. This clearly shows that also after irradiation with iron ions there are far more γH2AX foci compared to 5hmC foci and this gives a first indication that the difference in 5hmC and γH2AX foci is not due to detection differences of the single signals. However to fully exclude this possibility, the same analysis should be made using heavy ions with higher LET.

5hmC is mainly associated with euchromatic regions [Kubiura et al., 2012], which was confirmed in this work using intensity profiles (Figure 5-21). Namely, 5hmC co-localized with γH2AX at sites, located outside of heterochromatic chromocenters. However, 5hmC depends on pre-existing 5mC and 5mC of promoter regions is mainly located in heterochromatin [Shen et al., 2013]. In recent studies [Jakob et al., 2011], a movement of DSBs (marked by γH2AX) from the interior to the heterochromatic periphery, where repair may proceed, was observed. Since 5hmC spatial location was investigated one hour after irradiation, one could speculate that 5mC located in heterochromatin is oxidized to 5hmC, the latter being transported to the border of heterochromatin (similar to γH2AX). Should 5hmC only be formed in heterochromatin, this could explain why there are less 5hmC foci compared to γH2AX foci, since γH2AX is also generated in euchromatic regions. It is questionable whether the heterochromatic amount of AG cells can account for the differences in 5hmC and γH2AX foci number. In that case it might be of help to investigate whether 5hmC formation is different for damage induced inside or outside of heterochromatic regions. Additionally, in this study 5hmC spatial location was only investigated one hour after irradiation with heavy ions. Therefore, it might be of interest to investigate whether after short times after irradiation 5hmC is still located inside of chromocenters. This can be performed by targeted irradiation of chromocenters, as described previously [Jakob et al., 2011].

In addition, there is also evidence for DNA methylation in gene bodies which is higher than DNA methylation in promoter regions and where DNA methylation is more clearly related to the presence of transcribed regions than to transcription repression. On the other hand, gene expression is positively correlated to open chromatin, resulting in a link between gene body methylation, transcription and open chromatin [Jjingo et al., 2012]. As already mentioned 5hmC is mainly associated to euchromatin and is dependent on 5mC abundance. Assuming that only DSB induction in gene bodies will lead to 5hmC formation, this will result in a 5hmC foci number, that will be lower than that of γH2AX foci, which itself will be formed at all DSBs after IR.

Additionally, analysis of 5hmC and γH2AX foci kinetics after irradiation with X-rays and heavy ions revealed that whenever a 5hmC focus was observed this always co-localized with a

γH2AX focus. This observation gives further insights on a 5hmC involvement in the DSB repair.

6.7.1 5hmC might serve as a binding platform for proteins of the DSB repair

Since there were indications that 5hmC might be involved in the response to IR induced DSBs, the question was, what kind of function 5hmC takes over in this process.

As already mentioned above, 5hmC might be transported out of the heterochromatin or heterochromatic regions may get decondensed so that 5hmC can be found in euchromatic regions. In those euchromatic regions repair takes place and in this context 5hmC might serve as a marker for DSBs or a binding platform for proteins involved in chromatin remodeling or repair. In this thesis, the influence of DNA-PKcs inhibition on 5hmC foci formation and persistence was investigated. It is known that γH2AX foci formation is not dependent on DNA-PKcs activity. Conversely, repair of DSBs is strongly affected by DNA-PKcs inhibition, indicated by increased γH2AX foci and their persistence over time [Bee et al., 2013]. This was confirmed in this doctoral thesis (Figure 5-24). Similarly, 5hmC foci persistence was increased in cells treated with DNA-PK inhibitor, demonstrating that not only DSB repair but also 5hmC foci kinetics depend on the enzymatic activity of DNA-PK (Figure 5-24). Therefore, if the repair is slowed down due to DNA-PK inhibition (Figure 5-24), 5hmC might also persist as a marker for DSBs or a binding platform for repair factors until repair is accomplished.

6.8 Conclusions and perspectives

In this work it was shown that expression of TET2 catalytic domain increases 5hmC levels in different cell lines. Furthermore, overexpressed TET2 catalytic domain accumulated to nucleoli, suggesting a possible TET2 enzymatic function in rDNA demethylation processes. While irradiation alone did not change global 5hmC levels it was enhanced by irradiation in addition to TET2CD-GFP overexpression. Ectopically expressed TET2 catalytic domain is recruited to UV laser induced damage, while recruitment of endogenous TET2 to DNA damage was observed after irradiation with X-rays and heavy ions. Proteins of the TET family are known to oxidize 5mC to 5hmC. In good agreement local 5hmC accumulation was found at damage sites after X-ray and ion irradiation. Whereby 5hmC foci kinetics followed γH2AX kinetics and release of 5hmC rely on repair kinetics shown by inhibition of DNA-PK enzymatic activity.

Increasing evidence suggest that the DNA damage response is closely connected to chromatin conformation changes in a process comprising the access to the break, followed by the repair of the break and finally the restoration of chromatin (reviewed in [Soria et al., 2012]). Both the access to the break and the restoration of DNA need extensive chromatin conformation changes allowing access to the DNA by repair proteins. Since unmodified cytosines as well as 5hmC are correlated to an open chromatin state, it is likely that these factors play a major role in chromatin conformation changes in the DNA damage response. However, this might not be directed by the presence of cytosine or 5hmC alone but might rather be achieved by recruiting selective 5hmC-binding proteins or excluding 5mC-binding proteins. Additionally, also specific binders for 5caC or 5fC, the oxidative derivatives of 5hmC, might contribute to chromatin conformation changes in response to irradiation. For example it is reported [Yildirim et al., 2011] on two antagonistic chromatin regulators (MBD3/NuRD and Brg1 (Brahma-Related Gene 1)) that specifically bind 5hmC but not 5mC, which are important for expression or repression of certain genes in ESCs. Since there are several chromatin remodelers known to be

involved in the repair of DSBs, it is not unlikely that those are specifically attracted by 5hmC although specific investigations were not performed so far.

Besides recruiting chromatin remodeling factors, 5hmC and its derivatives are also known to direct DNA repair factors to DNA. Namely it is reported [Spruijt et al., 2013] that TDG, Bloom and p53 were recruited to modified cytosines (most pronounced for 5fC).

In order to fulfill its function as a binding platform different from 5mC, 5hmC needs to be oxidized from 5mC as a response to DNA damage. Since replication related DNA demethylation processes are too slow to be involved in those fast DNA repair processes, only fast enzymatically catalyzed DNA demethylation processes come into question. Therefore TET enzymes, known to be able to oxidize 5mC to 5hmC or 5fC and 5caC, respectively, were considered. The fact that TET2 is recruited to DSBs and that 5hmC accumulates at DSBs after irradiation with X-rays and heavy ions in a very short time frame, suggests that TET2 might be involved in a process where 5mC is converted to 5hmC and finally to cytosine to change chromatin accessibility around the DSB or to serve as a binding platform distinct from 5mC.

While 5hmC may contribute to a proper DNA repair process, 5mC conversion to 5hmC may also have deleterious effects if 5mC is not restored properly. It is known that oncogenes and repeat elements are methylated to assure their transcriptional repression. A loss of DNA methylation instead may reactivate repeat elements and oncogenes and therefore may contribute to carcinogenesis [Robertson, 2002, Weisenberger et al., 2005, Das and Singal, 2004]. Therefore 5mC demethylation must be a tightly controlled mechanism ensuring proper formation of 5hmC and its derivatives as well as 5mC restoration.

7 Outlook

In this work first indications of a DNA demethylation process in the response to IR induced DSBs are given. This process is likely to be TET2-driven, though confirmation is still needed. Therefore in further studies it must be investigated whether TET2 or other TET proteins are needed for the formation of 5hmC foci at damage sites. Therefore, it would be paramount to establish a functional knockdown of TET proteins and to investigate 5hmC formation as a part of the DNA demethylation process in TET-depleted cells. Meanwhile several groups have established TET knockout cells that might be used instead of knockdown cells. Furthermore it is of interest to examine, why 5hmC and γH2AX foci number differ. In this work it is discussed that 5hmC may only be formed in heterochromatic promoter regions. Therefore, with targeted irradiation inside or outside of heterochromatic regions, differences in 5hmC accumulation might be investigated.

Additionally it should be investigated whether also 5mC and other 5mC derivatives (5fC and 5caC) can be found at damage sites, which will further consolidate a TET-driven demethylation process. In this context a time course of 5mC and 5mC derivative formation may give insights on how fast the demethylation process takes place. Like for 5hmC, this might be performed by microscopic analysis. However, it is questionable whether 5fC and 5caC are detectable due to their low abundance.

In this work, transfection of TET2 catalytic domain as well as irradiation concomitant to transfection, led to 5hmC accumulation in NIH/3T3 cells. In future experiments it should be investigated whether 5hmC accumulation is accompanied by a loss of 5mC amount, which can be performed by microscopic or flow cytometry analysis. This will give a further indication that 5mC is oxidized to 5hmC and that a TET2 driven demethylation process takes place. Including TET2 mutants will further help to investigate whether 5hmC formation is dependent on TET2. Additionally, it might be worth investigating whether also TET1 and TET3 overexpression leads to 5hmC formation.

8 Bibliography

[Agarwal et al., 2006] Agarwal, S., Tafel, A. A., and Kanaar, R. (2006). DNA double-strand break repair and chromosome translocations. *DNA Repair (Amst.)*, 5(9-10):1075–1081.

[Aguilera et al., 2010] Aguilera, O., Fernandez, A. F., Munoz, A., and Fraga, M. F. (2010). Epigenetics and environment: a complex relationship. *J. Appl. Physiol.*, 109(1):243–251.

[Alberts et al., 2002] Alberts, B., Johnson, A., Lewis, J., Raff, M., Roberts, K., and Walter, P. (2002). *Molecular Biology of the Cell, 4th edition*. New York: Garland Science.

[Antwih et al., 2013] Antwih, D. A., Gabbara, K. M., Lancaster, W. D., Ruden, D. M., and Zielske, S. P. (2013). Radiation-induced epigenetic DNA methylation modification of radiation-response pathways. *Epigenetics*, 8:1–10.

[Aypar et al., 2011] Aypar, U., Morgan, W. F., and Baulch, J. E. (2011). Radiation-induced epigenetic alterations after low and high LET irradiations. *Mutation Research*, 10:24–33.

[Bakkenist and Kastan, 2003] Bakkenist, C. J. and Kastan, M. B. (2003). DNA damage activates ATM through intermolecular autophosphorylation and dimer dissociation. *Nature*, 421(6922):499–506.

[Bee et al., 2013] Bee, L., Fabris, S., Cherubini, R., Mognato, M., and Celotti, L. (2013). The efficiency of homologous recombination and non-homologous end joining systems in repairing double-strand breaks during cell cycle progression. *PLoS ONE*, 8(7):e69061.

[Bekker-Jensen and Mailand, 2010] Bekker-Jensen, S. and Mailand, N. (2010). Assembly and function of DNA double-strand break repair foci in mammalian cells. *DNA Repair (Amst.)*, 9(12):1219–1228.

[Berger et al., 2009] Berger, S. L., Kouzarides, T., Shiekhattar, R., and A.Shilatifard (2009). An operational definition of epigenetics. *Genes Dev.*, 23:781–783.

[Bethe, 1930] Bethe, H. (1930). Zur Theorie des Durchgangs schneller Korpuskularstrahlen durch Materie. *Annalen der Physik*, 397:325–400.

[Beucher et al., 2009] Beucher, A., Birraux, J., Tchouandong, L., Barton, O., Shibata, A., Conrad, S., Goodarzi, A. A., Krempler, A., Jeggo, P. A., and Lobrich, M. (2009). ATM and Artemis promote homologous recombination of radiation-induced DNA double-strand breaks in G2. *EMBO J.*, 28(21):3413–3427.

[Bhutani et al., 2010] Bhutani, N., Brady, J. J., Damian, M., Sacco, A., Corbel, S. Y., and Blau, H. M. (2010). Reprogramming towards pluripotency requires AID-dependent DNA demethylation. *Nature*, 463(7284):1042–1047.

[Bhutani et al., 2011] Bhutani, N., Burns, D. M., and Blau, H. M. (2011). DNA demethylation dynamics. *Cell*, 146:866–872.

[Bloch, 1933] Bloch, F. (1933). Zur Bremsung rasch bewegter Teilchen beim Durchgang durch Materie. *Annalen der Physik*, 408:285–320.

[Bártová et al., 2010] Bártová, E., Horáková, A. H., Uhlírová, R., Raška, I., Galiová, G., Orlova, D., and Kozubek, S. (2010). Structure and epigenetics of nucleoli in comparison with non-nucleolar compartments. *Journal of Histochemistry & Cytochemistry*, 58:391–403.

[Castro et al., 1994] Castro, G. D., Stamato, C. J., and Castro, J. A. (1994). 5-methylcytosine attack by free radicals arising from bromotrichloromethane in a model system: structures of reaction products. *Free Radic. Biol. Med.*, 17:419–428.

[Chaudhry and Omaruddin, 2012] Chaudhry, M. A. and Omaruddin, R. A. (2012). Differential DNA methylation alterations in radiation-sensitive and -resistant cells. *DNA and Cell Biology*, 31(6):908–916.

[Chen et al., 2012] Chen, C.-C., Wang, K.-Y., and Shen, C.-K. J. (2012). The mammalian de novo DNA methyltransferases Dnmt3a and Dnmt3b are also DNA 5-hydroxymethyl cytosine dehydroxymethylases. *The Journal of Biological Chemistry*, 287:33116–33121.

[Chen and Riggs, 2011] Chen, Z. X. and Riggs, A. D. (2011). DNA methylation and demethylation in mammals. *J. Biol. Chem.*, 286(21):18347–18353.

[Christmann et al., 2003] Christmann, M., Tomicic, M. T., Roos, W. P., and Kaina, B. (2003). Mechanisms of human DNA repair: an update. *Toxicology*, 193(1-2):3–34.

[Cuozzo et al., 2007] Cuozzo, C., Porcellini, A., Angrisano, T., Morano, A., Lee, B., Pardo, A. D., Messina, S., Iuliano, R., Fusco, A., Santillo, M. R., Muller, M. T., Chiariotti, L., Gottesman, M. E., and Avvedimento, E. V. (2007). DNA damage, homology-directed repair, and DNA methylation. *PLoS Genetics*, 3:1144–1162.

[Dalton and Bellacosa, 2012] Dalton, S. R. and Bellacosa, A. (2012). DNA demethylation by TDG. *Epigenomics*, 4(4):459–467.

[Das and Singal, 2004] Das, P. M. and Singal, R. (2004). DNA methylation and cancer. *J. Clin. Oncol.*, 22(22):4632–4642.

[Deaton and Bird, 2011] Deaton, A. M. and Bird, A. (2011). CpG islands and the regulation of transcription. *Genes Dev.*, 25(10):1010–1022.

[Deplus et al., 2013] Deplus, R., Delatte, B., Schwinn, M. K., Defrance, M., Mendez, J., Murphy, N., Dawson, M. A., Volkmar, M., Putmans, P., Calonne, E., Shih, A. H., Levine, R. L., Bernard, O., Mercher, T., Solary, E., Urh, M., Daniels, D. L., and Fuks, F. (2013). TET2 and TET3 regulate GlcNAcylation and H3K4 methylation through OGT and SET1/COMPASS. *The EMBO Journal*, 32:1–11.

[Gehring et al., 2009] Gehring, M., Reik, W., and Henikoff, S. (2009). DNA demethylation by DNA repair. *Trends Genet.*, 25(2):82–90.

[Globisch et al., 2010] Globisch, D., Munzel, M., Muller, M., Michalakis, S., Wagner, M., Koch, S., Bruckl, T., Biel, M., and Carell, T. (2010). Tissue distribution of 5-hydroxymethylcytosine and search for active demethylation intermediates. *PLoS ONE*, 5(12):e15367.

[Goetz et al., 2011] Goetz, W., Morgan, M. N. M., and Baulch, J. E. (2011). The effect of radiation quality on the genomic DNA methylation profiles in irradiated human cell lines. *Radiation Research*, 175:575–587.

[Goodarzi et al., 2010] Goodarzi, A. A., Jeggo, P., and Lobrich, M. (2010). The influence of heterochromatin on DNA double strand break repair: Getting the strong, silent type to relax. *DNA Repair (Amst.)*, 9(12):1273–1282.

[Goodhead, 1994] Goodhead, D. T. (1994). Initial events in the cellular effects of ionizing radiations: clustered damage in DNA. *Int. J. Radiat. Biol.*, 65(1):7–17.

[Guo et al., 2011] Guo, J. U., Su, Y., Zhong, C., Ming, G. L., and Song, H. (2011). Emerging roles of TET proteins and 5-hydroxymethylcytosines in active DNA demethylation and beyond. *Cell Cycle*, 10(16):2662–2668.

[Ha et al., 2011] Ha, K., Lee, G. E., Palii, S. S., Brown, K. D., Takeda, Y., Liu, K., Bhalla, K. N., and Robertson, K. D. (2011). Rapid and transient recruitment of DNMT1 to DNA double-strand breaks is mediated by its interaction with multiple components of the DNA damage response machinery. *Hum. Mol. Genet.*, 20(1):126–140.

[Haber, 2000] Haber, J. E. (2000). Partners and pathways repairing a double-strand break. *Trends Genet.*, 16:259–264.

[Hackett et al., 2013] Hackett, J. A., Sengupta, R., Zylicz, J. J., Murakami, K., Lee, C., Down, T. A., and Surani, M. A. (2013). Germline DNA demethylation dynamics and imprint erasure through 5-hydroxymethylcytosine. *Science*, 339:448–452.

[Hall and Giaccia, 2012] Hall, E. J. and Giaccia, A. J. (2012). *Radiobiology for the radiologist*. Lippincott Williams & Wilkins.

[Han et al., 2013] Han, K., Lee, J., Km, H.-S., Yang, K., and Yi, J. M. (2013). Dna methylation of mobile genetic elements in human cancers. *Genes & Genomics*, 35:265–271.

[Hanawalt, 2000] Hanawalt, P. C. (2000). DNA repair. The bases for Cockayne syndrome. *Nature*, 405(6785):415–416.

[Hashimoto et al., 2012a] Hashimoto, H., Liu, Y., Upadhyay, A. K., Chang, Y., Howerton, S. B., Vertino, P. M., Zhang, X., and Cheng, X. (2012a). Recognition and potential mechanisms for replication and erasure of cytosine hydroxymethylation. *Nucleic Acids Res.*, 40(11):4841–4849.

[Hashimoto et al., 2012b] Hashimoto, H., Zhang, X., and Cheng, X. (2012b). Excision of thymine and 5-hydroxymethyluracil by the MBD4 DNA glycosylase domain: structural basis and implications for active DNA demethylation. *Nucleic Acids Research*, 40:8276–8284.

[He and Hannon, 2004] He, L. and Hannon, G. J. (2004). MicroRNAs: small RNAs with a big role in gene regulation. *Nat. Rev. Genet.*, 5(7):522–531.

[He et al., 2011] He, Y.-F., Li, B.-Z., Li, Z., Liu, P., Wang, Y., Tang, Q., Ding, J., Jia, Y., Chen, Z., Li, L., Sun, Y., Li, X., Dai, Q., Song, C.-X., Zhang, K., He, C., and Xu, G.-L. (2011). Tet-mediated formation of 5-carboxylcytosine and its excision by TDG in mammalian DNA. *Science*, 333:1303–1307.

[Hegde et al., 2008] Hegde, M. L., Hazra, T. K., and Mitra, S. (2008). Early steps in the DNA base excision/single-strand interruption repair pathway in mammalian cells. *Cell Res.*, 18(1):27–47.

[Hu et al., 2013] Hu, L., Li, Z., Cheng, J., Rao, Q., Gong, W., Liu, M., Shi, Y. G., Zhu, J., Wang, P., and Xu, Y. (2013). Crystal structure of TET2-DNA complex: Insight into TET-mediated 5mc oxidation. *Cell*, 155:1–11.

[Huang et al., 2013] Huang, S., Zhu, Z., Wang, Y., Wang, Y., Xu, L., Chen, X., Xu, Q., Zhang, Q., Zhao, X., Yu, Y., and Wu, D. (2013). Tet1 is required for Rb phosphorylation during G1/S phase transition. *Biochemical and Biophysical Research Communications*, 434:241–244.

[Illingworth and Bird, 2009] Illingworth, R. S. and Bird, A. P. (2009). CpG islands – 'A rough guide'. *FEBS Letters*, 583:1713–1720.

[Inoue et al., 2011] Inoue, A., Shen, L., Dai, Q., He, C., and Zhang, Y. (2011). Generation and replication-dependent dilution of 5fC and 5caC during mouse preimplantation development. *Cell Research*, 21:1670–1676.

[Iqbal et al., 2011] Iqbal, K., Jinb, S.-G., Pfeifer, G. P., and Szabó, P. E. (2011). Reprogramming of the paternal genome upon fertilization involves genome-wide oxidation of 5-methylcytosine. *PNAS*, 108:3642–3647.

[Ito et al., 2010] Ito, S., D'Alessio, A. C., Taranova, O. V., Hong, K., Sowers, L. C., and Zhang, Y. (2010). Role of Tet proteins in 5mc to 5hmc conversion, ES-cell self-renewal and inner cell mass specification. *Nature*, 466:1129–1135.

[Ito et al., 2011] Ito, S., Shen, L., Dai, Q., Wu, S. C., Collins, L. B., Swenberg, J. A., He, C., and Zhang, Y. (2011). Tet proteins can convert 5-methylcytosine to 5-formylcytosine and 5-carboxylcytosine. *Science*, 333(6047):1300–1303.

[Iurlaro et al., 2013] Iurlaro, M., Ficz, G., Oxley, D., Raiber, E.-A., Bachman, M., Booth, M. J., Andrews, S., Balasubramanian, S., and Reik, W. (2013). A screen for hydroxymethylcytosine and formylcytosine binding proteins suggests functions in transcription and chromatin regulation. *Genome Biology*, 14:R119.

[Jakob et al., 2003] Jakob, B., Scholz, M., and Taucher-Scholz, G. (2003). Biological imaging of heavy charged-particle tracks. *Radiat. Res.*, 159(5):676–684.

[Jakob et al., 2011] Jakob, B., Splinter, J., Conrad, S., Voss, K. O., Zink, D., Durante, M., Lobrich, M., and Taucher-Scholz, G. (2011). DNA double-strand breaks in heterochromatin elicit fast repair protein recruitment, histone H2AX phosphorylation and relocation to euchromatin. *Nucleic Acids Research*, 39(15):6489–6499.

[Jakob et al., 2009] Jakob, B., Splinter, J., Durante, M., and Taucher-Scholz, G. (2009). Live cell microscopy analysis of radiation-induced DNA double-strand break motion. *Proc. Natl. Acad. Sci. U.S.A.*, 106(9):3172–3177.

[Jjingo et al., 2012] Jjingo, D., Conley, A. B., Yi, S. V., Lunyak, V. V., and Jordan, I. K. (2012). On the presence and role of human gene-body DNA methylation. *Oncotarget*, 3(4):462–474.

[Kim et al., 2013] Kim, J.-G., Park, M.-T., Heo, K., Yang, K.-M., and Yi, J. M. (2013). Epigenetics meets radiation biology as a new approach in cancer treatment. *International Journal of Molecular Sciences*, 14:15059–15073.

[Kim and Wilson, 2012] Kim, Y. J. and Wilson, D. M. (2012). Overview of base excision repair biochemistry. *Curr Mol Pharmacol*, 5(1):3–13.

[Kinner et al., 2008] Kinner, A., Wu, W., Staudt, C., and Iliakis, G. (2008). Gamma-H2AX in recognition and signaling of DNA double-strand breaks in the context of chromatin. *Nucleic Acids Res.*, 36(17):5678–5694.

[Ko et al., 2013] Ko, M., An, J., Bandukwala, H. S., Chavez, L., Äijö, T., Pastor, W. A., Segal, M. F., Li, H., Koh, K. P., Lähdesmäki, H., Hogan, P. G., Aravind, L., and Rao, A. (2013). Modulation of TET2 expression and 5-methylcytosine oxidation by the CXXC domain protein IDAX. *Nature*, 497:122–136.

[Koh et al., 2011] Koh, K. P., Yabuuchi, A., Rao, S., Huang, Y., Cunniff, K., Nardone, J., Laiho, A., Tahiliani, M., Sommer, C. A., Mostoslavsky, G., Lahesmaa, R., Orkin, S. H., Rodig, S. J., Daley, G. Q., and Rao, A. (2011). Tet1 and Tet2 regulate 5-hydroxymethylcytosine production and cell lineage specification in mouse embryonic stem cells. *Cell*, 8:200–213.

[Kohli and Zhang, 2013] Kohli, R. M. and Zhang, Y. (2013). TET enzymes, TDG and the dynamics of DNA demethylation. *Nature*, 502:472–479.

[Kong et al., 2009] Kong, X., Mohanty, S. K., Stephens, J., Heale, J. T., Gomez-Godinez, V., Shi, L. Z., Kim, J.-S., Yokomori, K., and Berns, M. W. (2009). Comparative analysis of different laser systems to study cellular responses to DNA damage in mammalian cells. *Nucleic Acids Research*, 37:e68.

[Kraft, 2008] Kraft, G. (2008). *Tumortherapie mit schweren Ionen.* Verein zur Förderung der Tumortherapie mit schweren Ionen e.V.

[Kubiura et al., 2012] Kubiura, M., Okano, M., Kimura, H., Kawamura, F., and Tada, M. (2012). Chromosome-wide regulation of euchromatin-specific 5mc to 5hmc conversion in mouse ES cells and female human somatic cells. *Chromosome Research*, 20:837 – 848.

[Kudo et al., 2012] Kudo, Y., Tateishi, K., Yamamoto, K., Yamamoto, S., Asaoka, Y., Ijichi, H., Nagae, G., Yoshida, H., Aburatani, H., and Koike, K. (2012). Loss of 5-hydroxymethylcytosine is accompanied with malignant cellular transformation. *Cancer Sci.*, 103(4):670–676.

[Kuhmann et al., 2011] Kuhmann, C., Weichenhan, D., Rehli, M., Plass, C., Schmezer, P., and Popanda, O. (2011). DNA methylation changes in cells regrowing after fractioned ionizing radiation. *Radiotherapy and Oncology*, 101:116–121.

[Langemeijer et al., 2009] Langemeijer, S. M. C., Kuiper, R. P., Berends, M., Knops, R., Aslanyan, M. G., Massop, M., Stevens-Linders, E., van Hoogen, P., van Kessel, A. G., Raymakers, R. A. P., Kamping, E. J., Verhoef, G. E., Verburgh, E., Hagemeijer, A., Vandenberghe, P., de Witte, T., van der Reijden, B. A., and Jansen, J. H. (2009). Acquired mutations in TET2 are common in myelodysplastic syndromes. *Nature Genetics*, 41:838–843.

[Le May et al., 2010] Le May, N., Egly, J. M., and Coin, F. (2010). True lies: the double life of the nucleotide excision repair factors in transcription and DNA repair. *J Nucleic Acids*, 2010.

[Leonhardt et al., 1992] Leonhardt, H., Page, A. W., Weier, H. U., and Bestor, T. H. (1992). A targeting sequence directs DNA methyltransferase to sites of DNA replication in mammalian nuclei. *Cell*, 71(5):865–873.

[Li et al., 2007] Li, B., Carey, M., and Workman, J. L. (2007). The role of chromatin during transcription. *Cell*, 128:707–719.

[Li et al., 2004] Li, Q., Lau, A., Morris, T. J., Guo, L., Fordyce, C. B., and Stanley, E. F. (2004). A syntaxin 1, Galpha(o), and N-type calcium channel complex at a presynaptic nerve terminal: analysis by quantitative immunocolocalization. *The Journal of Neuroscience*, 24:4070–7081.

[Lister et al., 2009] Lister, R., Pelizzola, M., Dowen, R. H., Hawkins, R. D., Hon, G., Tonti-Filippini, J., Nery, J. R., Lee, L., Ye, Z., Ngo, Q.-M., Edsall, L., Antosiewicz-Bourget, J., Stewart, R., Ruotti, V., Millar, A. H., Thomson, J. A., Ren, B., and Ecker, J. R. (2009). Human DNA methylomes at base resolution show widespread epigenomic differences. *Nature*, 462:315–322.

[Liutkeviciute et al., 2009] Liutkeviciute, Z., Lukinavicius, G., Masevicius, V., Daujotyte, D., and Klimasauskas, S. (2009). Cytosine-5-methyltransferases add aldehydes to DNA. *Nat. Chem. Biol.*, 5(6):400–402.

[Lorsbach et al., 2003] Lorsbach, R. B., Moore, J., Mathew, S., Raimondi, S. C., Mukatira, S. T., and Downing, J. R. (2003). TET1, a member of a novel protein family, is fused to MLL in acute myeloid leukemia containing the t(10;11)(q22;q23). *Leukemia*, 3:637–641.

[Lowry et al., 1951] Lowry, O. H., Rosebrough, N. J., Farr, A. L., and Randall, R. J. (1951). Protein measurement with the Folin phenol reagent. *J. Biol. Chem.*, 193(1):265–275.

[Milutinovic et al., 2003] Milutinovic, S., Zhuang, Q., Niveleau, A., and Szyf, M. (2003). Epigenomic stress response. Knockdown of DNA methyltransferase 1 triggers an intra-S-phase arrest of DNA replication and induction of stress response genes. *J. Biol. Chem.*, 278(17):14985–14995.

[Mortusewicz et al., 2005] Mortusewicz, O., Schermelleh, L., Walter, J., Cardoso, M. C., and Leonhardt, H. (2005). Recruitment of DNA methyltransferase I to DNA repair sites. *Proc. Natl. Acad. Sci. U.S.A.*, 102(25):8905–8909.

[Munro, 1970] Munro, T. R. (1970). The relative radiosensitivity of the nucleus and cytoplasm of Chinese hamster fibroblasts. *Radiat. Res.*, 42(3):451–470.

[Murata-Kamiya et al., 1999] Murata-Kamiya, N., Kamiya, H., Karino, N., Ueno, Y., Kaji, H., Matsuda, A., and Kasai, H. (1999). Formation of 5-formyl-2'-deoxycytidine from 5-methyl-2'-deoxycytidine in duplex DNA by Fenton-type reactions and gamma-irradiation. *Nucleic Acids Res.*, 27(22):4385–4390.

[Nakamura et al., 2012] Nakamura, T., Liu, Y.-J., Nakashima, H., Umehara, H., Inoue, K., Matoba, S., Tachibana, M., Ogura, A., Shinkai, Y., and Nakano, T. (2012). PGC7 binds histone H3K9me2 to protect against conversion of 5mc to 5hmc in early embryos. *Nature*, 486:415–419.

[O'Hagan et al., 2008] O'Hagan, H. M., Mohammad, H. P., and Baylin, S. B. (2008). Double strand breaks can initiate gene silencing and SIRT1-dependent onset of DNA methylation in an exogenous promoter CpG island. *PLoS Genetics*, 4:e1000155.

[Orlowski et al., 2011] Orlowski, C., Mah, L.-J., Vasireddy, R. S., El-Osta, A., and Karagiannis, T. C. (2011). Double-strand breaks and the concept of short- and long-term epigenetic memory. *Chromosoma*, 120:129–149.

[Otani et al., 2013] Otani, J., Kimura, H., Sharif, J., Endo, T. A., Mishima, Y., Kawakami, T., Koseki, H., Shirakawa, M., Suetake, I., and Tajima, S. (2013). Cell cycle-dependent turnover of 5-hydroxymethyl cytosine in mouse embryonic stem cells. *PLoS ONE*, 8(12):e82961.

[Pardo et al., 2009] Pardo, B., Gómez-González, B., and Aguilera, A. (2009). DNA repair in mammalian cells: DNA double-strand break repair: how to fix a broken relationship. *Cellular and Molecular Life Sciences*, 66:1039–1056.

[Pastor et al., 2013] Pastor, W. A., Aravind, L., and Rao, A. (2013). TETonic shift: biological roles of TET proteins in DNA demethylation and transcription. *Nature Reviews Molecular Cell Biology*, 14:341–356.

[Peddi et al., 2010] Peddi, P., Loftin, C. W., Dickey, J. S., Hair, J. M., Burns, K. J., Aziz, K., Francisco, D. C., Panayiotidis, M. I., Sedelnikova, O. A., Bonner, W. M., Winters, T. A., and Georgakilas, A. G. (2010). DNA-PKcs deficiency leads to persistence of oxidatively induced clustered DNA lesions in human tumor cells. *Free Radic. Biol. Med.*, 48(10):1435–1443.

[Polo and Jackson, 2011] Polo, S. E. and Jackson, S. P. (2011). Dynamics of DNA damage response proteins at DNA breaks: a focus on protein modifications. *Genes Dev.*, 25(5):409–433.

[Popp et al., 2010] Popp, C., Dean, W., Feng, S., Cokus, S. J., Andrews, S., Pellegrini, M., Jacobsen, S. E., and Reik, W. (2010). Genome-wide erasure of DNA methylation in mouse primordial germ cells is affected by AID deficiency. *Nature*, 463(7284):1101–1105.

[Rai et al., 2008] Rai, K., Huggins, I. J., James, S. R., Karpf, A. R., Jones, D. A., and Cairns, B. R. (2008). DNA demethylation in zebrafish involves the coupling of a deaminase, a glycosylase, and gadd45. *Cell*, 135(7):1201–1212.

[Robertson, 2002] Robertson, K. D. (2002). DNA methylation and chromatin - unraveling the tangled web. *Oncogene*, 21(35):5361–5379.

[Rogakou et al., 1999] Rogakou, E. P., Boon, C., Redon, C., and Bonner, W. M. (1999). Megabase chromatin domains involved in DNA double-strand breaks in vivo. *J. Cell Biol.*, 146(5):905–916.

[Sambrook et al., 1989] Sambrook, J., Fritsch, E. F., and Maniatis, T. (1989). *Molecular Cloning*. Cold Spring Harbor Laboratory Press.

[Santoro and Grummt, 2005] Santoro, R. and Grummt, I. (2005). Epigenetic mechanism of rRNA gene silencing: temporal order of NoRC-mediated histone modification, chromatin remodeling, and DNA methylation. *Mol. Cell. Biol.*, 25(7):2539–2546.

[Schaefer et al., 2013] Schaefer, A., Karaulanov, E., Stapf, U., Doderlein, G., and Niehrs, C. (2013). Ing1 functions in DNA demethylation by directing Gadd45a to H3K4me3. *Genes Dev.*, 27(3):261–273.

[Schmitz et al., 2009] Schmitz, K.-M., Schmitt, N., Hoffmann-Rohrer, U., Schäfer, A., Grummt, I., and Mayer, C. (2009). TAF12 recruits Gadd45a and the nucleotide excision repair complex to the promoter of rRNA genes leading to active DNA demethylation. *Molecular Cell*, 33:344–353.

[Scholz, 2003] Scholz, M. (2003). Effects of ion radiation on cells and tissues. *Advances in Polymer Science*, 162:95–155.

[Schomacher, 2013] Schomacher, L. (2013). Mammalian DNA demethylation - multiple faces and upstream regulation. *Epigenetics*, 8:679–684. review demethylation including GADD45.

[Sharif et al., 2007] Sharif, J., Muto, M., Takebayashi, S., Suetake, I., Iwamatsu, A., Endo, T. A., Shinga, J., Mizutani-Koseki, Y., Toyoda, T., Okamura, K., Tajima, S., Mitsuya, K., Okano, M., and Koseki, H. (2007). The SRA protein Np95 mediates epigenetic inheritance by recruiting Dnmt1 to methylated DNA. *Nature*, 450(7171):908–912.

[Shen et al., 2013] Shen, L., Wu, H., Diep, D., Yamaguchi, S., D'Alessio, A. C., Fung, H. L., Zhang, K., and Zhang, Y. (2013). Genome-wide analysis reveals TET- and TDG-dependent 5-methylcytosine oxidation dynamics. *Cell*, 153(3):692–706.

[Soria et al., 2012] Soria, G., Polo, S. E., and Almouzni, G. (2012). Prime, repair, restore: the active role of chromatin in the DNA damage response. *Mol. Cell*, 46(6):722–734.

[Splinter et al., 2010] Splinter, J., Jakob, B., Lang, M., Yano, K., Engelhardt, J., Hell, S. W., Chen, D. J., Durante, M., and Taucher-Scholz, G. (2010). Biological dose estimation of UVA laser microirradiation utilizing charged particle-induced protein foci. *Mutagenesis*, 25:289–97.

[Spruijt et al., 2013] Spruijt, C. G., Gnerlich, F., Smits, A. H., Pfaffeneder, T., Jansen, P. W., Bauer, C., Munzel, M., Wagner, M., Muller, M., Khan, F., Eberl, H. C., Mensinga, A., Brinkman, A. B., Lephikov, K., Muller, U., Walter, J., Boelens, R., van Ingen, H., Leonhardt, H., Carell, T., and Vermeulen, M. (2013). Dynamic readers for 5-(hydroxy)methylcytosine and its oxidized derivatives. *Cell*, 152(5):1146–1159.

[Tahiliani et al., 2009] Tahiliani, M., Koh, Y., Shen, K. P., Pastor, W. A., Bandukwala, H., Brudno, Y., Agarwal, S., Iyer, L. M., Liu, D. R., Aravind, L., and Rao, A. (2009). Conversion of 5-methylcytosine to 5-hydroxymethylcytosine in mammalian DNA by MLL partner TET1. *Science*, 324:930–935.

[Tan and Shi, 2012] Tan, L. and Shi, Y. G. (2012). Tet family proteins and 5-hydroxymethylcytosine in development and disease. *Development*, 139:1895–1902.

[Taucher-Scholz et al., 1996] Taucher-Scholz, G., Heilmann, J., and Kraft, G. (1996). Induction and rejoining of DNA double-strand breaks in CHO cells after heavy ion irradiation. *Advances in Space Research*, 18:83–92.

[Thomson et al., 2012] Thomson, J. P., Lempiainen, H., Hackett, J. A., Nestor, C. E., Muller, A., Bolognani, F., Oakeley, E. J., Schubeler, D., Terranova, R., Reinhardt, D., Moggs, J. G., and Meehan, R. R. (2012). Non-genotoxic carcinogen exposure induces defined changes in the 5-hydroxymethylome. *Genome Biol.*, 13(10):R93.

[Thurman et al., 2012] Thurman, R. E., Rynes, E., Humbert, R., Vierstra, J., Maurano, M. T., Haugen, E., Sheffield, N. C., Stergachis, A. B., Wang, H., Vernot, B., Garg, K., John, S., Sandstrom, R., Bates, D., Boatman, L., Canfield, T. K., Diegel, M., Dunn, D., Ebersol, A. K., Frum, T., Giste, E., Johnson, A. K., Johnson, E. M., Kutyavin, T., Lajoie, B., Lee, B. K., Lee, K., London, D., Lotakis, D., Neph, S., Neri, F., Nguyen, E. D., Qu, H., Reynolds, A. P., Roach, V., Safi, A., Sanchez, M. E., Sanyal, A., Shafer, A., Simon, J. M., Song, L., Vong, S., Weaver, M., Yan, Y., Zhang, Z., Zhang, Z., Lenhard, B., Tewari, M., Dorschner, M. O., Hansen, R. S., Navas, P. A., Stamatoyannopoulos, G., Iyer, V. R., Lieb, J. D., Sunyaev, S. R., Akey, J. M., Sabo, P. J., Kaul, R., Furey, T. S., Dekker, J., Crawford, G. E., and Stamatoyannopoulos, J. A. (2012). The accessible chromatin landscape of the human genome. *Nature*, 489(7414):75–82.

[Ting et al., 2006] Ting, A. H., McGarvey, K. M., and Baylin, S. B. (2006). The cancer epigenome–components and functional correlates. *Genes Dev.*, 20(23):3215–3231.

[Tollefsbol, 2011] Tollefsbol, T., editor (2011). *Handbook of Epigenetics - The New Molecular and Medical Genetics*. Elsevier.

[Toouli et al., 2002] Toouli, C. D., Huschtscha, L. I., Neumann, A. A., Noble, J. R., Colgin, L. M., Hukku, B., and Redde, R. R. (2002). Comparison of human mammary epithelial cells immortalized by simian virus 40 t-antigen or by the telomerase catalytic subunit. *Oncogene*, 21:128–139.

[Valinluck and Sowers, 2007] Valinluck, V. and Sowers, L. C. (2007). Endogenous cytosine damage products alter the site selectivity of human DNA maintenance methyltransferase DNMT1. *Cancer Res.*, 67(3):946–950.

[Ward, 1975] Ward, J. F. (1975). Radiation-induced strand breakage in DNA. *Basic Life Sci.*, 5B:471–472.

[Ward, 1994] Ward, J. F. (1994). The complexity of DNA damage: relevance to biological consequences. *Int. J. Radiat. Biol.*, 66(5):427–432.

[Watt and Molloy, 1988] Watt, F. and Molloy, P. L. (1988). Cytosine methylation prevents binding to DNA of a HeLa cell transcription factor required for optimal expression of the adenovirus major late promoter. *Genes Dev.*, 2:1136–1143.

[Weisenberger et al., 2005] Weisenberger, D. J., Campan, M., Long, T. I., Kim, M., Woods, C., Fiala, E., Ehrlich, M., and Laird, P. W. (2005). Analysis of repetitive element DNA methylation by MethyLight. *Nucleic Acids Res.*, 33(21):6823–6836.

[Williams et al., 2007] Williams, E. S., Stap, J., Essers, J., Ponnaiya, B., Luijsterburg, M. S., Krawczyk, P. M., Ullrich, R. L., Aten, J. A., and Bailey, S. M. (2007). DNA double-strand breaks are not sufficient to initiate recruitment of TRF2. *Nature Genetics*, 39:696–698.

[Wu and Zhang, 2011] Wu, H. and Zhang, Y. (2011). Mechanisms and functions of Tet protein-mediated 5-methylcytosine oxidation. *Genes*, 25:2436–2452.

[Wu and Zhang, 2014] Wu, H. and Zhang, Y. (2014). Reversing DNA methylation: mechanisms, genomics, and biological functions. *Cell*, 156(1-2):45–68.

[Wu and Zhang, 2010] Wu, S. C. and Zhang, Y. (2010). Active DNA demethylation: many roads lead to Rome. *Nat. Rev. Mol. Cell Biol.*, 11(9):607–620.

[Wyatt and Cohen, 1953] Wyatt, G. R. and Cohen, S. S. (1953). The bases of the nucleic acids of some bacterial and animal viruses: the occurrence of 5-hydroxymethylcytosine. *Biochem. J.*, 55(5):774–782.

[Yildirim et al., 2011] Yildirim, O., Li, R., Hung, J. H., Chen, P. B., Dong, X., Ee, L. S., Weng, Z., Rando, O. J., and Fazzio, T. G. (2011). Mbd3/NURD complex regulates expression of 5-hydroxymethylcytosine marked genes in embryonic stem cells. *Cell*, 147(7):1498–1510.

[Zhang et al., 2012] Zhang, L., Lu, X., Lu, J., Liang, H., Dai, Q., Xu, G. L., Luo, C., Jiang, H., and He, C. (2012). Thymine DNA glycosylase specifically recognizes 5-carboxylcytosine-modified DNA. *Nat. Chem. Biol.*, 8(4):328–330.

[Zhang et al., 1999] Zhang, Y., Ng, H.-H., Erdjument-Bromage, H., Tempst, P., Bird, A., and Reinberg, D. (1999). Analysis of the NuRD subunits reveals a histone deacetylase core complex and a connection with DNA methylation. *Genes Dev.*, 13:1924–1935.

9 Appendix

9.1 Publications and contributions to scientific meetings

9.1.1 Publications

M. Herrlitz, F. Natale, A. L. Leifke, M. Durante, G. Taucher-Scholz (2013). Active DNA Methylation Changes in Response to Ionizing Radiation. GSI Scientific Report 2012, S.431

M. Herrlitz, F. Natale, A. L. Leifke, M. Durante, G. Taucher-Scholz (2014). Active DNA Demethylation in Response to Ionizing Radiation. GSI Scientific Report 2013

9.1.2 Contributions to scientific meetings

Teile der Arbeit wurden als Tagungsbeiträge veröffentlicht.

12th Biennial Meeting of the DGDR / 15th Annual Meeting of the GBS; Munich (2012)
Poster: “Changes of epigenetic DNA and histone modifications in response to ionizing radiation“
M. Herrlitz, I. Müller, F. Natale, M. Durante und G. Taucher-Scholz

IMB Conference – DNA Demethylation, DNA Repair and Beyond; Mainz (2012)
Poster: “Active DNA Methylation changes in response to ionizing radiation”
M. Herrlitz, F. Natale, M. Durante und G. Taucher-Scholz

15th Annual Meeting of the GBS; Darmstadt (2013)
Poster: “Are Tet – enzymes involved in methylation changes after exposure to ionizing radiation?”
M. Herrlitz, F. Natale, M. Durante und G. Taucher-Scholz

9.2 Lebenslauf

Der Lebenslauf ist in der Online-Version aus Gründen des Datenschutzes nicht enthalten.

9.3 Danksagungen

Herzlich bedanken möchte ich mich an dieser Stelle bei Herrn Prof. Dr. Marco Durante für die Ermöglichung, meine Dissertation in der Abteilung Biophysik des GSI anzufertigen.

Bei Frau Prof. Dr. Cristina Cardoso möchte ich mich herzlich für die Übernahme des Zweitgutachtens und die Diskussionsbereitschaft meines Themas bedanken.

Außerdem bedanke ich mich bei Frau Prof. Dr. Gisela Taucher-Scholz für die umfassende Betreuung, ihre Diskussionsbereitschaft und die Vermittlung von umfangreichem Fachwissen.

Besonders bedanken möchte ich mich bei Dr. Francesco Natale und Dr. Iris Müller für die tolle Betreuung und Unterstützung, die Ideen und die Ratschläge. Danke außerdem für die Aufmunterungen, wenn es mal nicht so gut lief und für das freundschaftliche Verhältnis.

Anna Lena Leifke möchte ich nicht nur für die tatkräftige Unterstützung im Labor danken, sondern auch für eine sehr schöne Zeit, in der ich nicht nur eine spitzen Kollegin sondern auch eine echte Freundin gefunden habe.

Dr. Nicole Averbeck möchte ich dafür danken, dass sie bei Fragen immer einen Rat hatte. Außerdem danke ich ihr für das freundschaftliche Verhältnis, das sich in den letzten Jahren entwickelt hat. „Ich werde dich und das „Happy Office“ vermissen.“

Bei Gudrun Becker, Dr. Burkhard Jakob sowie bei allen weiteren Mitgliedern und ehemaligen Mitgliedern der DNA Gruppe möchte ich mich für die tolle Teamarbeit und das freundliche Arbeitsklima bedanken.

Rayees Khan, Wolfgang Becher, Günter Lenz, Dr. Michael Scholz und Dr. Thomas Friedrich möchte ich für die hervorragende Planung von allen Strahlzeiten und die Hilfe bei der Bestrahlung danken.

Allen Mitgliedern der Biophysik danke ich für das angenehme und freundliche Arbeitsklima.

Außerdem möchte ich mich für die Finanzierung durch das Beilstein Institut im Projekt „NanoBiC“ und die Finanzierung durch das Frankfurt Institute for Advanced Studies bedanken.

Ein ganz lieber Dank geht an meine Familie, Freunde und meinen Freund Alexander, die immer an mich geglaubt haben und mir stets eine große Stütze waren.

9.4 Ehrenwörtliche Erklärung

Ich erkläre hiermit ehrenwörtlich, dass ich die vorliegende Arbeit entsprechend den Regeln guter wissenschaftlicher Praxis selbstständig und ohne unzulässige Hilfe Dritter angefertigt habe.

Sämtliche aus fremden Quellen direkt oder indirekt übernommenen Gedanken sowie sämtliche von Anderen direkt oder indirekt übernommenen Daten, Techniken und Materialien sind als solche kenntlich gemacht. Die Arbeit wurde bisher bei keiner anderen Hochschule zu Prüfungszwecken eingereicht.

Darmstadt, den 15.05.2014

.....

Maren Linda Herrlitz